

INVESTIGATION OF SECONDARY CURRENT PRODUCED  
BY AN ISOLATED BLOCK IN A TWO-DIMENSIONAL  
TURBULENT FLOW

A Thesis

by

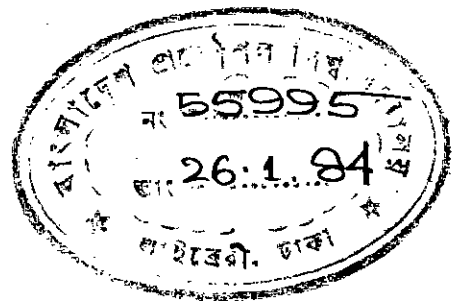
MD. AKRAM HOSSAIN

Submitted to the Department of Mechanical Engineering of  
Bangladesh University of Engineering and Technology, Dhaka  
in partial fulfilment of the requirements for the degree

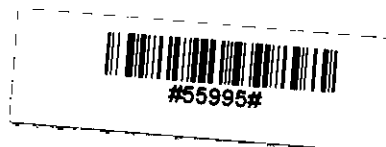
of

MASTER OF SCIENCE IN MECHANICAL ENGINEERING

620.114  
1983  
MDA



December, 1983




INVESTIGATION OF SECONDARY CURRENT PRODUCED  
BY AN ISOLATED BLOCK IN A TWO-DIMENSIONAL  
TURBULENT FLOW


A Thesis


by

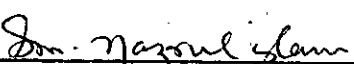
MD. AKRAM HOSSAIN

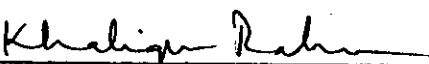
Approved as to style and content by:

  
(Dr. Dipak Kanti Das) : Chairman  
Professor,  
Dept. of Mechanical Engg.,  
BUET, Dhaka.

  
(Dr. A.M. Aziz-ul Haq) : Member  
Professor and Head,  
Dept. of Mechanical Engg.,  
BUET, Dhaka.

  
(Dr. M.A. Taher Ali) : Member  
Professor,  
Dept. of Mechanical Engg.,  
BUET, Dhaka.

  
(Dr. S.M. Nazrul Islam) : Member  
Associate Professor,  
Dept. of Mechanical Engg.,  
BUET, Dhaka.

  
(Dr. Khaliquur Rahman) : Member  
Professor,  
Dept. of Chemical Engg.,  
BUET, Dhaka.

December, 1983

CERTIFICATE OF RESEARCH

. Certified that the work presented in this thesis is the result of the investigation carried out by the candidate under the supervision of Dr. Dipak Kanti Das, at the Department of Mechanical Engineering, BUET, Dhaka.

*2012/2012*

---

Candidate

*Dipak Kanti Das*

---

Supervisor

DECLARATION

I do hereby declare that neither this thesis nor any part thereof has been submitted or is being concurrently submitted in candidature for any degree at any other university.

*ATTENAR*

---

Candidate

## ACKNOWLEDGEMENTS

I would like to express my sincere gratitude to Dr. Dipak Kanti Das, Professor of Mechanical Engineering Department whose, guidance, advice and continuous help have helped me to perform this research work.

I wish to express my gratefulness to Dr. S.M. Nazrul Islam and Dr. M.A. Taher Ali for their suggestions and inspiration at many steps of the experiment.

My gratitude is also to Dr. A.M. Aziz-ul- Huq for his interest into my work.

Special thank is due to Mr. Binoy Bhushan Shaha, Photographer of Metallurgical Engineering Department for his sincere co-operation for photographic works.

Thanks are also due to Mr. Md. Shahabuddin of Fluid Mechanics Laboratory of Mechanical Engineering Department for his help in various steps of the experiment and also to Mr. Md. Abdul Malek for typing the thesis.

ABSTRACT

Investigation of secondary current produced by an isolated block in the two dimensional, incompressible, turbulent boundary layer on a smooth plate was performed. Mean velocity profiles of undisturbed and disturbed (by the presence of isolated block) flows were measured. It was found that distortions of velocity profiles due to the presence of isolated blocks are slightly dependent on shape of the obstacle of same aspect ratio, but broadly they are similar. Distortions of velocity profiles are well significant in the down-stream of the disturbed region having negative wake effect indicating the presence of secondary current. Secondary current was measured by a two-tube yaw-meter, and both triangular and s-shape hodographs (or polar plots) were found. The hodograph of the experiment agreed well with the  $(p_2, q_2 = 2)$  family of hodograph model. A mathematical derivation of  $(p_2, q_2 = 2)$  family of model was also presented.

## CONTENTS

	Page
Certificate of Research	iii
Declaration	iv
Acknowledgement	v
Abstract	vi
Contents	vii
Figures and Table	ix
Nomenclature	xiii
Chapter 1      INTRODUCTION	
1.1      General Outline	1
1.2      Motivation Behind the Present Investigation	1
1.3      Features of the Present Work	3
Chapter 2      LITERATURE SURVEY	
2.1      Flow Past Obstacles	6
2.2      Turning Flow without Obstacles	11
Chapter 3      METHODS OF INVESTIGATION	
3.1      Determination of Wall Shear Velocity	14
3.2      Determination of Boundary Layer Parameters	16
Chapter 4      EXPERIMENTAL SET-UP AND PROCEDURE	
4.1.1    The wind tunnel	17
4.1.2    The blocks	18
4.1.3    Instrumentation and apparatus	19

	Page
4.1.4 Measurement procedure	19
4.2 Investigation of Secondary Current	21
4.3 Flow Visualisation	22
Chapter 5 MATHEMATICAL MODEL OF $(p_2, q_2 = 2)$ FAMILY OF HODOGRAPH	
5.1 Introduction	24
5.2 Mathematical Model of $(p_2, q_2=2)$ Family of Hodograph	25
Chapter 6 DISCUSSION ON EXPERIMENTAL RESULTS	
6.1 Introduction	29
6.2 Undisturbed Mean Flow Properties	29
6.3 Disturbed Flows	32
6.4 Flow Visualisation	34
6.5 Calibration of the Yaw-meter and Measurement of Flow Angle	35
6.6 Cross and Cross-over Flow	36
6.7 Comparison of the Model with Experiment	38
Chapter 7 CONCLUSIONS	
7.1 Introduction	40
7.2 Results	40
7.3 Conclusion	41
References	42
Appendix	102



## FIGURES AND TABLE

<u>Figure</u>	<u>Experimental Set-up and Procedure</u>	<u>Page</u>
4.A	Open Circuit Blower Type Wind Tunnel	45
4.B	Height Gauge, Manometer and the Block inside test section	45
4.C	Static Tapping on the test section	46
4.D	Probe-carrying shaft and Dial of the Yaw-meter	47
4.1	Diagram of Blocks and the Yaw-meter	48
4.2	Schematic Diagram of the tunnel working section showing position of static tapping and grid points	49
4.3	Diagram showing grid points downstream of the block	50
<u>Undisturbed Flow</u>		
6.1	Static pressure distribution in the wind tunnel	52
6.2	Mean velocity profiles at grid points $L_1, M_1, R_1$	53
6.3	Mean velocity profiles at grid points $L_2, M_2, R_2$	54
6.4	Mean velocity profiles at grid points $L_3, M_3, R_3$	55
6.5	Mean velocity profiles at grid points $L_4, M_4, R_4$	56
6.6	Mean velocity profiles at grid points $(L_1, M_1, R_1), (L_2, M_2, R_2), (L_3, M_3, R_3), (L_4, M_4, R_4)$	57
6.7	Mean velocity profiles at grid points $(L_1, L_2, L_3, L_4), (M_1, M_2, M_3, M_4), (R_1, R_2, R_3, R_4)$	58
6.8	The Universal law of the wall	59
<u>Disturbed Flow</u>		
6.9	Mean velocity profiles for the right circular cylinder at grid points $L_1, M_1$	62
6.10	Mean velocity profiles for the right circular cylinder at grid points $L_2, M_2, R_2$	63

<u>Figure</u>	Page
6.11 Mean velocity profiles for the right circular cylinder at grid points $L_3, M_3, R_3$	64
6.12 Mean velocity profiles for the right circular cylinder at grid points $L_4, M_4, R_4$	65
6.13 Mean velocity profiles for the rounded head cylinder at grid points $L_1, R_1$	66
6.14 Mean velocity profiles for the rounded head cylinder at grid points $L_2, M_2, R_2$	67
6.15 Mean velocity profiles for the rounded head cylinder at grid points $L_3, M_3, R_3$	68
6.16 Mean velocity profiles for the rounded head cylinder at grid points $L_4, M_4, R_4$	69
6.17 Mean velocity profiles for the cone at grid points $L_1, R_1$	70
6.18 Mean velocity profiles for the cone at grid points $L_2, M_2, R_2$	71
6.19 Mean velocity profiles for the cone at grid points $L_3, M_3, R_3$	72
6.20 Mean velocity profiles for the cone at grid points $L_4, M_4, R_4$	73
6.21 Mean velocity profiles for the right circular cylinder, the rounded head cylinder and the cone at grid points $L_1, L_2, L_3, L_4$	74
6.22 Mean velocity profiles for the right circular cylinder, the rounded head cylinder and the cone at grid points $M_2, M_3, M_4$	75
6.23 Mean velocity profiles for the right circular cylinder, the rounded head cylinder and the cone at grid points $R_1, R_2, R_3, R_4$	76

#### Flow Visualisation

6.24 Flow pattern of undisturbed flow	78
6.25 Flow pattern for the right circular cylinder	79
6.26 Flow pattern for the rounded head cylinder	80
6.27 Flow pattern for the cone	81

<u>Figure</u>	<u>Plots of <math>\gamma/\delta</math> vs. Flow Angle</u>	<u>Page</u>
6.28	Calibration of the Yaw-meter	83
6.29	$\gamma/\delta$ vs. flow angle for the right circular cylinder at grid points $L_1, L_2, R_1, R_2$	84
6.30	$\gamma/\delta$ vs. flow angle for the right circular cylinder at grid points $L_3, L_4, R_3, R_4$	85
6.31	$\gamma/\delta$ vs. flow angle for the right circular cylinder at grid points $M_2, M_3, M_4$	86
6.32	$\gamma/\delta$ vs. flow angle for the rounded head cylinder at grid points $L_1, L_2, R_1, R_2$	87
6.33	$\gamma/\delta$ vs. flow angle for the rounded head cylinder at grid points $L_3, L_4, R_3, R_4$	88
6.34	$\gamma/\delta$ vs. flow angle for the rounded head cylinder at grid points $M_2, M_3, M_4$	89
6.35	$\gamma/\delta$ vs. flow angle for the cone at grid points $L_1, L_2, R_1, R_2$	90
6.36	$\gamma/\delta$ vs. flow angle for the cone at grid points $L_3, L_4, R_3, R_4$	91
6.37	$\gamma/\delta$ vs. flow angle for the cone at grid points $M_2, M_3, M_4$	92

#### Hodographs

6.38	Hodograph for the right circular cylinder at grid points $R_1, R_2, R_3, R_4$	94
6.39	Hodograph for the right circular cylinder at grid points $L_1, L_2, L_3, L_4$	95
6.40	Hodograph for the right circular cylinder at grid points $M_2, M_3, M_4$	96
6.41	Hodograph for the rounded head cylinder at grid points $R_1, R_2, R_3, R_4$	97
6.42	Hodograph for the rounded head cylinder at grid points $L_1, L_2, L_3, L_4$	98

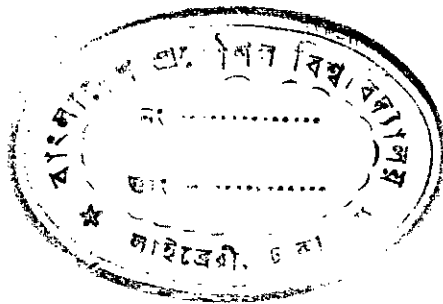
<u>Figure</u>		Page
6.43	Hodograph for the rounded head cylinder at grid points $M_2, M_3, M_4$	99
6.44	Hodograph for the cone at grid points $R_1, R_2, R_3, R_4, L_1, L_2, L_3, L_4$	100
6.45	Hodograph for the cone at grid points $M_2, M_3, M_4$	101

TABLE

6.A	Boundary Layer Parameters	60
-----	---------------------------	----

<u>Symbols</u>	<u>Nomenclature</u>
A, B	constants in Hodograph Model
A', A''	constants in Johnston's model
B', k	constants of Law of the wall (Eqn. 3.1)
$C_f$	co-efficient of skin-friction
$C_1, C_2, C_3, C_4$	constants of Eqn. (6.3)
d	diameter of isolated block
$P_i, q_j$	Hodograph model parameters
$P_2, q_2$	A family of Hodograph model
$R_e$	Reynolds number
$S_d$	separation distance
u	local mean velocity
U	free stream velocity
$U_0$	wall shear velocity
W	tangential component of mean velocity
y	ordinate of the axis
$\delta$	boundary layer thickness
$\delta_1$	displacement thickness
$\delta_2$	momentum thickness
$\delta_3$	energy thickness
$\nu$	kinematic viscosity
$\theta'$	angle of inclination of the yaw-meter
$\theta$	flow angle
$\rho$	density
$\xi$	$\frac{u}{U}$

CHAPTER 1  
INTRODUCTION



1.1 General Outline

Now-a-days one of the most interesting and challenging problems of Engineering Fluid mechanics is to analyse and determine three-dimensional turbulent boundary layer particularly to predict its major characteristics about or within an arbitrary shaped surface with its attendant free-stream flow field. It is quite significant to note that though three-dimensional turbulent boundary layers are more common than two-dimensional ones, the amount of research effort which has been and continues to be expanded on the latter problems is disproportionately large. But the problem that has generated interest among designers of turbomachinery and fluid dynamics concerns the nature of the boundary layer on a flat wall under the influence of a turning mean flow. Whereas few attempts have been made to study three-dimensional boundary layers either experimentally or theoretically and as far as the development of calculation method is concerned, the great majority of investigators have never ventured into three dimensions, presumably being deterred by the large number of velocity and shear stress components that have to be considered.

1.2 Motivation Behind the Present Investigation

Many practical problems involve flows of turning mean flow. For instance flow on the end wall bounding a compressor

cascade, flow over rivet heads, mechanical joints of a ship-hull, etc. In calculating the ship resistance or the resistance experienced by any aerodynamic or hydrodynamic surfaces it is necessary to consider the effect of three-dimensional single protuberances in the layer caused by the radial pressure gradient imposed on the layer by the curvature of the mean flow. The presence of such three-dimensional bodies in a boundary layer flow, creates vigorous distortions of the velocity profiles and turbulence quantities especially in the near region of the down-stream flow, giving rise to additional resistance (due to form drag) on the surface concerned. The effect generally observed is a skewing of the boundary-layer velocity vectors towards the centre of curvature of the mean flow.

The three-dimensional boundary layer may be classified as either collateral or skewed. The collateral layer is similar to a two-dimensional boundary layer in that a single plane passed normal to the bounding surface and containing the free-stream velocity vector will also contain all of the velocity vectors in a boundary layer velocity profile as well, e.g. a plane of symmetry flow. In the skewed profile there exists a cross-flow velocity component normal to this plane defined by the surface normal and free-stream direction.

Since almost all three-dimensional boundary layer problems are of turbulent flows, it is important to investigate the nature of disturbances as affected by the presence of

three dimensional obstacles. Keeping in view the above points of interest, attempts have been made to expand the knowledge in above mentioned fields.

### 1.3 Features of the Present Work

The total work presented in this thesis has been divided in following parts, e.g. (a) study of mean velocity profiles of undisturbed and disturbed flows (disturbed by the presence of obstacles), (b) study of boundary layer parameters (e.g. displacement thickness, momentum thickness, energy thickness, etc.), (c) Investigation of secondary current and its modelling.

In order to facilitate the above studies three obstacles of different geometry, but of same aspect ratio were placed in the free stream flow in a wind tunnel.

A comprehensive review of the relevant literature has been presented in Chapter 2.

Methods of investigation has been described in Chapter 3. The investigations described the development of turbulent boundary layer and measurement of boundary layer parameters.

In order to compare disturbed velocity profiles with undisturbed ones, mean velocity profiles for the undisturbed flows and disturbed flows were measured in the working



section of the wind tunnel at zero pressure gradient. For disturbed flows three isolated blocks (a right circular cylinder, a rounded head cylinder and a cone) having same aspect ratio (1" dia and 1" height) were chosen and set up individually at a selected grid point along the centre line of the test plate of the rectangular duct of the wind tunnel. The experimental technique used to measure different quantities for all experiments, reported in this thesis has been described in Chapter 4.

A mathematical model popularly known as  $(p_i, q_j)$  family of Hodograph model has been presented in Chapter 5. A family of hodograph model for the cross-flow velocity components of three-dimensional turbulent boundary layer was presented by Shanebrook and Hatch (1972). The principal advantage of this family is its flexibility which allows a wide variety of possible shapes for the hodograph. An extension of the above model with little modification has been used here to conform the present investigation.

In Chapter 6, discussion of results of velocity profiles behind obstacles were presented. A comparison was made with the undisturbed flows. Values of displacement thickness, momentum thickness and energy thickness were also determined. An elaborate experimental study has been carried out for the investigation of secondary current. Possible cross-flow were measured at each grid point for each block

by a two-tube Yaw-meter. It was found that in the disturbed boundary layer, cross-flow velocity components were present, confirming that the flows under investigation were three-dimensional in nature.

In Chapter 7, conclusions drawn from the investigations and the proposals for future work has been presented. It is hoped that the present work would be able to provide some useful information to the researchers and designers working on turbulent boundary layer, a three-dimensional one in particular.

.....

CHAPTER 2  
LITERATURE SURVEY

Not too many researchers investigated incompressible three-dimensional turbulent boundary layer flows. However, some important ones are mentioned below.

2.1 Flow Past Obstacles

Schlichting (1936) experimented on the measurement of the velocity field behind a row of spheres placed on a smooth flat surface. The pattern of curves of constant velocity clearly revealed that a kind of negative wake effect was present. The smallest velocities were found to be in the free gaps in which no spheres were present over the whole length of the plate; on the other hand, the largest velocities existed behind the rows of spheres where smaller velocities were expected.

Wieghardt (1943) carried out a large number of measurements on roughness in the special tunnel at Göttingen. The drag was measured with the aid of a balance which was attached to a rectangular test plate. The test plate was accommodated in a recess in the lower wall of the tunnel and it was free to move over a short distance. The difference between the drag on the test plate with and without the roughness elements (rectangular bars) gave the increased drag due to roughness. The author thought the increase

consisted of two terms. The first term is the form drag due to roughness itself and the second is due to the fact that the presence of roughness elements changes the velocity profile in its neighbourhood and hence the shearing stress on the wall as in the region of backflow behind the fillet.

Kuethé, Mckee and Curry (1946) investigated on three-dimensional turbulent boundary layer. They performed the experiment on a yawed wing of elliptical planform set up in a low-speed wind tunnel. Velocity profiles were measured by hot-wire anemometer and they found that the cross-flow profiles were of triangular shape.

Klebanoff and Diehl (1951) and Clauser (1956) also experimentally demonstrated that a rod placed parallel to the tunnel wall across a fully developed turbulent boundary layer violently distorted the velocity profile of the boundary layer. As the boundary layer proceeded downstream, this distortion died out and the boundary layer slowly returned to the original shape.

Hornung and Joubert (1963) investigated the mean velocity distribution in a low-speed three-dimensional turbulent boundary layer flow. They performed the experiment on a large scale model consisted of a flat plate on which secondary flow was generated by the pressure field introduced by a circular cylinder standing on the plate. They found that

the wall-wake model of Coles does not apply for flow of this kind and the model breaks down in the case of conically divergent flow with rising pressure, for example in the results of Kehl (1943). But the triangular model for the yawed turbulent boundary layer proposed by Johnston (1960) was confirmed with good correlation. The dimensionless velocity-defect profile was found to lie in a fairly narrow band when plotted against  $y/\delta$  for a wide variation of other parameters including the pressure gradient. They found that the law of the wall was applicable in the same form as for two-dimensional flow but for a more limited range of  $y$ .

Westkaemps (1968) showed that a cylinder protuberance mounted on a flat plate would cause the plate boundary layer to separate if the cylinder is long compared to the boundary layer thickness. An oil flow technique was used to obtain separation for several lengths and diameters of the cylindrical protuberances. From these data the author developed a relation for the prediction of the separation distance for a wide range of cylinder length and diameters. He found that for cylinders having a length to diameter ratio ( $L_d/d$ ) greater than 1.13 the non-dimensional separation distance ( $S_d/d$ ) has a constant value of 2.65. For smaller values of ( $L_d/d$ ), the relation is  $S_d/d = 2.42 (L_d/d)^{.7}$ .

A three-dimensional turbulent boundary layer accompanied with secondary currents and developing along a long streamwise bar of a rectangular cross-section placed on a flat plate was investigated experimentally by Furuya et.al. (1977). Two different wall configurations were provided by placing the longer sides of the rectangle perpendicular or parallel to the plate surface. They observed that the general behaviour of the flow is not much influenced by the change of the aspect ratio of the cross-section of the bar except in the region relatively near the leading edge. A self-preserving velocity profile in the plane of the flow symmetry of the three-dimensional turbulent boundary layer was proposed and comparison with the experimental results showed that the flow on the upper surface of the bar is, in fact, self-preserving.

Castro and Robins (1977) carried out an experimental investigation of the flow around surface-mounted cubes in turbulent flows. Measurements of body surface pressures and mean fluctuating velocities within the wake were taken. The flow was a simulated atmospheric boundary layer with a height ten times the body dimension. A similar experiment, on the flow past a cone placed on a flat plate, was also carried out by Okomoto, et. al. (1977). The vertex angle of the cone was varied  $60^\circ$ ,  $90^\circ$ ,  $120^\circ$  and  $150^\circ$ . The surface pressure distribution on the cone and the flat plate were

found to be similar for cones of vertex angles  $60^{\circ}$ - $120^{\circ}$ , but were different from those for vertex angle of  $150^{\circ}$ . This is thought to be because of the different flow separation and vortices. The separation points of the cones were obtained by the oil film method. The drag and lift coefficients were obtained from the surface-pressure distributions and it was found that the drag coefficient decreases as the vertex angle increases. Also negative wake effect was noticed in the wake of the cone on a flat plate.

Lee and Soliman (1977) carried out an experiment to investigate the influence of grouping parameters on the mean pressure distributions experienced by three dimensional bluff bodies immersed in a turbulent boundary. Different arrays of cubical roughness blocks were arranged and were tested with flows with different angles of attack. The authors had in mind a model of group of buildings and thus they concentrated on the problems of ventilation and environmental wind around buildings. From an architectural point of view this is particularly interesting.

Das (1980) experimented on flow recovery behind a three-dimensional cylindrical element using a pipe flow technique. To ascertain the effect of surface texture on the flow recovery, he investigated in pipes of different surfaces, smooth and rough. He described the flow recovery in terms of

mean flow properties and turbulence characteristics. In the downstream of the recovery zone a negative wake effect was observed and a cross-flow of s-shape which compared well with a proposed family of Hodograph model was found. The turbulence quantities are found to have an unusual but consistent distribution pattern in the recovery zone. However, the distortion of the mean flow and the turbulence quantities eventually dies out and the undisturbed flow characteristics are recovered at a further downstream position.

## 2.2 Turning Flow Without Obstacles

Gruschwitz (1935) performed an experiment in a turning passage of a rectangular cross-section preceeded by a straight rectangular duct in which a turbulent boundary layer had been caused to grow. At many stations on one of the flat walls, velocity profiles were determined by means of a traversed cylindrical, three-holed, stagnation pressure and angle probe. Static pressure was determined by means of wall-static taps.

Johnston (1960) carried out an experiment over the wall bounding a two-dimensional air-jet forced to flow against a perpendicular back wall. A uniform, collateral, turbulent boundary layer was caused to grow on the walls of



the rectangular entry duct. He measured velocity profiles on and around the plane of symmetry at many stations upstream of the separated regions that occur on the test-section walls ahead of the back wall. He achieved two objectives, e.g. (a) a mathematical model of the relationship between the cross-flow and mean flow components of the velocity vectors of the layer was established and secondly, (b) by utilization of the model some of the relationships required to carry out a boundary layer problem solution by the use of the momentum-integral equations were developed.

Klinksiek and Pierce (1970) carried out an experiment on the lateral flow in a low speed, three-dimensional, turbulent, incompressible boundary layer inside a recurving duct which was made to reverse itself completely. The test surface was floor wall of the sections. All profiles were measured in the test-section centre-line surfaces. They found that in the upstream of beginning of the bend a well-behaved two-dimensional turbulent boundary layer was developed. In the bend sections lateral and simultaneous lateral skewing were developed. They observed that when skewing existed in only one direction the polar velocity profiles indicated a near linear region as the floor of the channel was approached. With simultaneous lateral skewing a linear region was not apparent until flow reversal was near completion.

In spite of all these works the development of boundary layer and investigation on secondary current on a flat wall under the influence of a turning mean flow are still now very much in demand among the designers of turbomachinery and Fluid dynamics. So detailed experimental studies on cross-flow components of possible three-dimensional flows are essentially required.

## CHAPTER 3

### METHODS OF INVESTIGATION

The present thesis concerns the investigation of possible Secondary flow created by isolated blocks placed in the fully developed turbulent flow on a smooth flat plate. Calculation of different boundary layer parameters, co-efficient of skin friction, is essential for the purpose of the above investigation. Standard methods are used to determine all these parameters and properties.

#### 3.1 Determination of Wall Shear Velocity

Local velocity profile method has been used to determine the co-efficient of friction in the boundary layer flow. Von Karman demonstrated a universal velocity-distribution law from turbulent friction equation and a similar velocity-distribution law was deduced from Prandtl's mixing-length hypothesis for turbulent shearing stress by Schlichting, H., for a flat wall (rectangular channel).

The law of the wall for smooth surface is

$$\frac{u}{U_0} = \frac{1}{k} \log \frac{yU_0}{\nu} + B' \quad (3.1)$$

where  $k$  and  $B'$  are universal constants, the former also being known as Von Karman's constant. The numerical values are  $k = .41$  and  $B' = 4.9$ . These are the average values found by Clauser from various sources.

Now, multiplying both sides of (3.1) by  $\frac{U_0}{U} = \sqrt{\frac{C_f}{2}}$  and substituting for the constants, the following equation is obtained.

$$\begin{aligned} \frac{u}{U} &= 5.6 \sqrt{\frac{C_f}{2}} \log \frac{yU}{\nu} + 5.6 \sqrt{\frac{C_f}{2}} \left[ \log \sqrt{\frac{C_f}{2}} + .875 \right] \quad (3.2) \\ &= 5.6 \sqrt{\frac{C_f}{2}} \log \frac{yU}{\nu} + C \\ &= m \log \frac{yU}{\nu} + C \end{aligned}$$

or  $Y = mX + C$ , which is a linear equation (3.3)

where,  $Y = \frac{u}{U}$

$$\begin{aligned} m &= 5.6 \sqrt{\frac{C_f}{2}}, \text{ slope of the curve} \\ C &= 5.6 \sqrt{\frac{C_f}{2}} \left[ \log \sqrt{\frac{C_f}{2}} + .875 \right], \end{aligned}$$

intercept of the curve with the ordinate.

By plotting  $\frac{u}{U}$  versus  $\frac{yU}{\nu}$  for all the grid points in semi-log scale the value of  $m$  could be calculated from which the value of  $\sqrt{\frac{C_f}{2}}$  can be calculated.

By putting the value of  $\sqrt{\frac{C_f}{2}}$  in the equation

$$U_0 = \sqrt{\frac{C_f}{2}} U$$

the value of shear velocity can be found out.

Plotting  $\frac{u}{U_0}$  versus  $\frac{yU_0}{\nu}$  in semi-log scale, the equation (3.1), the law of the wall can fairly be proved.

### 3.2 Determination of Boundary Layer Parameters

The displacement thickness, momentum thickness and energy thickness are measured graphically from the standard integral equation of

$$\delta_1 = \int_{y=0}^{\infty} \left(1 - \frac{u}{U}\right) dy$$

$$\delta_2 = \int_{y=0}^{\infty} \frac{u}{U} \left(1 - \frac{u}{U}\right) dy$$

$$\delta_3 = \int_{y=0}^{\infty} \frac{u}{U} \left(1 - \frac{u^2}{U^2}\right) dy$$

where,  $\delta_1$  = displacement thickness

$\delta_2$  = momentum thickness

$\delta_3$  = energy thickness

Having measured the values of  $u$  and  $U$  for all grid points and plotting  $\frac{y}{\delta}$  versus  $\left(1 - \frac{u}{U}\right)$ ,  $\frac{u}{U} \left(1 - \frac{u}{U}\right)$  and  $\frac{u}{U} \left(1 - \frac{u^2}{U^2}\right)$  individually the values of the above parameters can be found out.

## CHAPTER 4

### EXPERIMENTAL SET-UP AND PROCEDURE

The present experiment mainly concerns the experimental investigation of possible cross-flow in incompressible two-dimensional turbulent boundary layer.

The investigation was divided into three parts. The first experiment involved the measurement of mean velocity distribution in the boundary layer developed on a smooth surface here in after known as undisturbed flow and measurement of the same on the smooth surface disturbed by placing an isolated block here in after known as disturbed flow.

The second one consisted of investigation of secondary current.

The third experiment involved the visual observation of the flow pattern and determination of non-dimensional separation distance.

The test was carried out in one of the Wind tunnels situated in the Fluid Mechanics Laboratory of the Mechanical Engineering Department. The details of the experimental set-up are as follows.

#### 4.1.1 The wind tunnel

The Wind tunnel was an open circuit blower type one with 3'x12"x8" working section (Fig. 4.A). This was a forced type Wind-tunnel. The blower was of axial type and driven

by 2.7 H.P. induction motor with r.p.m. of 2900. The blower casing was fitted with a settling chamber on the downstream side followed by a flow-straightener made of glass tubes. The floor and the top of the working section were made of smooth, perspex plate. Seven taps were drilled along the centre-line of the top surface of the test section. The holes were made to measure the pressure distribution longitudinally of the test section. The taps were connected with an inclined tube manometer.

#### 4.1.2 The blocks

Three blocks (Fig. 4.1), (a right circular cylinder, a rounded head cylinder and a cone) each with diameter and height of 1"x1" were made from wood. The surface of the blocks were made sufficiently smooth so that they can produce symmetrical distribution of flows on both sides of the centre line of the test plate when the blocks were placed at the selected grid point of the test plate and air was blown.

#### 4.1.3 Instrumentation and apparatus

(a) Traverse mechanism: A height gauge graduated in inch was used to carry the probes (pitot, yaw-meter and static tubes). The height gauge was set up at the exit end of the test section (Fig. 4B). The probes were fitted with

a drilled rod which was carried by the height gauge. By turning the sliding mechanism of the height gauge the probes could be traversed up and down or fixed at a particular position.

(b) A square head pitot tube of .035" O.D. was used for measurement of total head.

(c) Manometer: In all experiments, pressures detected by the pitot tube, static tube, yaw-meter, etc. were measured by manometer containing a bank of 28 tubes. For the magnification of the manometric head the manometer was always used with a certain inclination (1:4). The manometric fluid used, was water. The probes were connected with the manometer via flexible plastic tubes.

#### 4.1.4 Measurement procedure

At the beginning of the experiment the horizontal level of the test plate and the roof plate were checked by an spirit level. The no-flow reading of a particular tube in the manometer and the ambient temperature were recorded. The air was blown through the duct and manometric readings of the seven top centre-line taps (Fig. 4.2 and Fig. 4C) were measured. Measurements were taken twice, one at full opening of the two-wing butterfly valve and the other at half opening of the valve i.e. at two different velocities.



The longitudinal pressure gradient of the flow was checked and was made zero by adjusting the roof of the working section. A constant free-stream velocity was maintained for each experiment.

Twelve grid points were pre-selected on the test plate (Fig. 4.3). For accurate positioning of the grid points on the plate white paper with location of the above points was glued at the underside of the transparent test plate. to determine velocity profiles in the boundary layer the traverse mechanism carrying the pitot tube was placed outside the tunnel working section. The pitot tube was fixed horizontally such that it is parallel to free-stream flow direction. The tube was then traversed down to touch the test plate such that there exists no parallax. This was ensured by having no gap between the vertex of the pitot tube and its image reflected from the smooth, transparent test-plate. Having ensured this initial position of the pitot tube at a selected grid point the traverse mechanism was operated to displace the tube gradually upwards in close steps of 0.05 inch. In this way velocity profiles were determined for all other grid points for the undisturbed flow. Some 12 to 16 points were monitored in each profile.

To record velocity profiles for disturbed flow any of the wooden blocks was fixed at  $M_1$  by a screw from underneath. Boundary layer velocity profiles were then measured as before at each grid point. The same procedure was adopted for all other blocks.

## 4.2 Investigation of Secondary Current

A three-dimensional body when placed in a two-dimensional boundary layer flow creates vigorous distortion of the velocity profiles specially in the near region of the down stream flow. In the present investigation the main objective was to study the cross-flow created by isolated blocks on flat plate in two-dimensional turbulent boundary layer. From the mean flow measurements in the disturbed flow, it was evident that Secondary current existed, details of which would be revealed later. So arrangement was made to measure it.

A simple probe known as yaw-meter was made for the above purpose. Two hyperdermic tubes of 0.05 in. O.D. were soldered together to form a double-barrel probe. The tip of the barrel was then accurately filed to an equilateral  $60^\circ$  triangular head (Fig. 4.1). This end of the probe was used to search the flow direction while the other ends were connected to multitube manometer to monitor the deflections.

The Yaw-meter was first calibrated and for this purpose a special traverse mechanism was made. The mechanism consisted of a round probe-carrying shaft and a dial (Fig. 4.D). The Yawmeter was fixed with the traverse mechanism at a height from the base where there was no boundary layer effect. After the axial fan was switched on, readings of the multitube manometer were recorded. The tip of the yaw-meter

was rotated about the centre-line of the test section at an interval of two degrees. A chart was prepared showing angle of rotation of the yaw-meter versus non-dimensional pressure difference monitored by the yaw-meter.

The yaw-meter was then fitted with the traverse mechanism that was used to carry pitot tubes. With the blocks at the positions the readings at different grid points were taken for cross-current components.

#### 4.3 Flow Visualisation

Flow visualisation was necessary to examine visually the extent and behaviour of distorted zone. Here a primitive flow visualisation technique was arranged.

For the experiment a separate test plate of smooth, perspex sheet was used. The underside of the test plate was painted white so that the white paint could give a good contrast of photographs. A mixture of kerosene and lamp-black was prepared. The concentration of the mixture was to be carefully determined, otherwise if it is too thin, the whole pattern of velocity profiles would be washed away and if it is too thick again, it would not give a good flow-pattern. However the concentration of the mixture was determined by trial and error. After preparing such a mixture the test

plate was brushed uniformly by the mixture and the air was blown. Pattern started developing. After few minutes of air blowing the pattern was dried up and photograph was taken. Adopting the above procedure, flow patterns for undisturbed and disturbed flows (for all isolated blocks) were taken.

.....

## CHAPTER 5

### MATHEMATICAL MODEL OF ( $p_2, q_2 = 2$ ) FAMILY OF HODOGRAPH

#### 5.1 Introduction

Interest in the three-dimensional turbulent problem has increased in recent years because of frequent occurrence of secondary current effects in many engineering devices. Many reviews of the subject were made by Joubert, Perry and Brown (1967); Horlock, Norbury and Cook (1967); Francis and Pierce (1967). Of this review the model presented by Mager (1952),

$$\frac{W}{U} = B \frac{u}{U} \left(1 - \frac{y}{\delta}\right)^2 \quad (5.1)$$

assumed most success. However, there are reasons to believe that the above equation does not provide a complete general description of the cross-flow velocity component of three-dimensional turbulent boundary layers. To overcome this difficulties Gruschwitz(1935) was the first to propose a flexible model of hodograph (or polar plot) of  $\frac{W}{U}$  versus  $\frac{u}{U}$ . Later, Johnston (1960) proposed a triangular representation for the hodograph. Subsequently, many additional conditions were proposed and a variety of polynomial representations for the hodograph were developed and finally, by reviewing

these conditions a family of hodograph models were presented by Shanebrook and Hatch (1972), better known as  $(p_i, q_j)$  family of Hodograph models. The principal advantage of this family is its flexibility which allows a wide variety of possible shapes for the hodograph.

Now, a mathematical derivation of  $(p_2, q_2 = 2)$  family of hodograph method is presented and the obtained experimental results were compared with  $(p_2, q_2 = 2)$  family of model.

## 5.2 Mathematical Model of $(p_2, q_2 = 2)$ Family of Hodographs

Using equation (5.1) the boundary conditions represented are as follows:

$$\frac{W}{U} = 0 \text{ at } \frac{u}{U} = 0 \quad (a)$$

$$\frac{\partial(\frac{W}{U})}{\partial(\frac{u}{U})} = B \text{ at } \frac{u}{U} = 0 \quad (b)$$

$$\frac{W}{U} = 0 \text{ at } \frac{u}{U} = 1 \quad (c)$$

$$\frac{\partial(\frac{W}{U})}{\partial(\frac{u}{U})} = -A \text{ at } \frac{u}{U} = 1 \quad (d)$$

Several investigators e.g. Francis and Pierce (1967) Pierce and Klinksiek (1969) and Johnston (1960) have observed a near linear variation of the

experimental hodographs as the wall and boundary layer edge are approached. From a Taylor series expansion about

$$\xi = 0, \quad \text{where} \quad \xi = \frac{u}{U}$$

$$\frac{W}{U} = B \xi + \left( \frac{\partial^2 W}{\partial \xi^2} \right) \frac{\xi^2}{2!} + \left( \frac{\partial^3 W}{\partial \xi^3} \right) \frac{\xi^3}{3!} + \dots$$

and another about  $\xi = 1$ ,

$$\frac{W}{U} = -A (\xi - 1) + \left( \frac{\partial^2 W}{\partial \xi^2} \right) \frac{(\xi - 1)^2}{2!} + \left( \frac{\partial^3 W}{\partial \xi^3} \right) \frac{(\xi - 1)^3}{3!} + \dots$$

It can be seen that the observed linearities can be mathematically approximated by requiring one or more consecutive higher order derivatives to be forced to zero at the wall and/or boundary layer edge. The extent of linearity can be controlled by specifying the number of consecutive derivatives to be forced to zero. This gives at the wall,

$$\left( \frac{\partial^r W}{\partial \xi^r} \right)_{\xi=0} = 0, \quad r = 2, 3, \dots, j$$

and at the boundary layer edge,

$$\left( \frac{\partial^r W}{\partial \xi^r} \right)_{\xi=1} = 0 \quad r = 2, 3, \dots, k$$

So, for the present case of  $(p_2, q_2 = 2)$  family of hodographs

$$\left(\frac{\partial^2 W}{\partial \xi^2}\right)_{\xi=1} = 0, \quad \left(\frac{\partial^3 W}{\partial \xi^3}\right)_{\xi=1} = 0 \quad (e), \text{ for } q_2 = 2, \text{ and}$$

$$\left(\frac{\partial^2 W}{\partial \xi^2}\right)_{\xi=0} = 0, \quad \left(\frac{\partial^3 W}{\partial \xi^3}\right)_{\xi=0} = 0, \quad \dots \dots \left(\frac{\partial^{N+1} W}{\partial \xi^{N+1}}\right)_{\xi=0} = 0 \quad (f), \text{ for } p_2 = N$$

With the above boundary conditions it is apparent that the polynomial for  $\frac{W}{U} = f(\xi)$  will be of the form,

$$\frac{W}{U} = B\xi + C_1 \xi^{N+2} + C_2 \xi^{N+3} + \dots \dots \dots \quad (5.2)$$

The number of terms of the polynomial will be found from the conditions at the other boundary (i.e.  $\xi = 1$ ). Since at  $\xi = 1$ , there are four boundary conditions, e.g.

$$\frac{W}{U} = 0, \quad \frac{\partial(W/U)}{\partial \xi} = -A, \quad \frac{\partial^2(W/U)}{\partial \xi^2} = 0 \text{ and } \frac{\partial^3(W/U)}{\partial \xi^3} = 0,$$

So the number of constants will be four. Thus, the equation (5.2) will be,

$$\frac{W}{U} = B\xi + C_1 \xi^{N+2} + C_2 \xi^{N+3} + C_3 \xi^{N+4} + C_4 \xi^{N+5} \quad (5.3)$$

Putting the above four boundary conditions in equation (5.3), the governing equations become,

$$-B = C_1 + C_2 + C_3 + C_4$$

$$-A - B = C_1(N+2) + C_2(N+3) + C_3(N+4) + C_4(N+5)$$



$$0 = C_1(N+1)(N+2) + C_2(N+2)(N+3) + C_3(N+3)(N+4) + C_4(N+4)(N+5)$$

$$0 = C_1 N(N+1)(N+2) + C_2(N+1)(N+2)(N+3) + C_3(N+2)(N+3)(N+4) + C_4(N+3)(N+4)(N+5)$$

Putting these four equations in matrix form and finding the values of the constants and replacing  $N$  by  $p_2$  the required model can be achieved. That is,

$$\begin{aligned} \frac{W}{U} = & B \left[ \int - \frac{(p_2+2)(p_2+3)(p_2+4)}{6} \int^{(p_2+2)} + \frac{(p_2+1)(p_2+3)(p_2+4)}{2} \int^{(p_2+3)} \right. \\ & \left. - \frac{(p_2+1)(p_2+2)(p_2+4)}{2} \int^{(p_2+4)} + \frac{(p_2+1)(p_2+2)(p_2+3)}{6} \int^{(p_2+5)} \right] \\ & + A \left[ \frac{(p_2+3)(p_2+4)}{2} \int^{(p_2+2)} - \frac{(3p_2+7)(p_2+4)}{2} \int^{(p_2+3)} \right. \\ & \left. + \frac{(p_2+2)(3p_2+11)}{2} \int^{(p_2+4)} - \frac{(p_2+2)(p_2+3)}{2} \int^{(p_2+5)} \right] \quad (5.4) \end{aligned}$$

Now by choosing particular value of  $p_2$  and assigning values to the constants  $B$  and  $A$  the equation (5.4) can be used for calculating  $\frac{W}{U}$ . The calculated values of  $\frac{W}{U}$  were compared with the result of the experiment (Fig. 6.38 to 6.45) in the next chapter.

## CHAPTER 6

### DISCUSSION ON EXPERIMENTAL RESULTS

#### 6.1 Introduction

External flows over most bodies in hydrodynamics and aerodynamic applications, internal flows in pipes, channels and ducts as well as the complex flow pattern in turbomachinery passages involve flows of turning mean flow. In calculating the resistance experienced by any aerodynamic or hydrodynamic surfaces, it is necessary to consider the effect of three-dimensional single protuberances. Presence of such three-dimensional body creates distortions of velocity profiles and gives rise to additional resistance to the surface concerned especially in the near region of downstream flow. So it was thought essential to study the detailed characteristics of mean flow behind such bodies. For experimental simplicity the investigation has been carried on a smooth plate of a rectangular duct (sec. 4.1.4). This chapter deals with the properties of the fully developed turbulent flow and monitoring the possible secondary current.

#### 6.2 Undisturbed Mean Flow Properties

Zero pressure gradient of the undisturbed free-stream flow was checked and established (sec. 4.1.4) and the static pressure distribution of the test section is shown

in Fig. 6.1 where  $P$  is the pressure difference between the atmospheric pressure and tunnel pressure at different sections. As stated earlier (sec. 4.1.4) a grid was selected for determining the velocity profiles. The grid was numbered as  $L_1, M_1, R_1, L_2, \dots, M_4, R_4$  as shown in Fig. 4.2 and Fig. 4.3. At each grid point velocity distribution was measured (sec. 4.1.4). The plots of the mean velocity profiles have been presented in Fig. 6.2 to 6.5. All the measurements were taken at a Reynolds number of  $9.8 \times 10^4$ , based on mean velocity and hydraulic diameter of the tunnel. From the plots of each grid point it is noticed that the distributions are uniform, similar and consistent resembling the fully developed boundary layer velocity profiles.

The superimposed velocity profiles of  $(L_1, M_1, R_1)$ ,  $(L_2, M_2, R_2)$ ,  $(L_3, M_3, R_3)$  and  $(L_4, M_4, R_4)$  are shown in Fig. 6.6 and that of  $(L_1, L_2, L_3, L_4)$ ,  $(M_1, M_2, M_3, M_4)$  and  $(R_1, R_2, R_3, R_4)$  are shown in Fig. 6.7. The former is done to check the transverse uniformity and the later for downstream similarity. From Fig. 6.6 and 6.7 it is noticed that the velocity profiles both transversely and longitudinally are collapsing on to a single curve giving a hint of near self preserving.

The universal logarithmic velocity distributions for smooth surface at grid points  $(L_2, L_3, L_4)$ ,  $(M_2, M_3, M_4)$  and  $(R_2, R_3, R_4)$  are shown in Fig. 6.8. The solid line in the figure represents equation 3.1 showing reasonable agreement. The logarithmic overlap is about 18% of the boundary layer.

In this context, it may be mentioned that  $U_0$  used in these plots have been calculated following the procedure described in section 3.1 and the values of B' and K were chosen 4.9 and .41 respectively.

The values of boundary layer parameters e.g. boundary layer thickness, displacement thickness, momentum thickness and energy thickness for all the profiles at  $L_1, M_1, R_1$  to  $L_4, M_4, R_4$  are calculated and presented in Table 6.A. It is noticed that at each grid point the value of the boundary layer thickness is greater than the displacement thickness and displacement thickness is greater than the corresponding momentum thickness, a typical boundary layer development concept. Moreover, boundary layer thickness at  $L_1$  position is smaller than that at  $L_2$  and the value at  $L_2$  is smaller than the value at  $L_3$  and the thickness at  $L_3$  is smaller than the value at  $L_4$ , showing that the boundary layer thickness is increasing in the downstream direction of the test-section. Similarly, it is observed that displacement thickness and momentum thickness are also increasing in the downstream direction of the test section with the increased value of the boundary layer thickness.

From the above data and logarithmic velocity distributions it is evident that the flow over the grid is a fully developed turbulent boundary layer flow.

### 6.3 Disturbed Flows

As stated earlier (sec. 4.1.4) a block was fixed at grid position  $M_1$  by a screw from underneath the test plate to record velocity profiles. At each grid point velocity distribution was measured. The same procedure was adopted for all other blocks. The plots of the mean velocity profiles for the right circular cylinder, the rounded head cylinder and the cone have been presented in Fig. 6.9 to 6.20. Undisturbed profiles (dashed lines) are superimposed on these profiles to account the distortions caused by the disturbed flow.

It is noticed from Fig. 6.9 to 6.12 of the right circular cylinder that the flow was disturbed at each grid point with maximum at  $L_2, M_2, R_2$  positions and minimum at  $L_4, M_4, R_4$  positions within the range of experiment. At  $M_2$  positions i.e. just behind the block the profile was distorted vigorously, giving rise to a positive wake effect at the middle portion of the profile and a negative wake trend at the lower portion of the profile. At all other grid positions negative wake effect were observed. At downstream positions the wake trend is going to be diminished indicating that the disturbed profile is recovering to its undisturbed profile.

From Fig. 6.13 to 6.16 of the rounded head cylinder it is observed that the distortion of profile is similar to that of the right circular cylinder, but with a lesser

degree of distortion. Here also at  $M_2$  position a positive wake effect is observed at the middle portion of the profile with a negative effect at the lower portion. Negative wake trend are observed at all other grid positions.

In Fig. 6.17 to 6.20 the profiles for the cone have been presented. Here also a similar trend is noticed as before with a positive wake effect at  $M_2$  position and negative wake effect at all other positions. However, the degree of distortion of profile and wake trend is least for the cone comparing to the previous two blocks.

Comparing the distortions of velocity profiles due to the presence of the blocks it is noticed that the distortion is maximum along the centre-line of the test-section i.e. at positions  $M_2, M_3, M_4$ . Of these the distortion of profile is maximum at position  $M_2$  and least at position  $M_4$  in the range of experiment indicating that the influence of disturbance is decreasing in the downstream direction.

Comparing the profiles with the undisturbed ones it is noticed that the nature of distributions are varying from position to position, which indicates that the flow streamline is not a straight line rather it is curlic one. This changing behaviour and wake trend of the streamlines strongly proves the existence of secondary current in the disturbed zone.

The superimposed velocity profiles of disturbed flows are shown in Fig. 6.21 for grid position  $L_1, L_2, L_3, L_4$ , in Fig. 6.22 for grid positions  $M_2, M_3, M_4$  and in Fig. 6.23 for positions  $R_1, R_2, R_3$  and  $R_4$ . The distortions of profiles at  $L_1, L_2, L_3, L_4$  and  $R_1, R_2, R_3, R_4$  show more or less uniform and similar for all the blocks. But at  $M_2, M_3, M_4$  positions the distortion of profiles varies largely. At  $M_2$  position the profiles are distorted vigorously. Moreover, it is noticed that the distortion and wake effect is maximum for the right circular cylinder and minimum for the cone.

#### 6.4 Flow Visualisation

Since from the above discussion it appeared that a secondary current existed, a visual appraisal of distortion of flow pattern was thought to be worth making. A simple lamp-black flow visualisation technique was used for this purpose (see sec. 4.3 for details). It is noticed that the streamline was straight for the undisturbed flow (Fig. 6.24), but when the isolated block is placed in the stream the flow lines (shown by lamp-black) are distorted out and are spread sideways having a clear indication of a cross current (Fig. 6.25 to 6.27). Photographs with scale show that distortion in the downstream are well prominent even after long distance, which means that disturbed flows require a reasonably long distance to recover the undisturbed profile.

Non-dimensional separation distance can also be measured from the photograph with scale. For the present case it is found that for obstacles having length to diameter ratio ( $L_d/d$ ) equal to 1.0, the non-dimensional separation distance ( $S_d/d$ ) are 2.24, 2.16 and 1.73 for the right circular cylinder, rounded head cylinder and the cone respectively. A similar result was also obtained by Westkaemps (1968). He found that for cylinders having a length to diameter ratio ( $L_d/d$ ) greater than 1.13 the non-dimensional separation distance ( $S_d/d$ ) has a constant value of 2.65. For smaller values of ( $L_d/d$ ), the relation is  $S_d/d = 2.42 (L_d/d)^{.7}$ .

#### 6.5 Calibration of the Yaw-meter and Measurement of Flow Angle

Then it was decided that the cross current was to be monitored. For this purpose a two-tube yaw-meter was made and calibrated (see sec. 4.2 for details). Fig. 6.28 shows the calibration of the yaw-meter. The yaw-meter helped to measure the angle of flow (with respect to main flow direction) and the tangential component of the flow (cross current) was calculated from that. Flow angles at all grid points of the blocks were measured and  $y/\delta$  versus flow angle, are presented in Fig. 6.29 to 6.37. It is noticed that flow was drastically affected in the inner region ( $M_2, M_3, M_4$  positions) and  $L_1, R_1$  positions. For  $L_1, R_1, M_2, M_3, M_4$  positions



of both the right circular cylinder and the rounded head cylinder and for all grid positions of the cone the flow assumes cross profile but for the  $L_2, L_3, L_4, R_2, R_3, R_4$  positions of the right circular cylinder and the rounded head cylinder the flow assumes cross-over profiles. It is also observed that the degree of deviation of the flow angle is greatest for the right circular cylinder and least for the cone.

It is noticed that at the downstream region where the flow proceeded towards recovery the deviation becomes smaller. Moreover, as the flow reached boundary layer the deviation was going to be deminished, which is usually expected.

### 6.6 Cross and Cross-over Flow

By measuring the flow angle, the tangential ( $W$ ) component of the mean velocity can be determined. By calculating  $W$ , the cross-flow profiles can be checked with any of the known models for three-dimensional turbulent boundary layer, e.g. Johnston (1960), who relates  $\frac{W}{U}$  to  $\frac{u}{U}$  by a hodograph model (or polar plot):

$$\frac{W}{U} = A' \frac{u}{U}, \text{ near the wall and}$$

$$\frac{W}{U} = A'' \left(1 - \frac{u}{U}\right), \text{ away from the wall.}$$

Plots of  $\frac{W}{U}$  versus  $\frac{u}{U}$  for different grid points of the blocks are presented in Fig. 5.38 to 5.45. Here for the cone the cross-flow profiles take only triangular form and for the right circular cylinder and the rounded head cylinder the profiles take both triangular and s-shapes. The s-shape profiles are better known as cross-over profiles. This type of profile was found by Klinksiek and Pierce (1970) inside a recurving duct wherein the flow was made to reverse itself completely and by Das (1980) behind a three-dimensional cylindrical element in a pipe flow. Gruschwitz (1935) found triangular hodographs in a turning passage of rectangular x-section preceeded by a straight rectangular duct and by Kuethe, Mckee and Curry (1949) on a yawed wing of elliptical planform and also by Johnston (1960) over a flat wall bounding a two-dimensional air-jet forced to flow against a perpendicular back wall.

It is noticed that when skewing existed in only one direction, the polar velocity profiles indicated a near linear region as the floor of the test section was approached. In case of simultaneous lateral skewing a linear region was not apparent until flow reversal was near completion.

The cross-over profile may be well defined by family of hodograph models proposed by Shanebrook, et. al. (1972).

### 6.7 Comparison of the Model with Experiment

For the present investigation a number of values of  $p_2$  starting from zero were chosen. For finding the values of B and A a reasonable average value of the slopes of the hodographs (Fig. 6.38 to 6.45) were taken, where

$$B = \frac{\partial(\frac{W}{U})}{\partial(\frac{u}{U})} \quad \text{at } \frac{u}{U} = 0 \text{ and}$$

$$- A = \frac{\partial(\frac{W}{U})}{\partial(\frac{u}{U})} \quad \text{at } \frac{u}{U} = 1$$

Then by putting the values of  $\xi$ , B, A, and  $p_2$  in equation (5.4) the values of  $\frac{W}{U}$  were calculated. For the present case it was found that by taking the value of  $p_2 = 10$ ,  $B = \tan 14.41^\circ = .257$  and  $A = \tan 24^\circ = .445$ , a reasonable agreement between the experiment and the equation (5.4) has been achieved.

A similar investigation was also made by Klinksiek and Pierce (1970) in a three-dimensional turbulent boundary layer inside a recurving duct which was made to reverse itself completely. They found a reasonable representations of the hodograph from  $(p_2, 0)$  family of models, as well as members of the  $(p_2, q_2 = 1)$  and  $(p_2, q_2 = 2)$  families.

Das (1980) investigated flow recovery behind a three-dimensional cylindrical element using a pipe flow technique.

The experimental data compared very well with the  $(p_2, q_2 = 1)$  family of hodograph model.

From the above representation it is seen that  $(p_2, q_2=2)$  family of model has a wide range of flexibility for the hodographs. This proves that  $(p_i, q_j)$  family of hodograph models has flexibility as its principal advantage. Due to this flexible nature, three-dimensional viscous flow fields which will require cross-flow models will find extensive use of  $(p_i, q_j)$  family of hodograph models in future applications.

.....

## CHAPTER 7

### CONCLUSIONS

#### 7.1 Introduction

The present dissertation is mainly an experimental one to investigate secondary current produced by an isolated block in three-dimensional turbulent boundary layer. For this mean velocity profiles of undisturbed and disturbed flows were determined. Boundary layer parameters of undisturbed flow were calculated. A lamp-black flow visualisation method was used to see the secondary flow. Due to the presence of isolated block in two-dimensional turbulent boundary layer, secondary current (or cross flow) was generated both in triangular and S-form (cross-over flow) and was represented by hodographs (or polar plots). A mathematical model of  $(p_2, q_2 = 2)$  family of hodograph model was presented and compared with the result of the experiment. From the above performances the following results were achieved.

#### 7.2 Results

a) Undisturbed nearly self-preserving, two-dimensional and fully developed turbulent boundary layer was established.

b) Distortions of velocity profiles due to isolated blocks are slightly dependent on shape of the obstacle, but broadly they are similar.

c) Distortions of velocity profiles are well significant in the downstream of the disturbed region having negative wake effect indicating the presence of secondary current.

d) Secondary flow was detected and both triangular and s-shape hodographs were found.

e) The hodograph of the experiment agrees well with the  $(p_2, q_2 = 2)$  family of hodograph model.

f) The flexible nature of  $(p_2, q_2 = 2)$  family of model proves that the  $(p_i, q_j)$  family of hodograph model has wide flexibility which allows a wide range of possible shapes for the hodograph.

### 7.3 Conclusion

Finally, it may be stated that the present work will be a helpful one to the future researchers and designers working on turbulent boundary layer, particularly a three-dimensional one. While estimating the development of turbulent boundary layer, the cross current component may be taken care of well by the  $(p_i, q_j)$  family of hodograph model. However, the need for checking the effects of aspect ratio of blocks is also underscored.

.....

## REFERENCES

1. Gruschwitz, Von E. (1935), "Turbulente Reibungsschichten mit Sekundarströmung," *Ingénieur - Archive*, Vol. VI, 1935 pp. 355-365.
2. Weighardt, K. (1943), "Erhöhung des turbulenten Reibungswiderstandes durch Oberflächenstörungen", *Techn. Berichte* 10, Heft 9 (1943).
3. Kuethe, A.M., Mecke, P.G. and Curry, W.H. (1946), "Measurements in the Boundary Layer of a Yawed Wing", NACA TN 1946.
4. Klenbanoff, P.S. and Diehl, F.W. (1951), "Some features of artificially thickened fully developed turbulent boundary layers with zero pressure gradient", NACA TN 2475.
5. Thompson, J.S. Holder D. W. Notes on wind-tunnel pressure measurements from operator's point of view. AGARD Report 164, 1958.
6. Johnston, J.P. (1960), "Three-dimensional Turbulent Boundary Layers", M.I.T. Gas turbine Lab. Report 39, 1957; also available as "On the Three-Dimensional Turbulent Boundary Layer at a plane of symmetry in a three-dimensional flow", *Journal of Basic Engineering TRANS, ASME, series D. Vol. 82, No.4, Dec. 1960, pp.622-628.*
7. Hornung, H. and Joubert, P. (1963), "The Mean Velocity Profile in Three-Dimensional Turbulent Boundary Layer", *Journal of Fluid Mechanics*, Vol. 15, 1963, pp. 368-385.
8. Westkaemper, J.C. (1968), "Turbulent Boundary Layer separation ahead of cylinders", *AIAA Journal*, Vol. 6, p. 1352.
9. Schlichting, H. (1968), "Boundary Layer Theory", Mc-Graw-Hill, New York, 6th Edition.

10. Klinksiek, W.F. and Pierce, F.J. (1970), "Simultaneous Lateral Skewing in a Three-Dimensional Turbulent Boundary Layer Flow", Journal of Basic Engineering, TRANS, ASME, Series D. Vol. 92, March, 1970, pp. 83-92.
11. Bryer, D.W. and Pankhurst, R.C. (1971), "Pressure-probe methods for determining wind speed and flow direction", Her Majesty's Stationery Office, England.
12. Shanebrook, J.R. and Hatch, D.E. (1972), "A Family of Hodograph Models for the Cross Flow Velocity Component of Three-Dimensional Turbulent Boundary Layer", Journal of Basic Engineering, TRANS, ASME, Series D, Vol. 94, June 1972, pp. 321-331.
13. Furuya, Y. Miyata, M. and Fujita, H. (1977), "Turbulent Boundary Layer along a streamwise bar of rectangular cross-section placed on a flat plate", Bulletin of the ASME, Vol. 20, No. 141, p. 315.
14. Castro, I.P. and Robins, A.G. (1977), "The flow around a surface mounted cube in uniform and turbulent streams", Journal of Fluid Mechanics, Vol. 79, p. 307.
15. Lee, B.E. and Soliman, F.F. (1977), "An investigation of the forces on three-dimensional bluff bodies in rough wall turbulent boundary layers", Journal of Fluid Engineering, Vol. 99, p. 503.
16. Das, D.K. (1980), "Recovery of a Disturbed Turbulent Shear Flow", Proceedings: Fifth ISME Conference, Dec.23,24, 1983 Allahbad, India.



EXPERIMENTAL SET-UP AND PROCEDURE

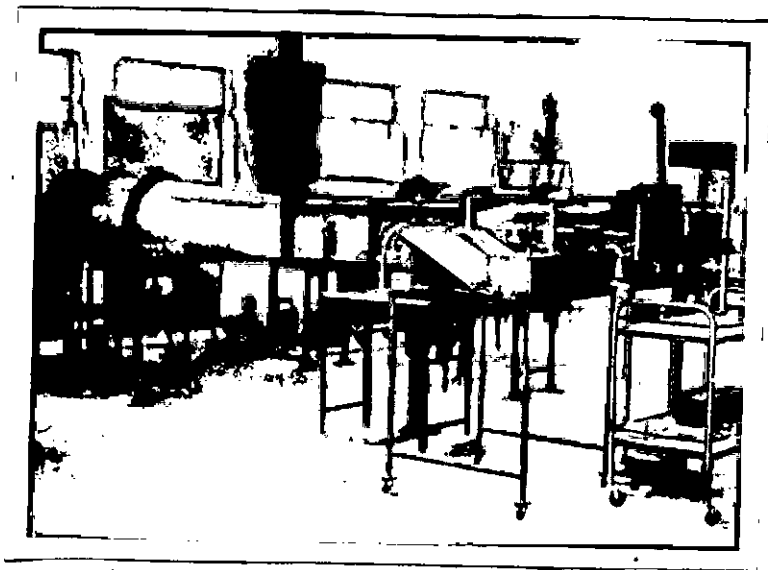


Fig. 4A Open Circuit Blower Type Wind Tunnel.

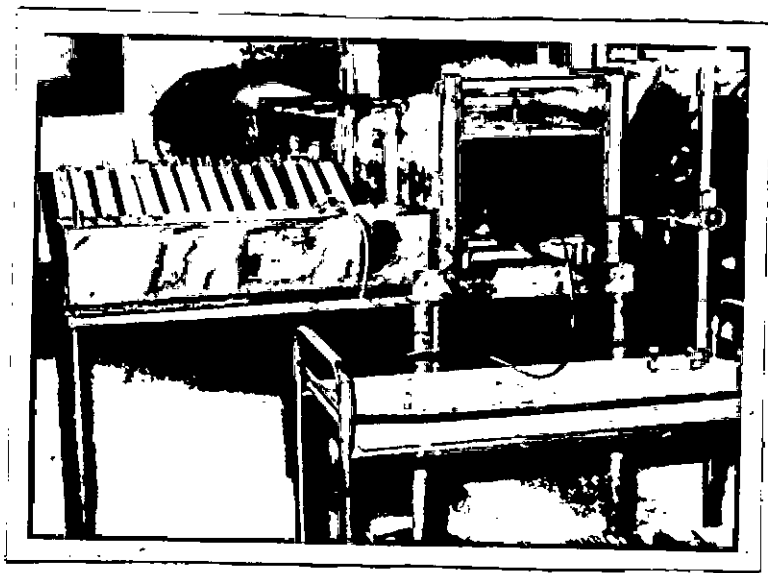


Fig. 4.B High Gauge, Manometer and the Block Inside the Test Section.



Fig. 4.C Static Tapping on the Test Section.

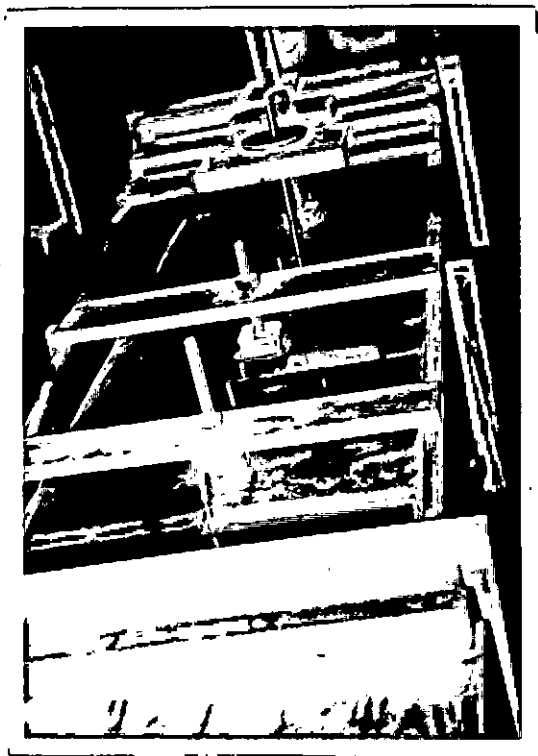
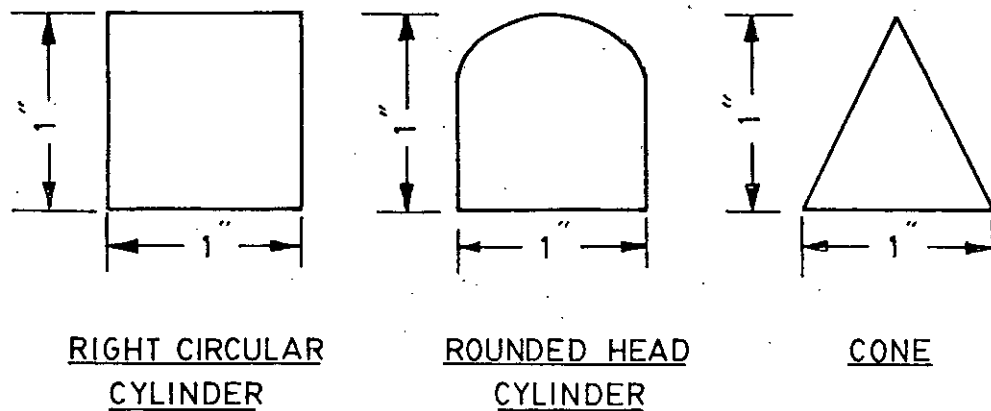


Fig. 4.D Probe-Carrying Shaft and Dial of the Yaw-Meter.



ISOLATED BLOCKS



FIG. 4-1 DIAGRAM OF BLOCKS AND THE YAW-METER

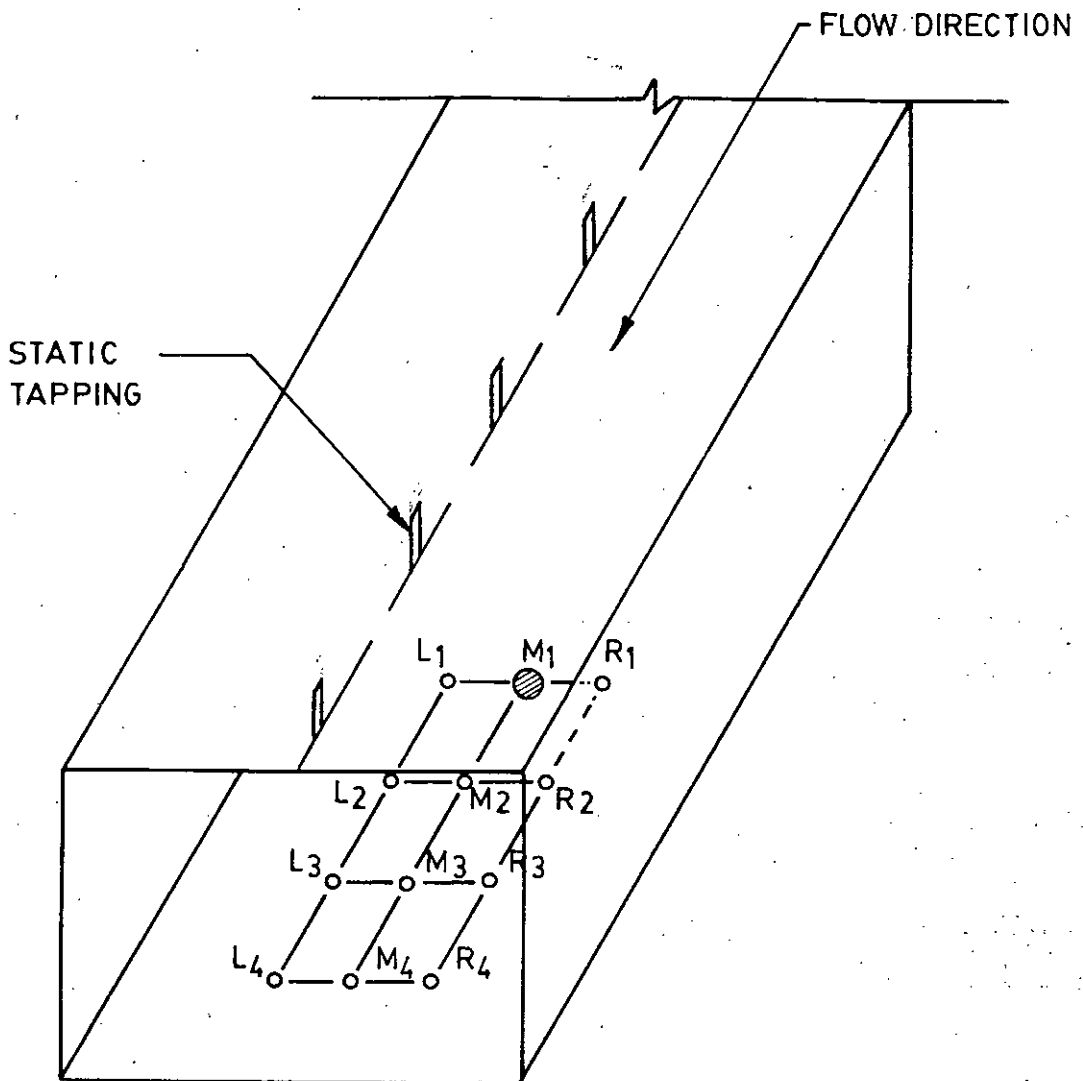


FIG. 4.2 SCHEMATIC DIAGRAM OF THE TUNNEL WORKING SECTION  
SHOWING POSITION OF STATIC TAPPING AND GRID POINTS

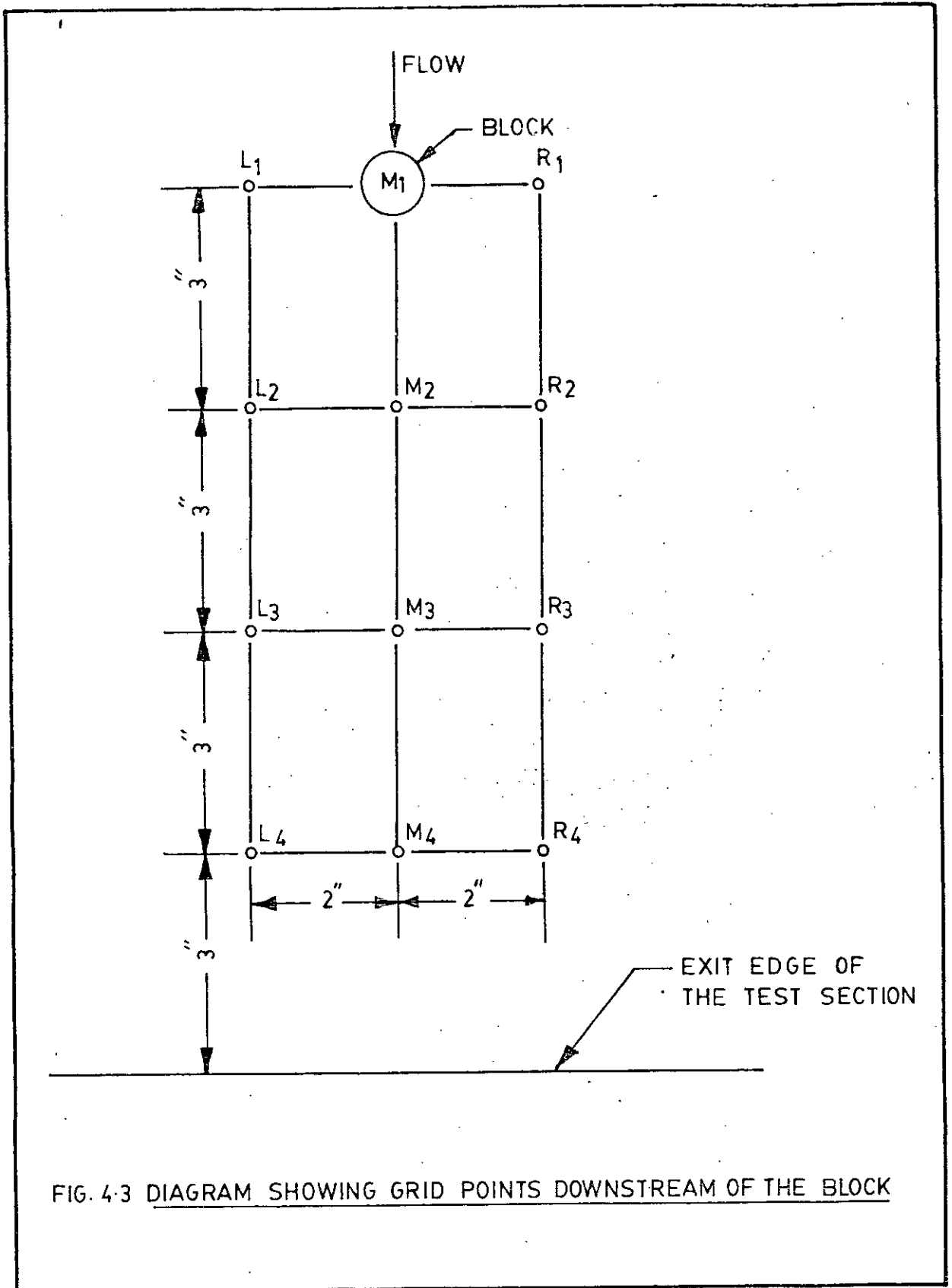


FIG. 4-3 DIAGRAM SHOWING GRID POINTS DOWNSTREAM OF THE BLOCK

UNDISTURBED FLOW



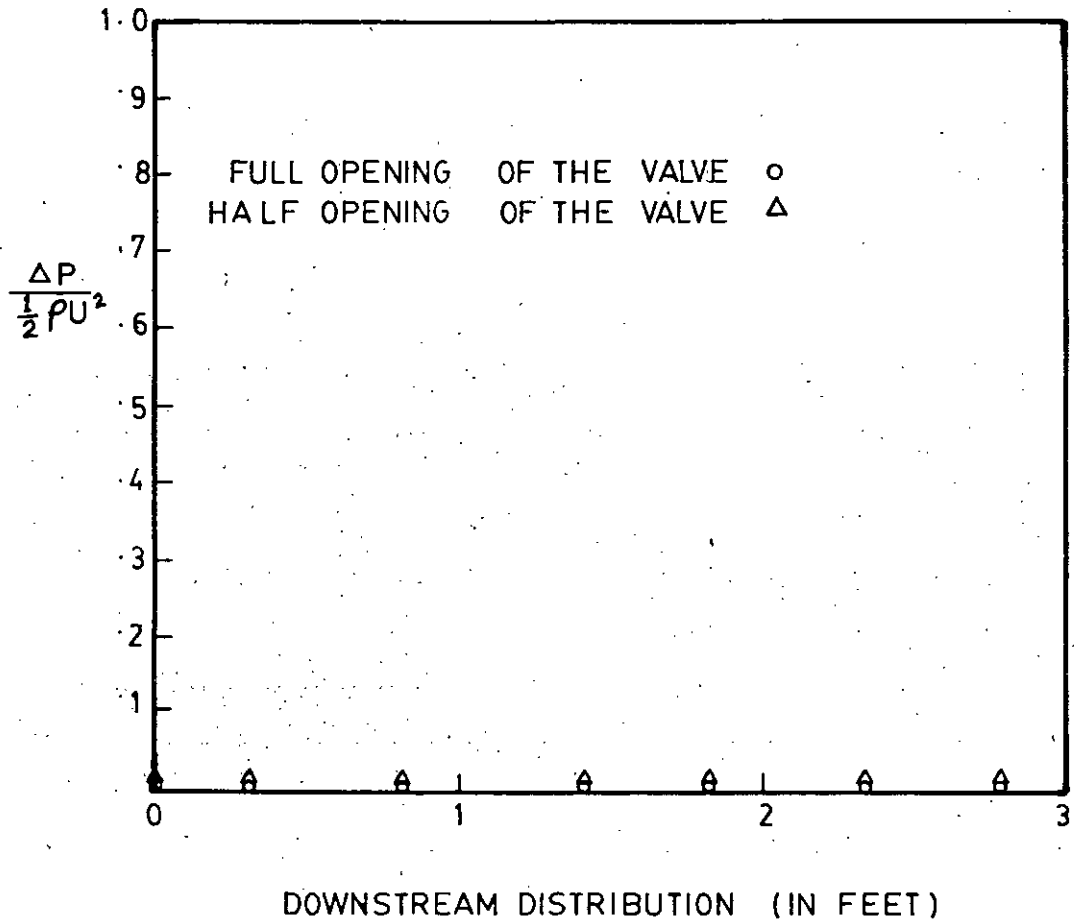


FIG-6.1 STATIC PRESSURE DISTRIBUTION IN THE WIND TUNNEL

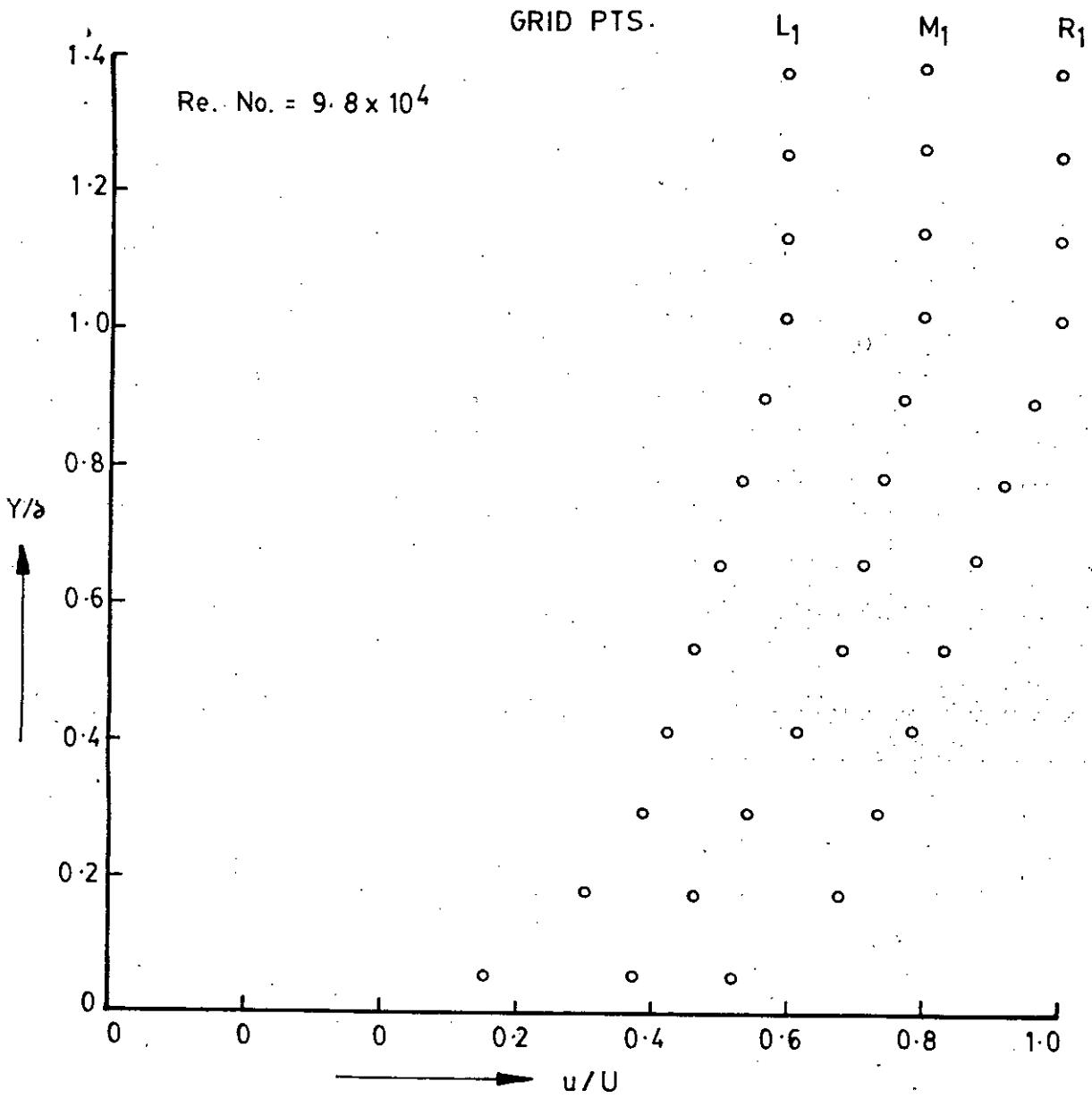


FIG. 6.2 MEAN VELOCITY PROFILES (UNDISTURBED FLOW)

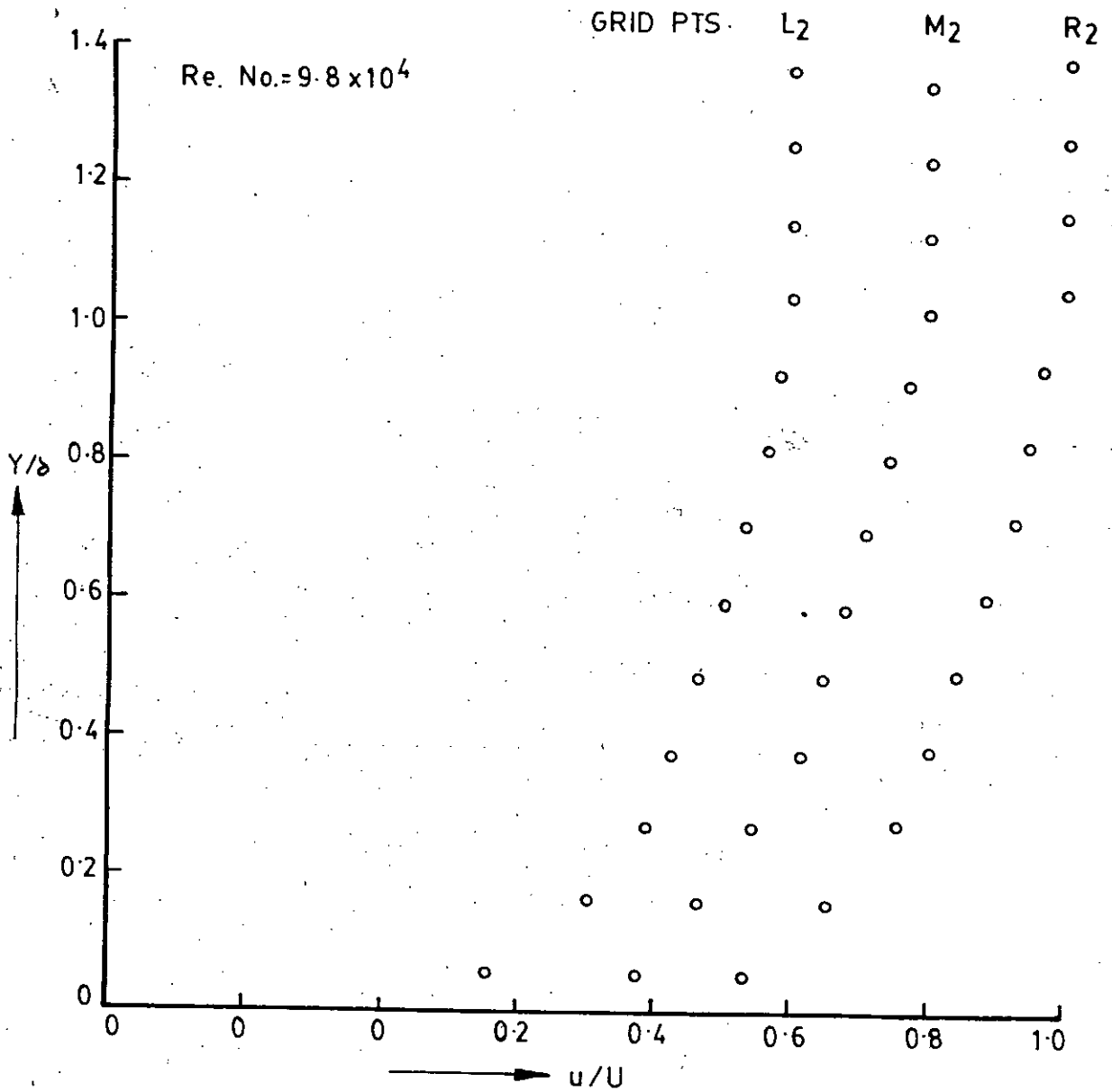


FIG. 6-3 MEAN VELOCITY PROFILES (UNDISTURBED FLOW)

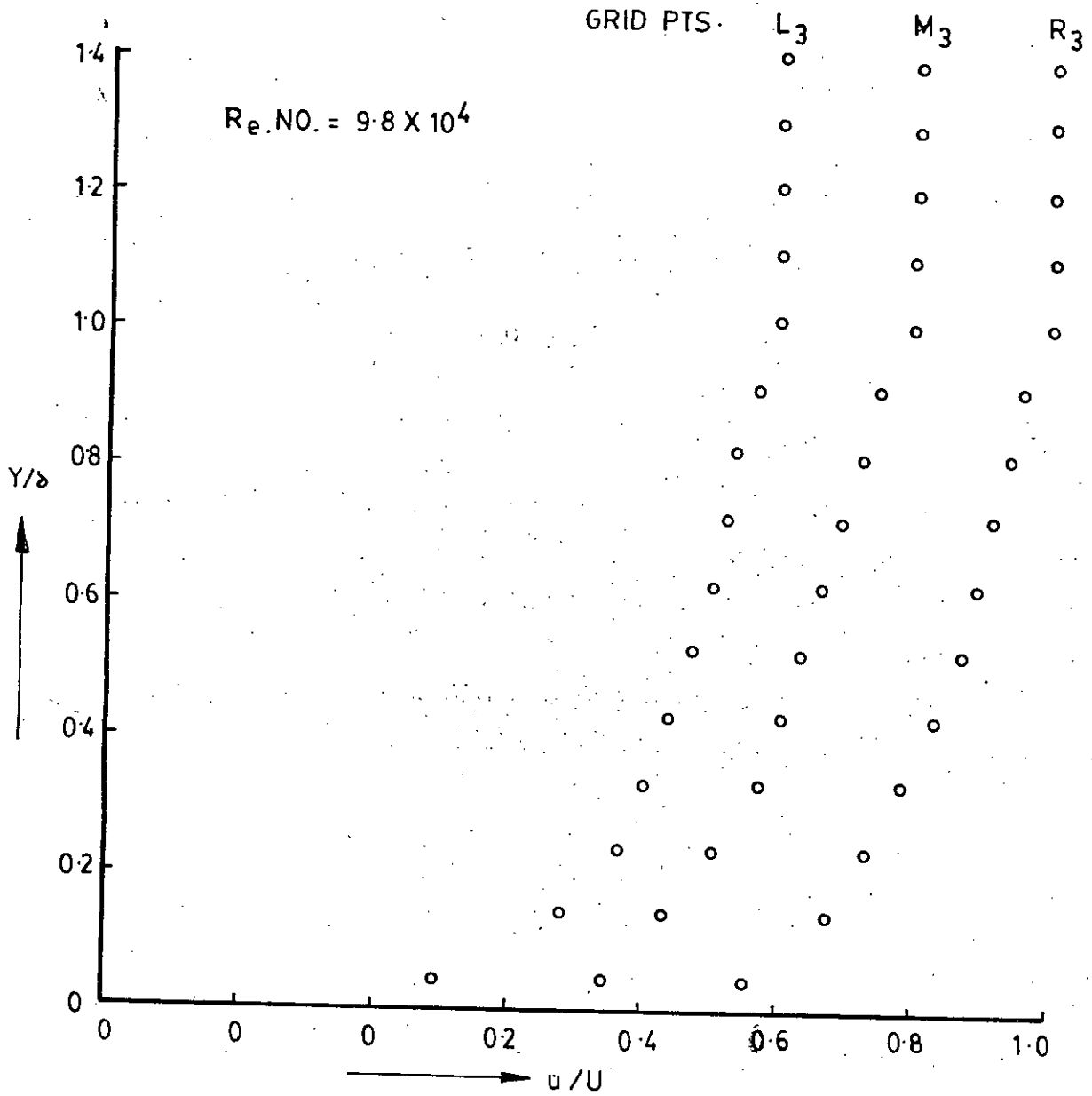


FIG. 6.4 MEAN VELOCITY PROFILES (UNDISTURBED FLOW)

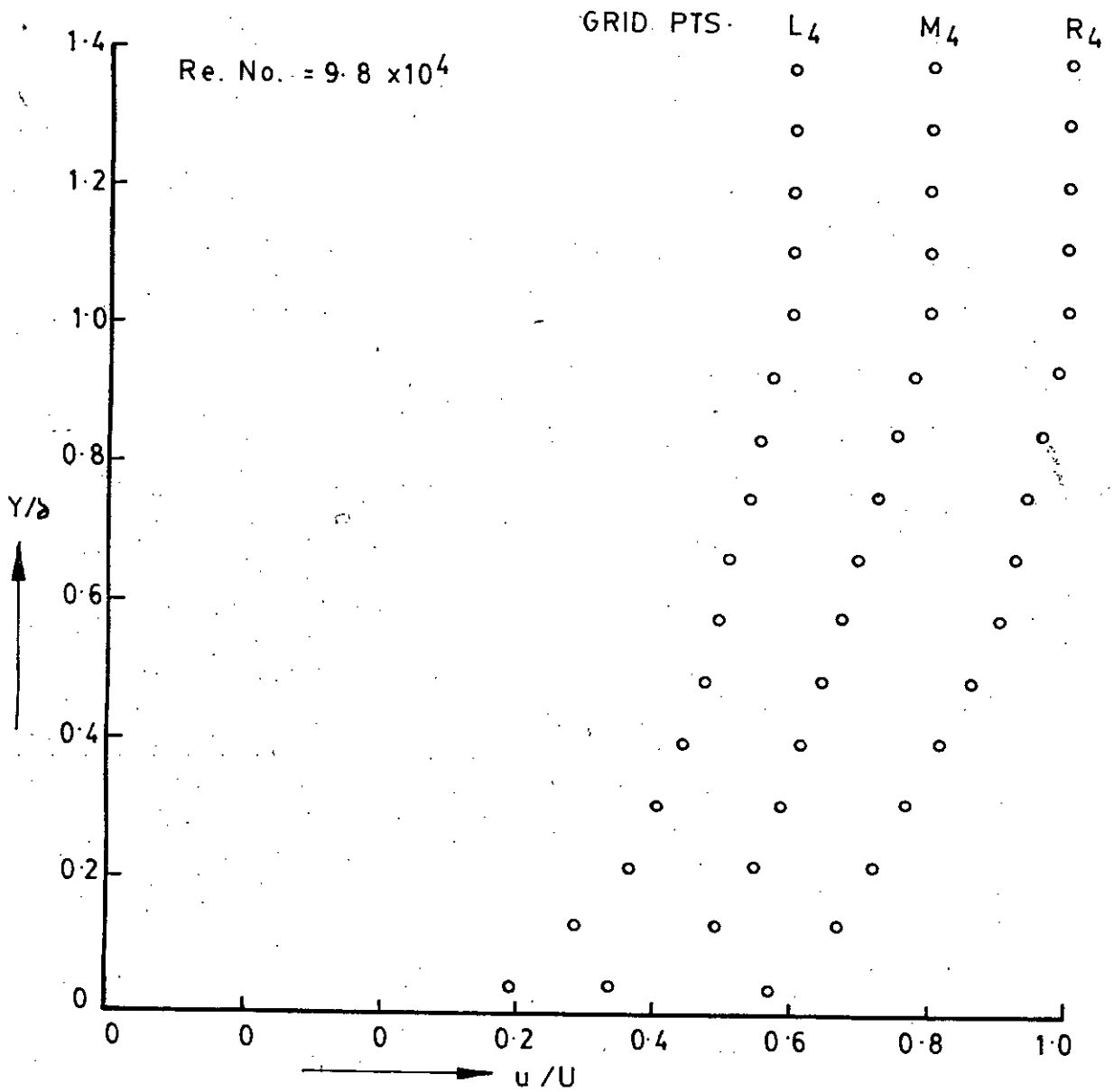


FIG. 6.5 MEAN VELOCITY PROFILES (UNDISTURBED FLOW)

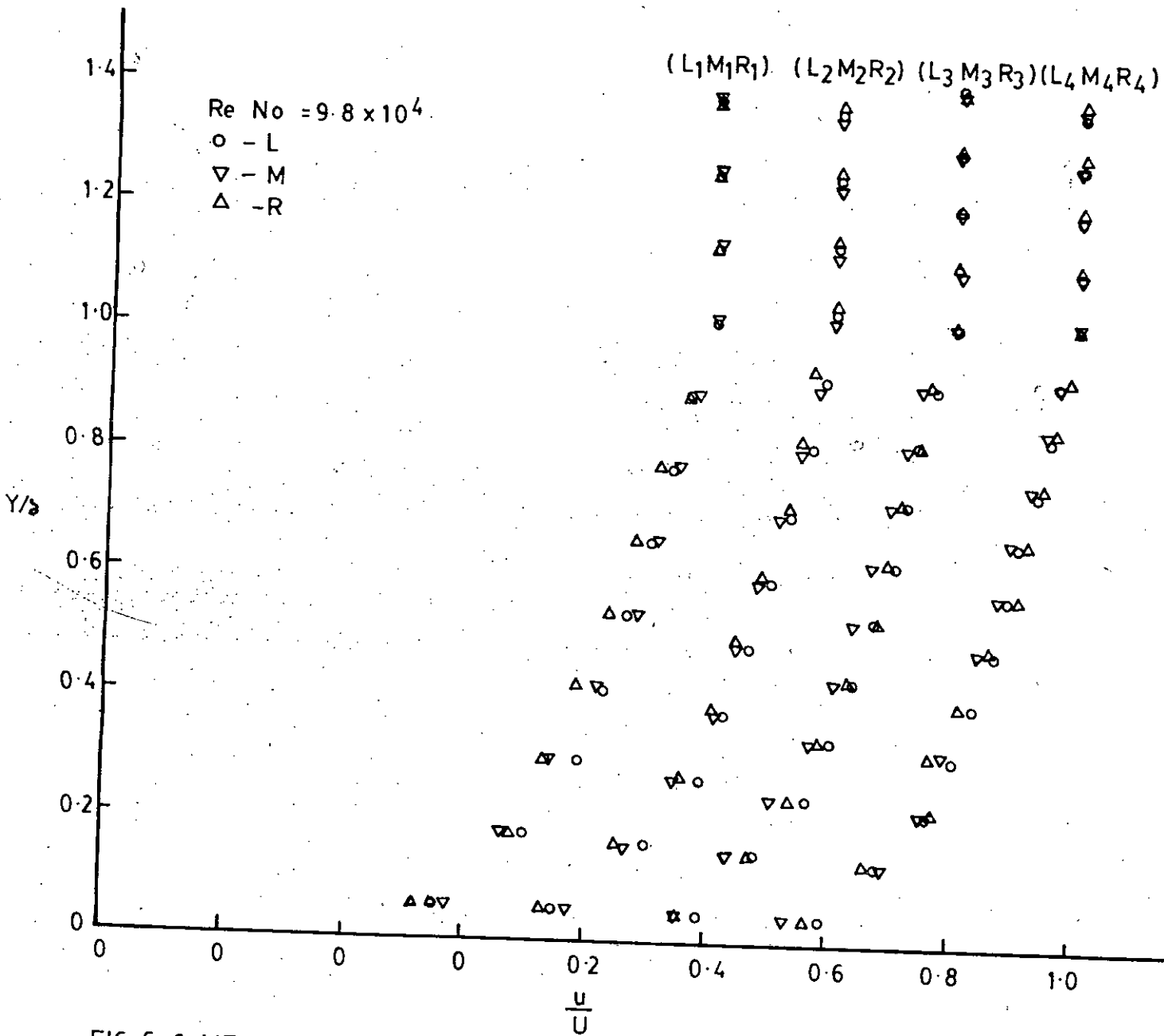


FIG. 6.6 MEAN VELOCITY PROFILES (UNDISTURBED FLOW)

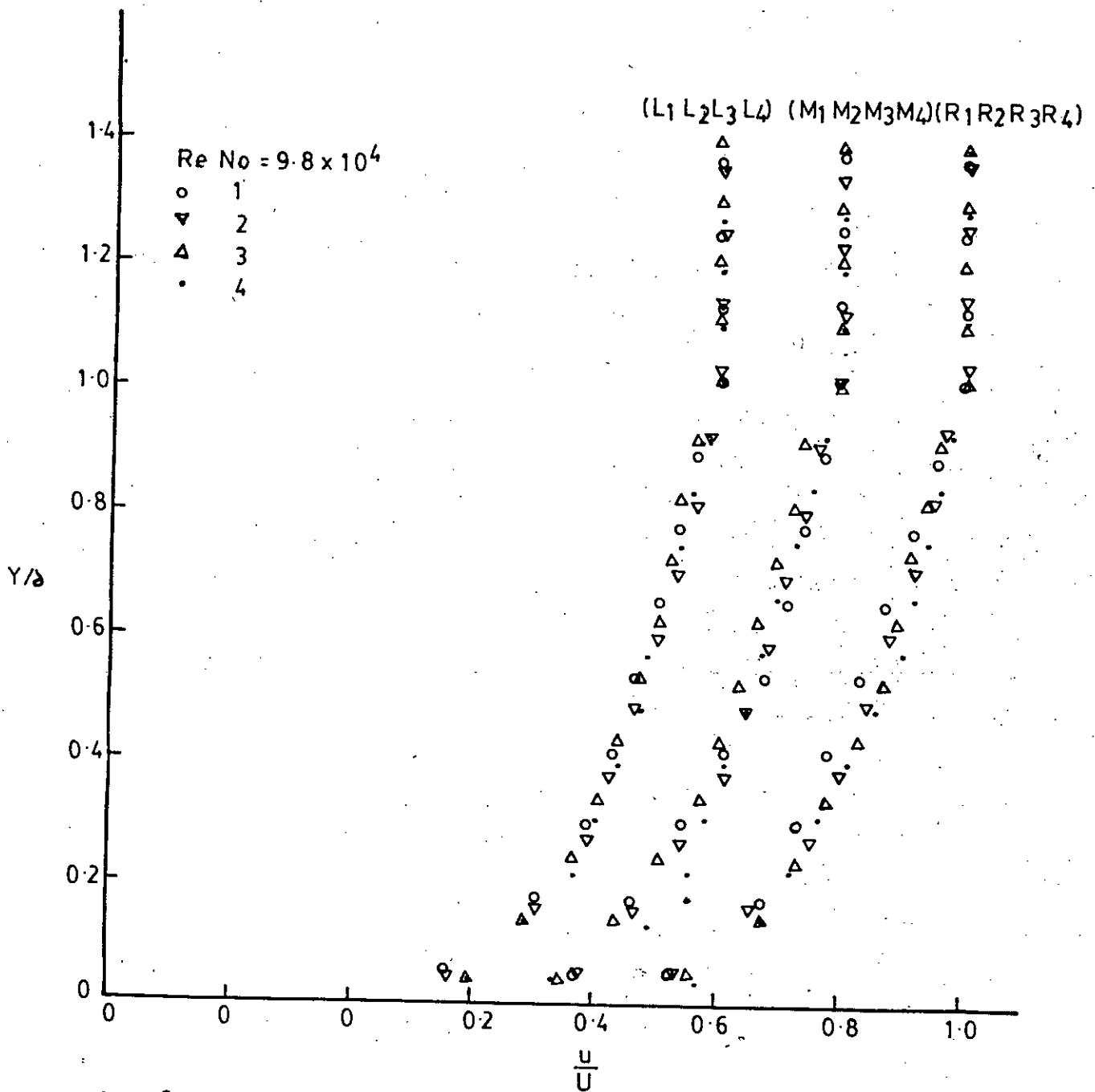


FIG. 6.7 MEAN VELOCITY PROFILES (UNDISTURBED FLOW)

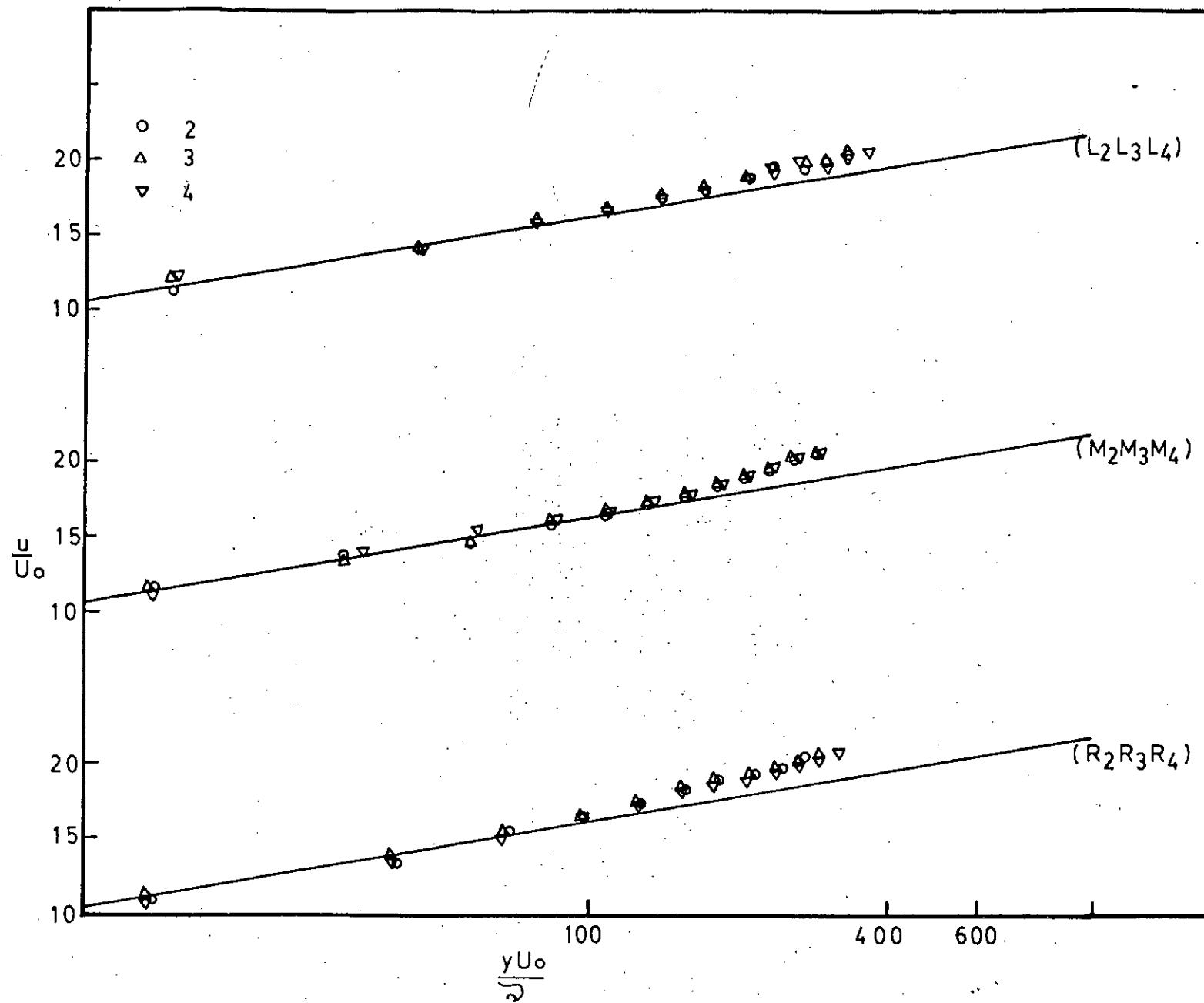


FIG. 6.8 THE UNIVERSAL LAW OF THE WALL (UNDISTURBED FLOW)



TABLE 6.A

Boundary Layer Parameters in inch

Grid pts.	$\delta$	$\delta_1$	$\delta_2$	$\delta_3$
L <sub>1</sub>	0.4159	0.0820	0.0673	0.1042
L <sub>2</sub>	0.4581	0.0865	0.0704	0.1117
L <sub>3</sub>	0.5154	0.0939	0.0757	0.1233
L <sub>4</sub>	0.5654	0.1072	0.0842	0.1355
M <sub>1</sub>	0.4151	0.0810	0.0625	0.1011
M <sub>2</sub>	0.4601	0.0899	0.0714	0.1141
M <sub>3</sub>	0.5189	0.1018	0.0815	0.1310
M <sub>4</sub>	0.5633	0.1059	0.0828	0.1334
R <sub>1</sub>	0.4170	0.0832	0.0694	0.1072
R <sub>2</sub>	0.4535	0.0840	0.0699	0.1085
R <sub>3</sub>	0.5175	0.0993	0.0790	0.1266
R <sub>4</sub>	0.5606	0.1039	0.0806	0.1308

Where,

 $\delta$  = Boundary layer thickness $\delta_1$  = Displacement thickness $\delta_2$  = Momentum thickness $\delta_3$  = Energy thickness

DISTURBED FLOW

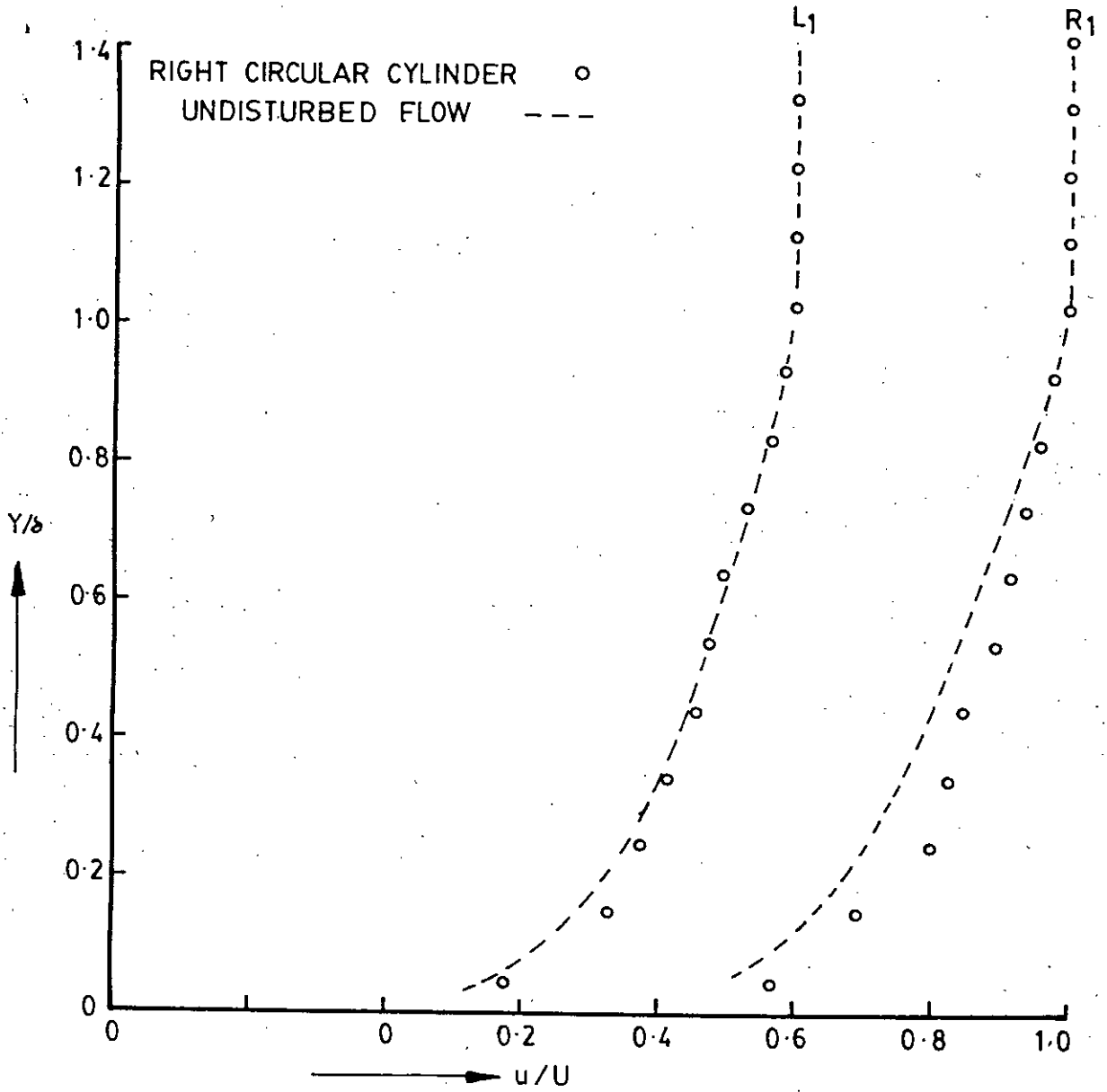


FIG. 6.9 MEAN VELOCITY PROFILES (DISTURBED FLOW)

55995

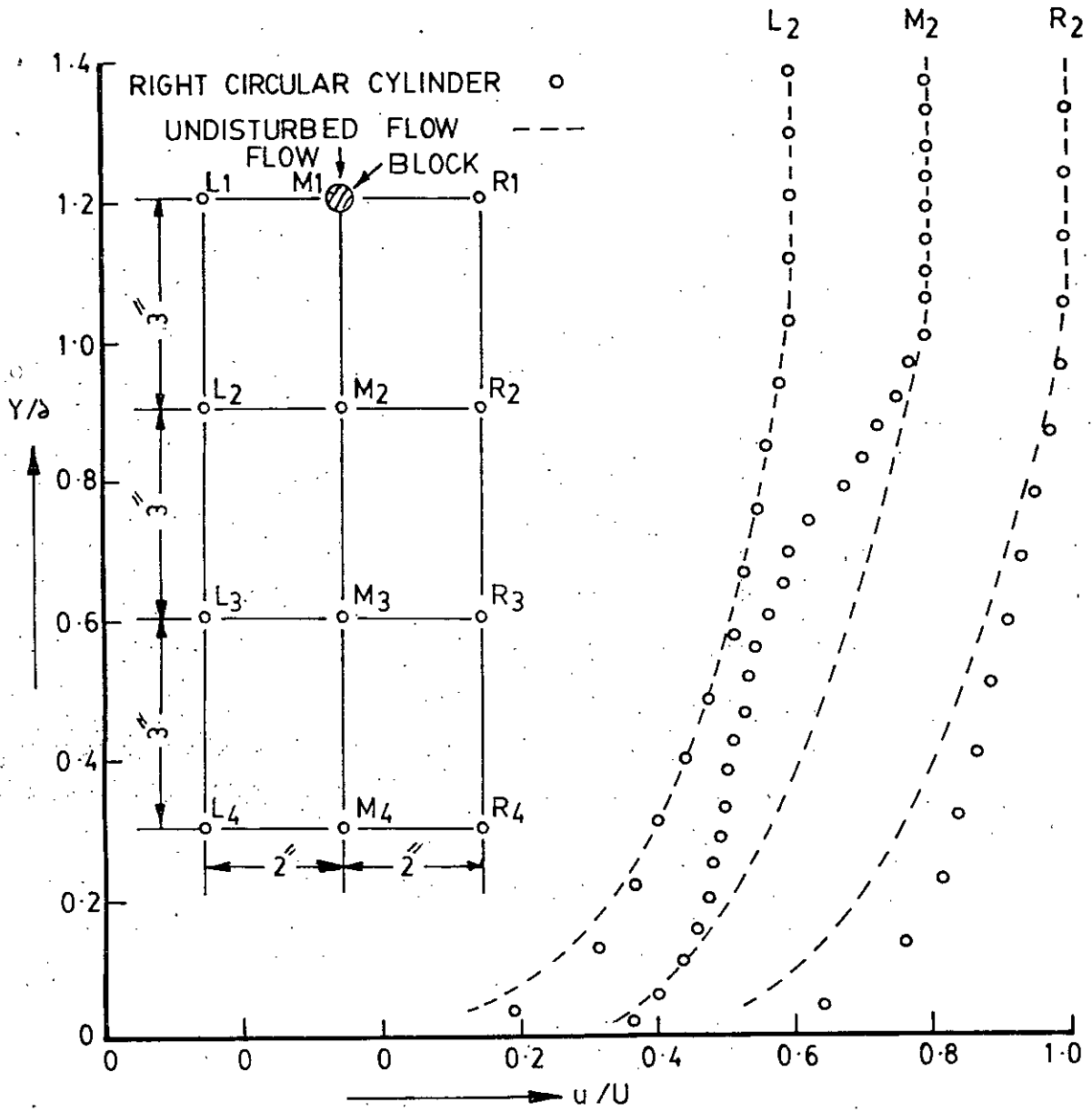


FIG. 6-10 MEAN VELOCITY PROFILES (DISTURBED FLOW)

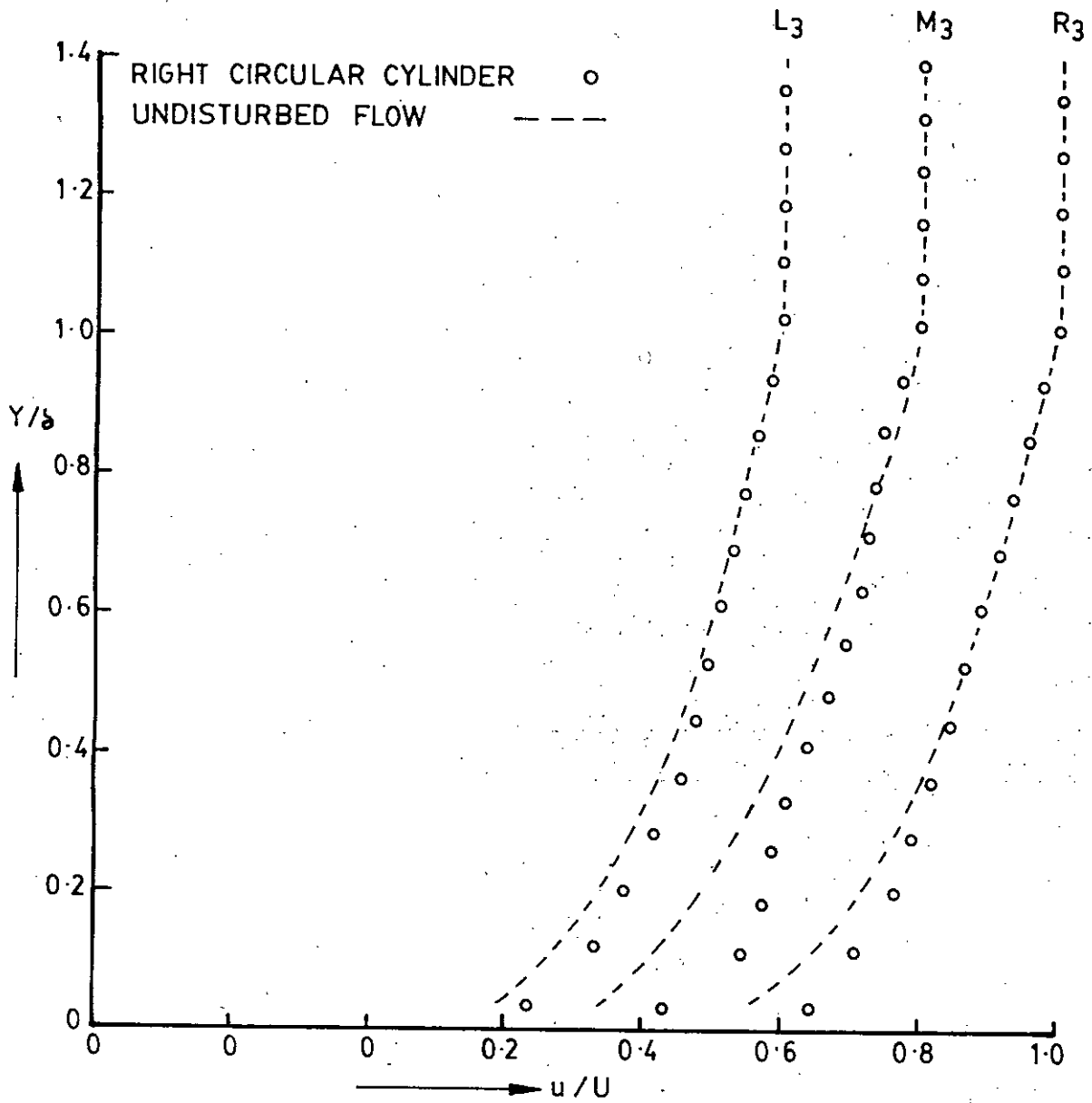


FIG.6.11 MEAN VELOCITY PROFILES (DISTURBED FLOW)

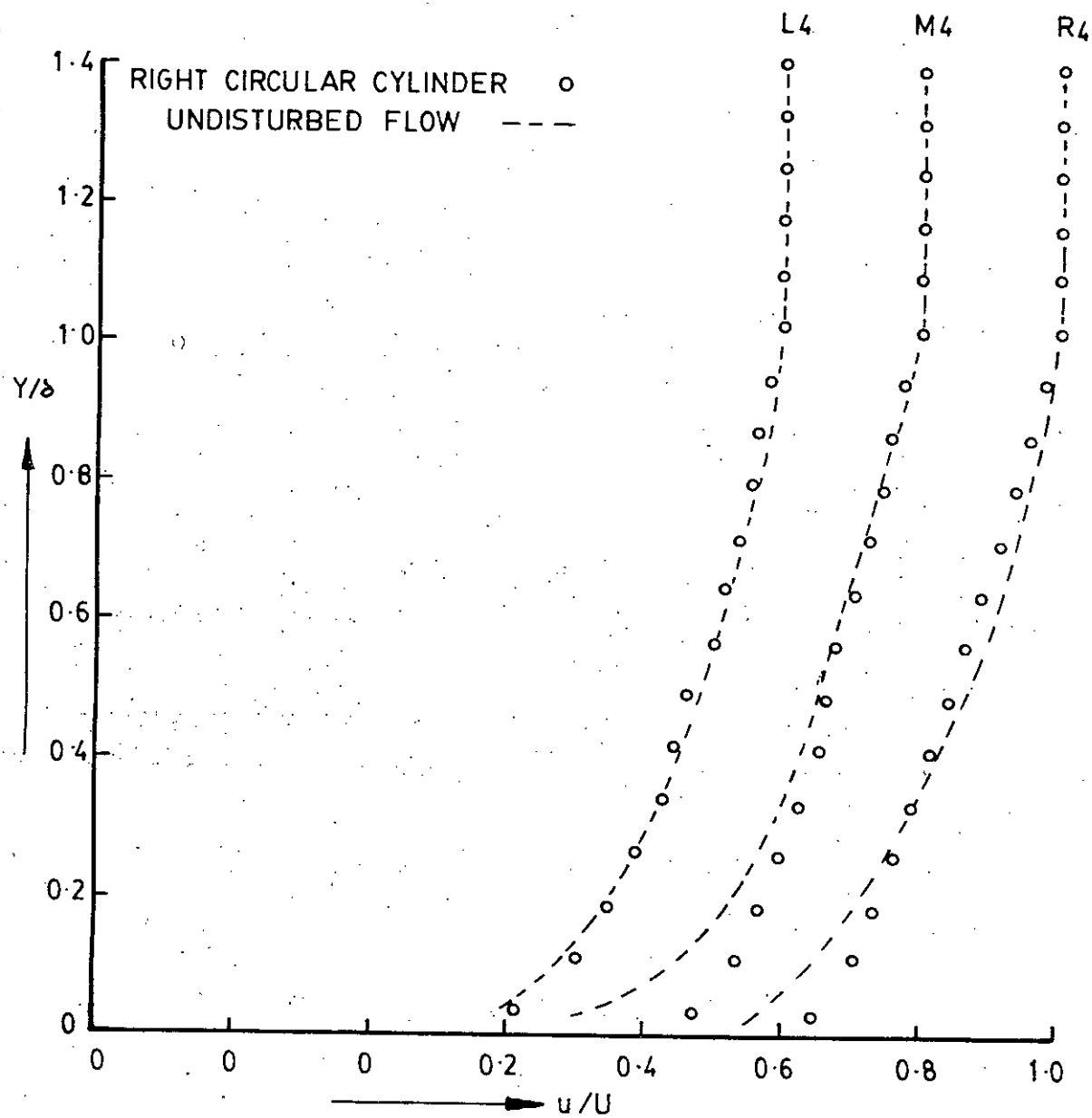


FIG-6-12 MEAN VELOCITY PROFILES (DISTURBED FLOW)

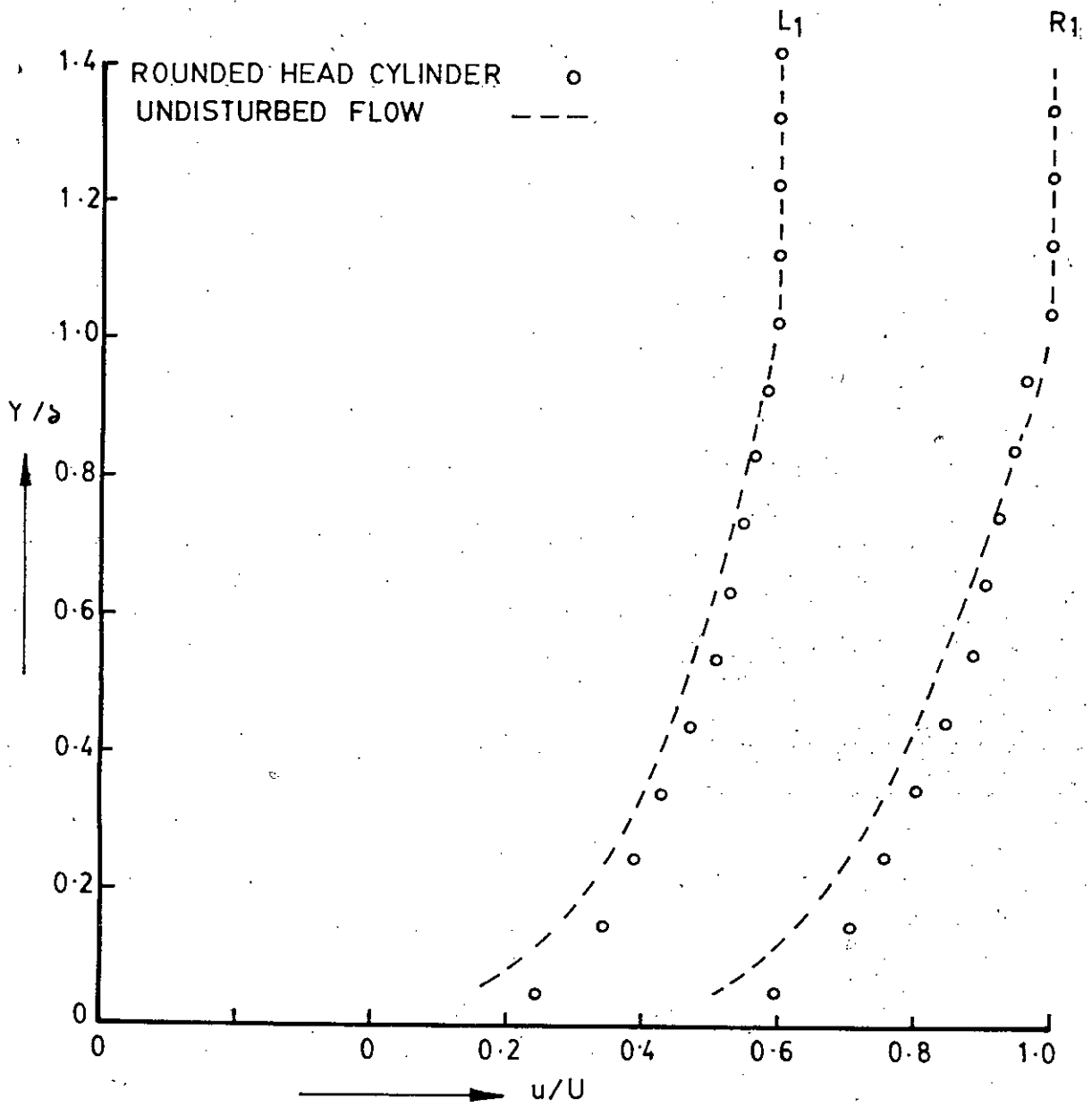


FIG. 6.13 MEAN VELOCITY PROFILES (DISTURBED FLOW)

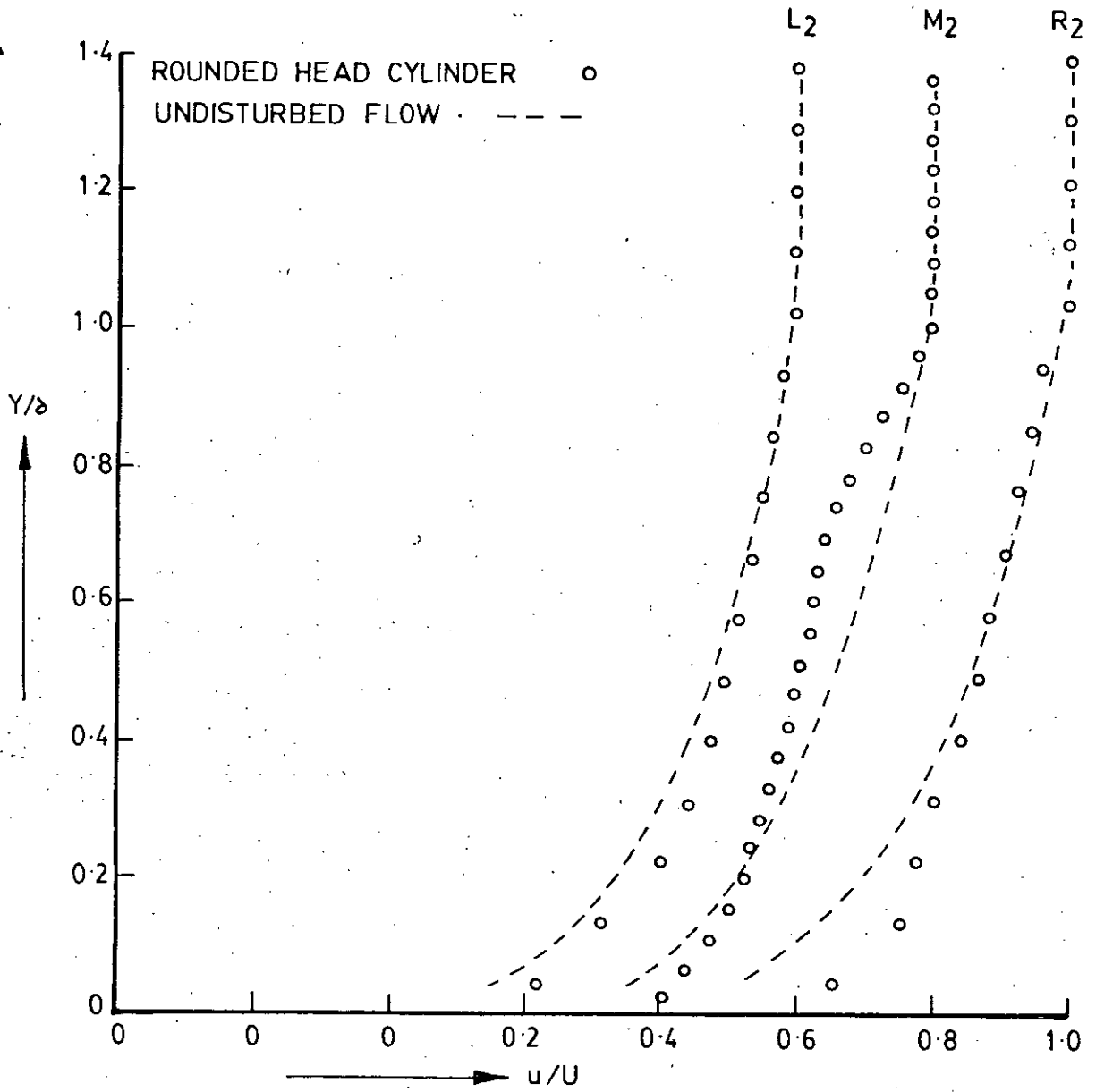


FIG. 6.14 MEAN VELOCITY PROFILES (DISTURBED FLOW)



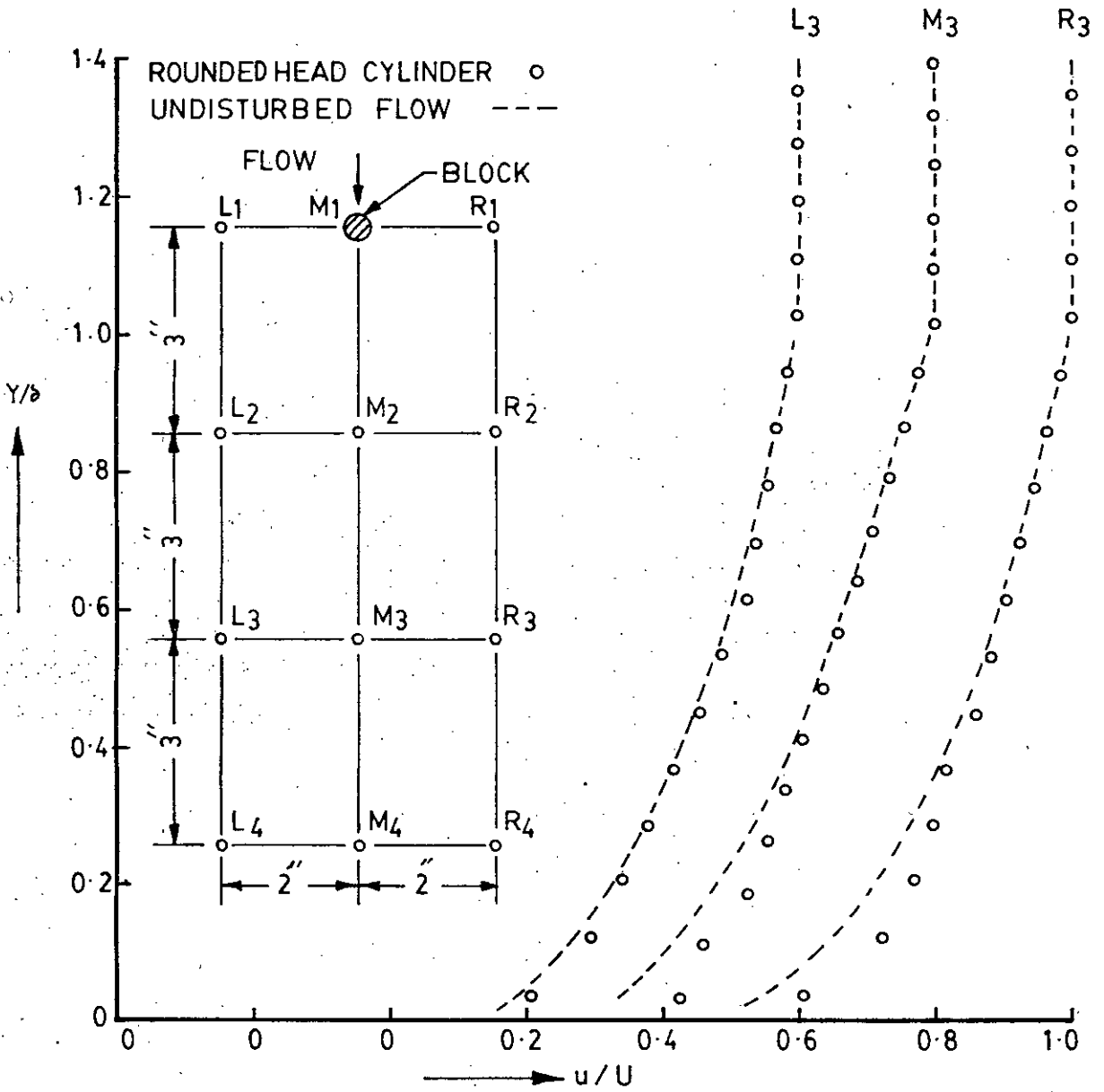


FIG-6-15 MEAN VELOCITY PROFILES (DISTURBED FLOW)

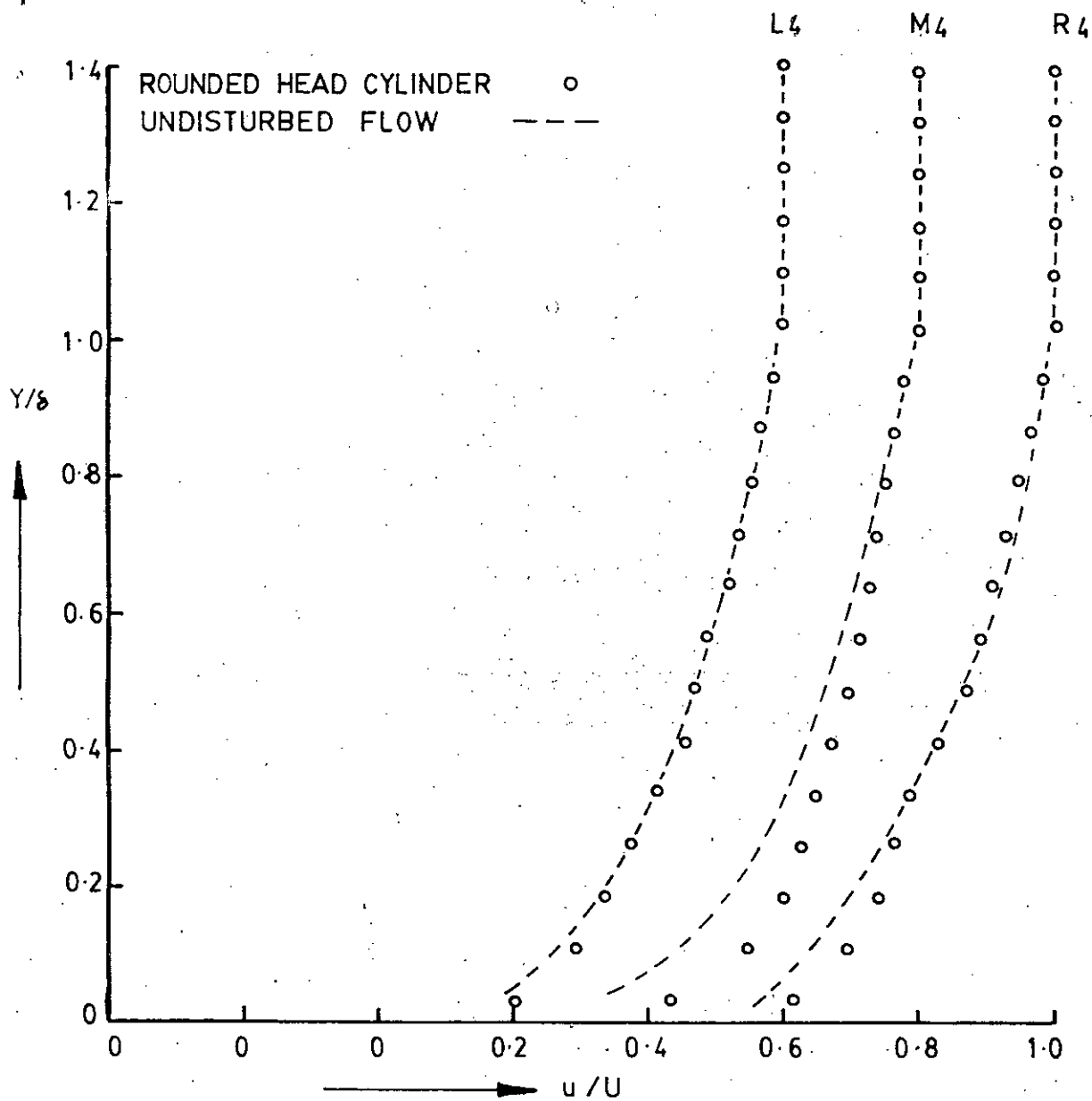


FIG. 6-16 MEAN VELOCITY PROFILES (DISTURBED FLOW)

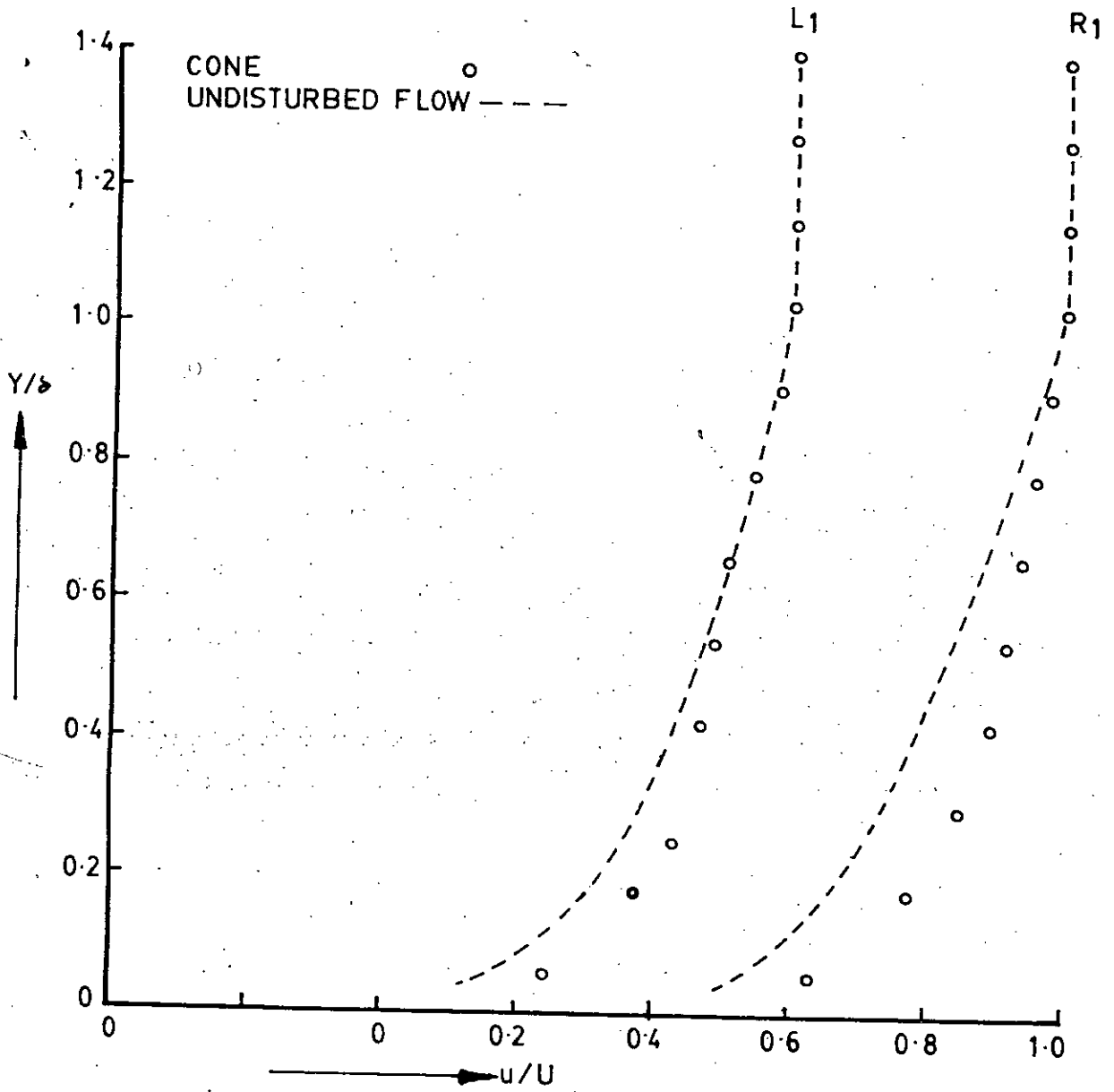


FIG. 6.17 MEAN VELOCITY PROFILES (DISTURBED FLOW).

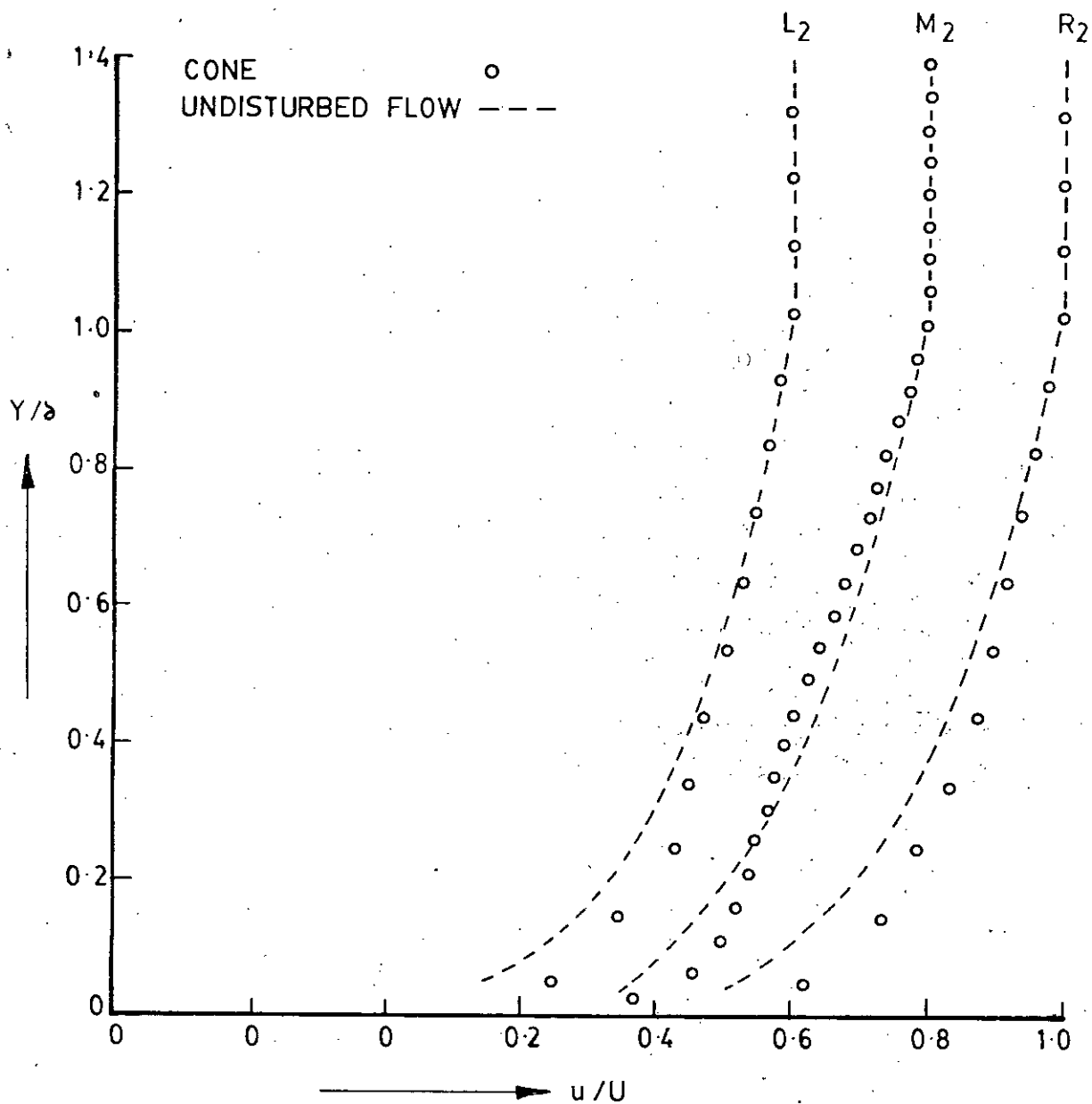


FIG. 6-18 MEAN VELOCITY PROFILES (DISTURBED FLOW)

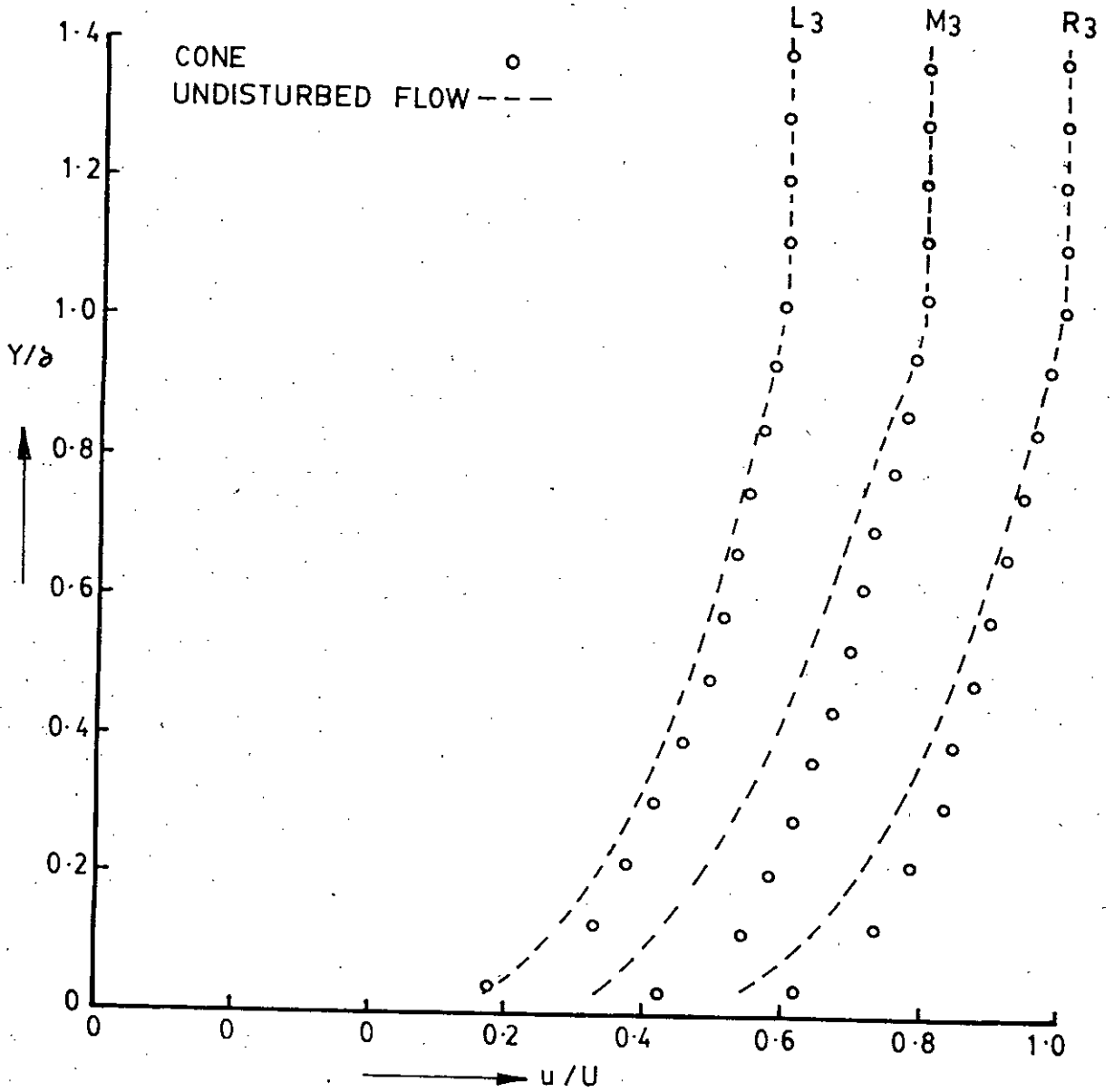


FIG. 6.19 MEAN VELOCITY PROFILES (DISTURBED FLOW)

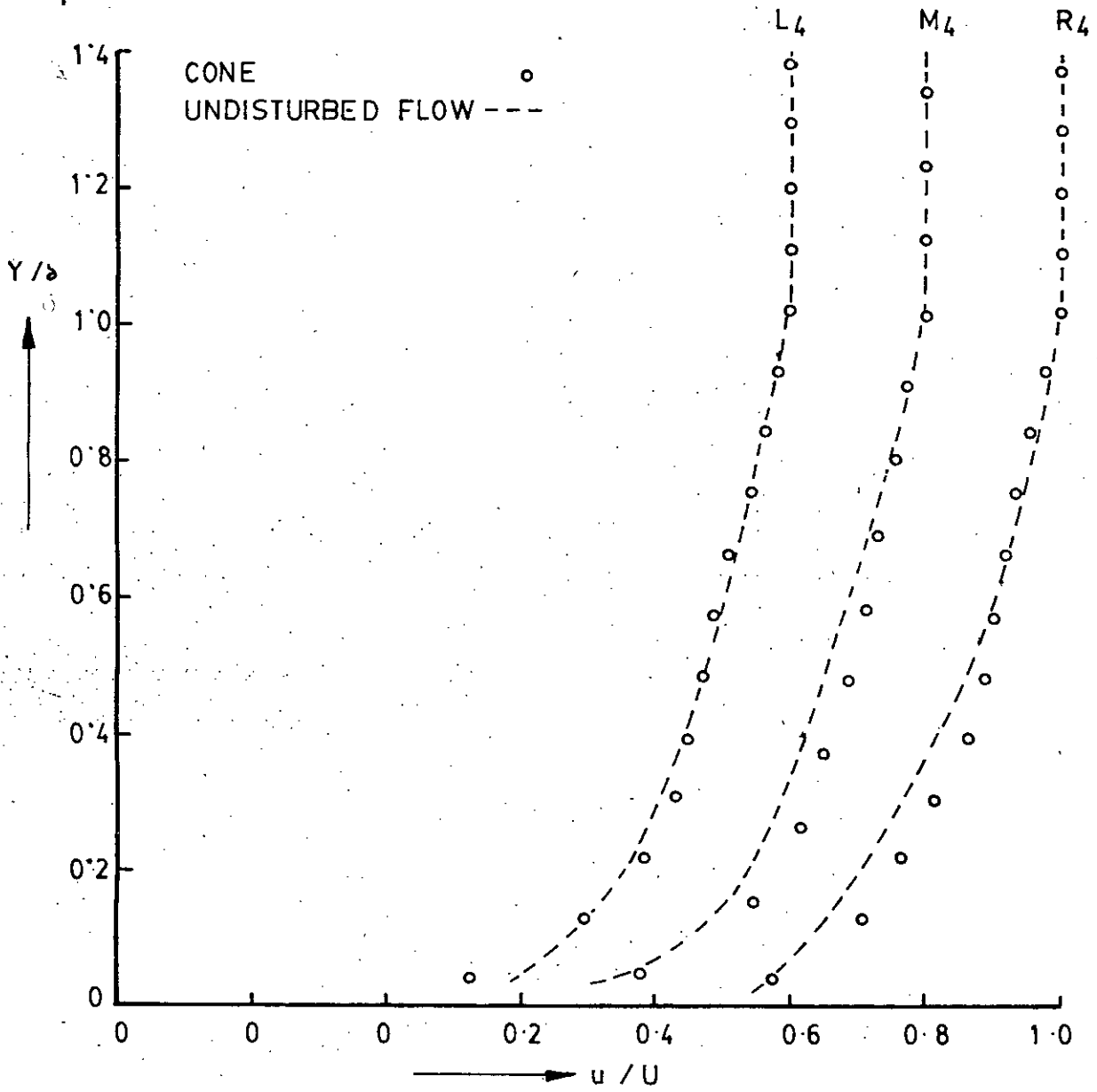


FIG. 6.20 MEAN VELOCITY PROFILES (DISTURBED FLOW)

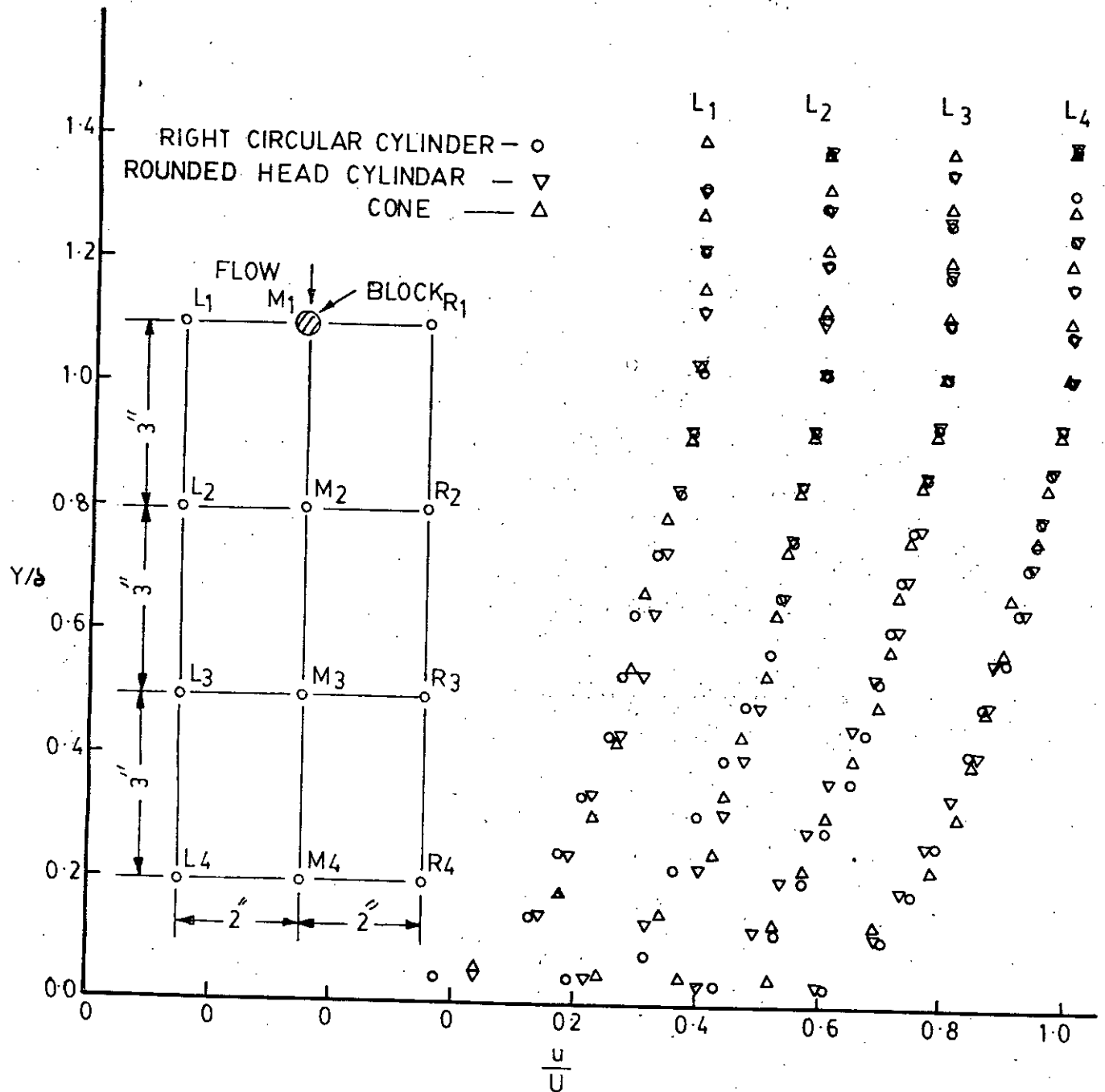


FIG. 6-21 MEAN VELOCITY PROFILES (DISTURBED FLOW)

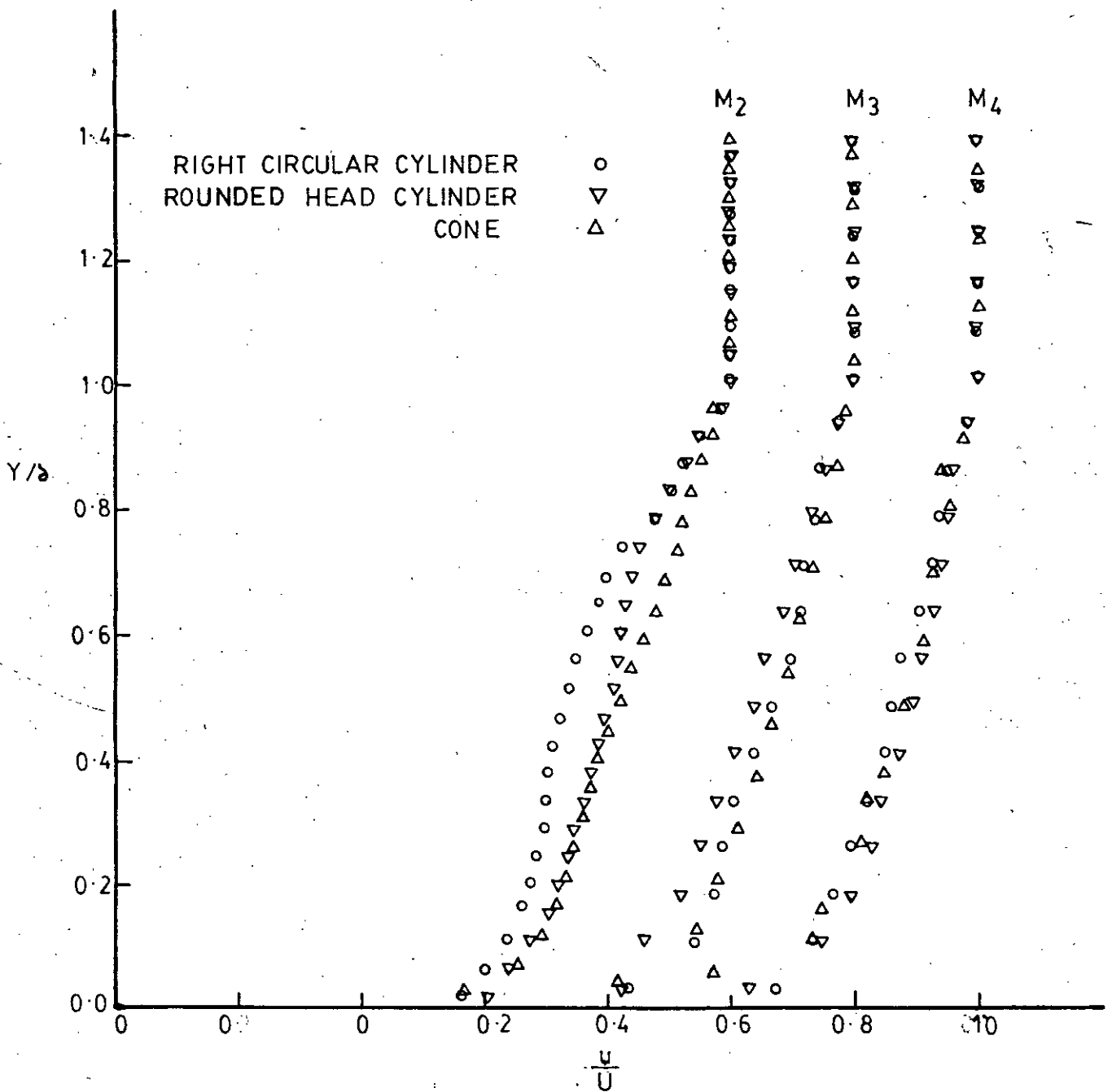


FIG. 6.22 MEAN VELOCITY PROFILES (DISTURBED FLOW)



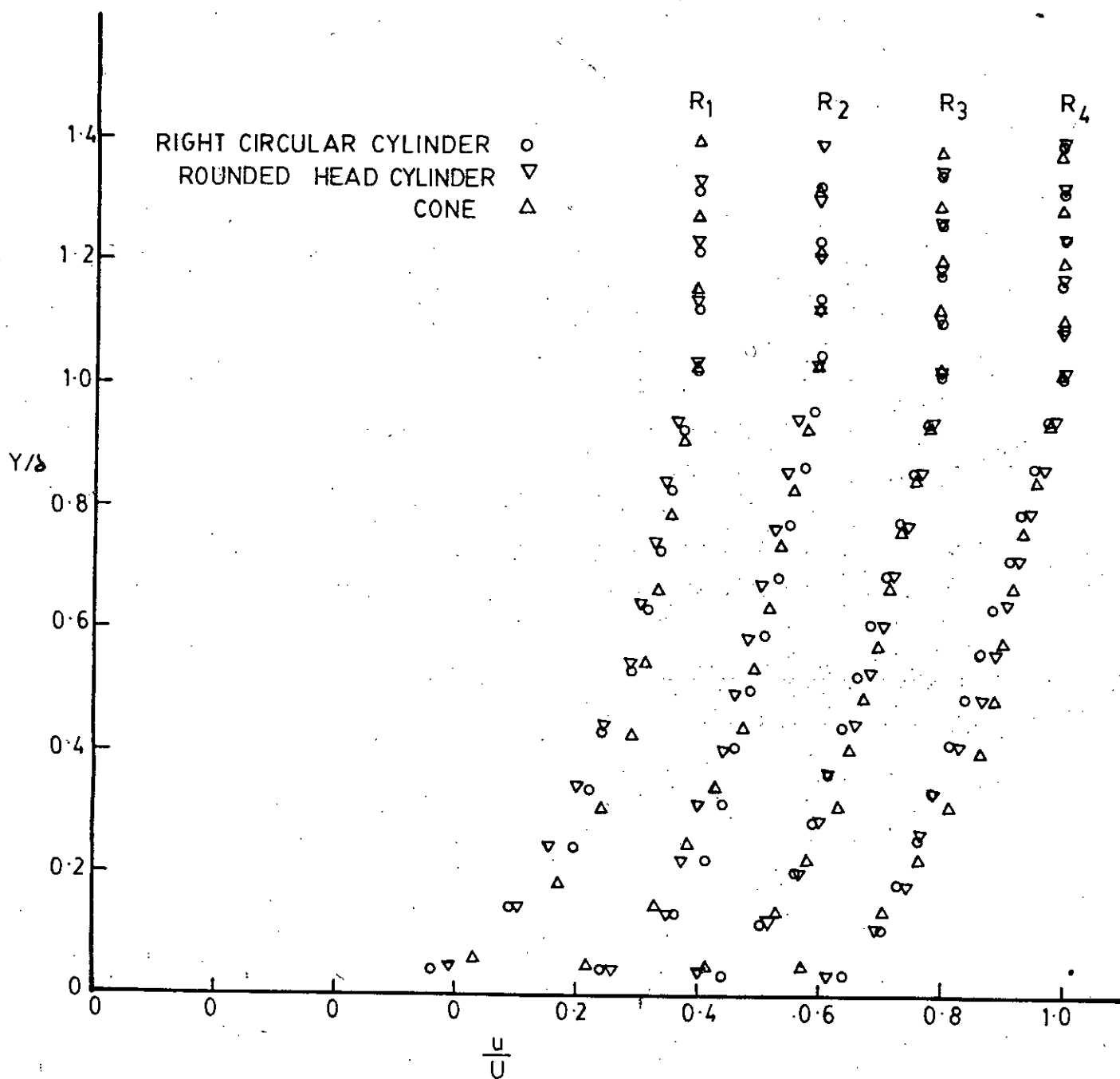
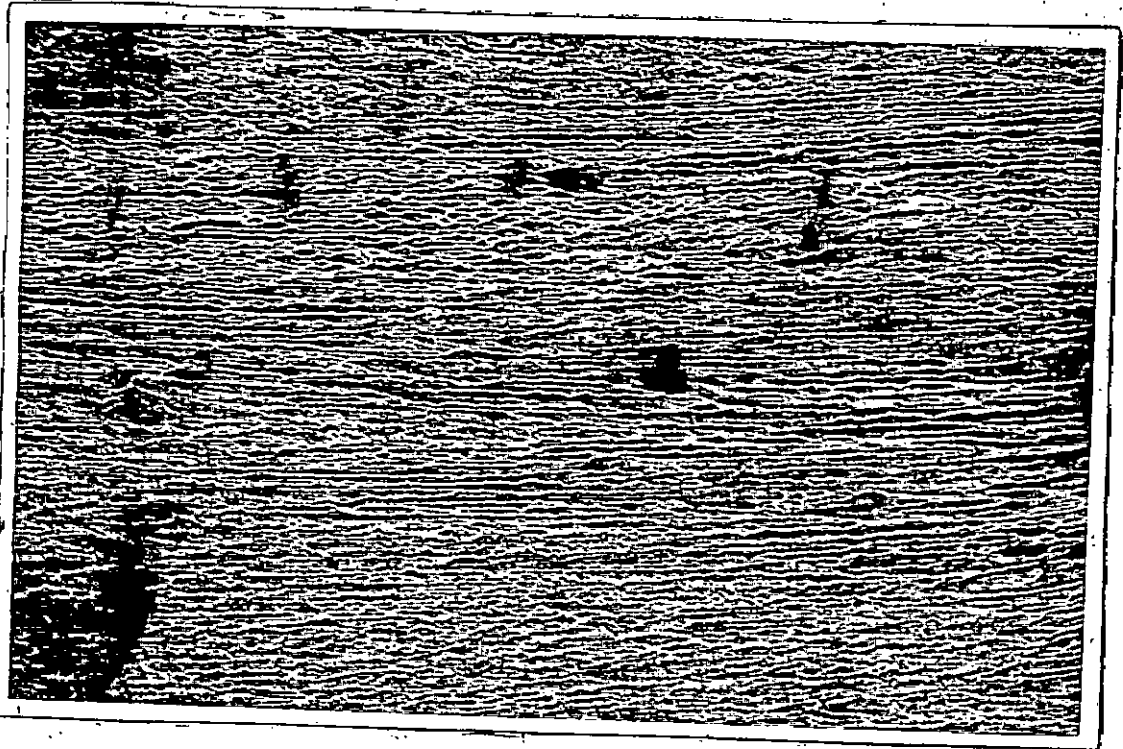
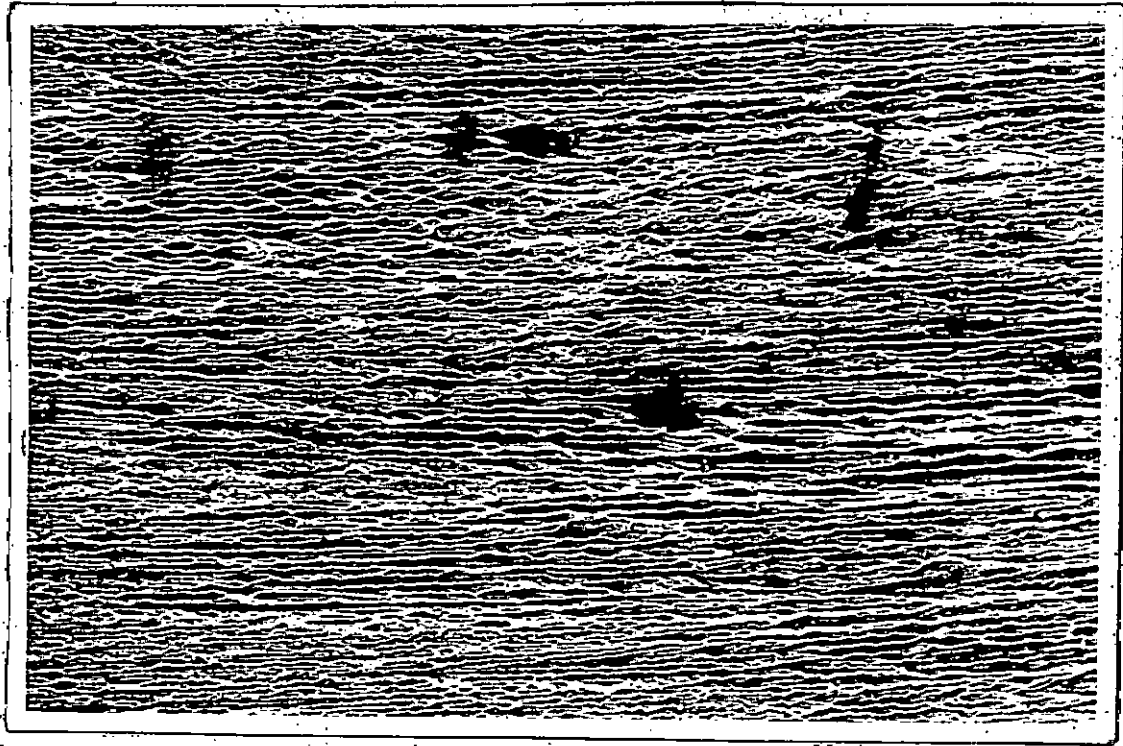


FIG. 6-23 MEANS VELOCITY PROFILES (DISTURBED FLOW)

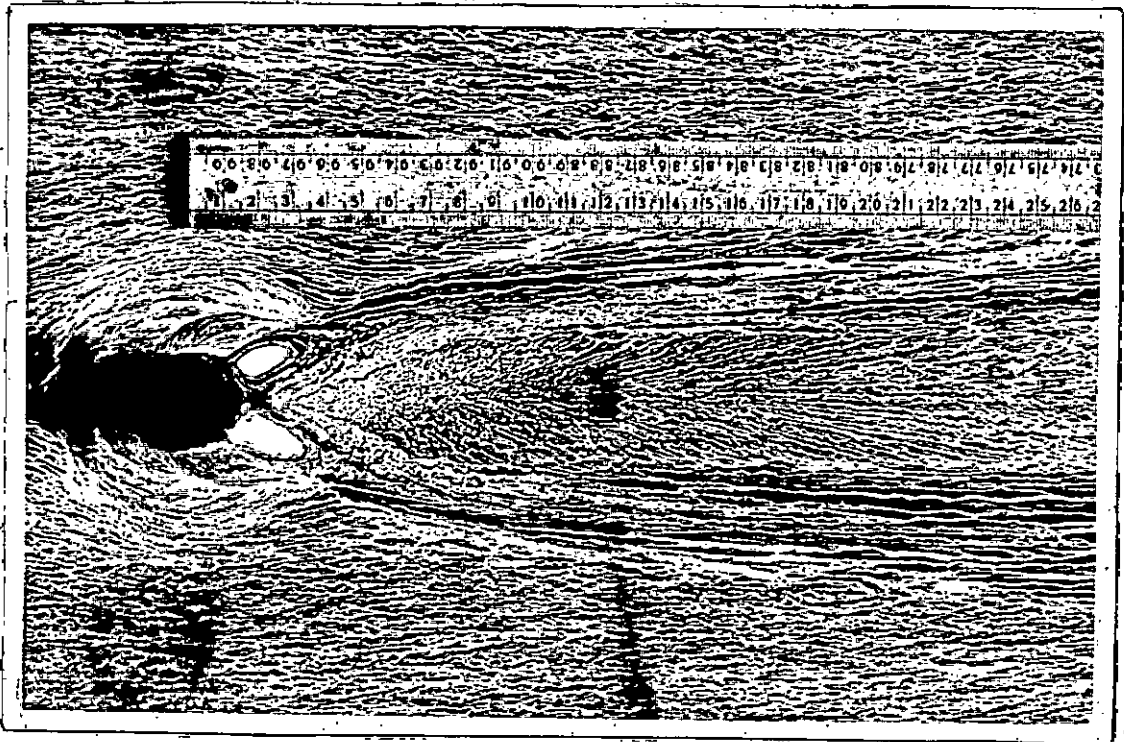
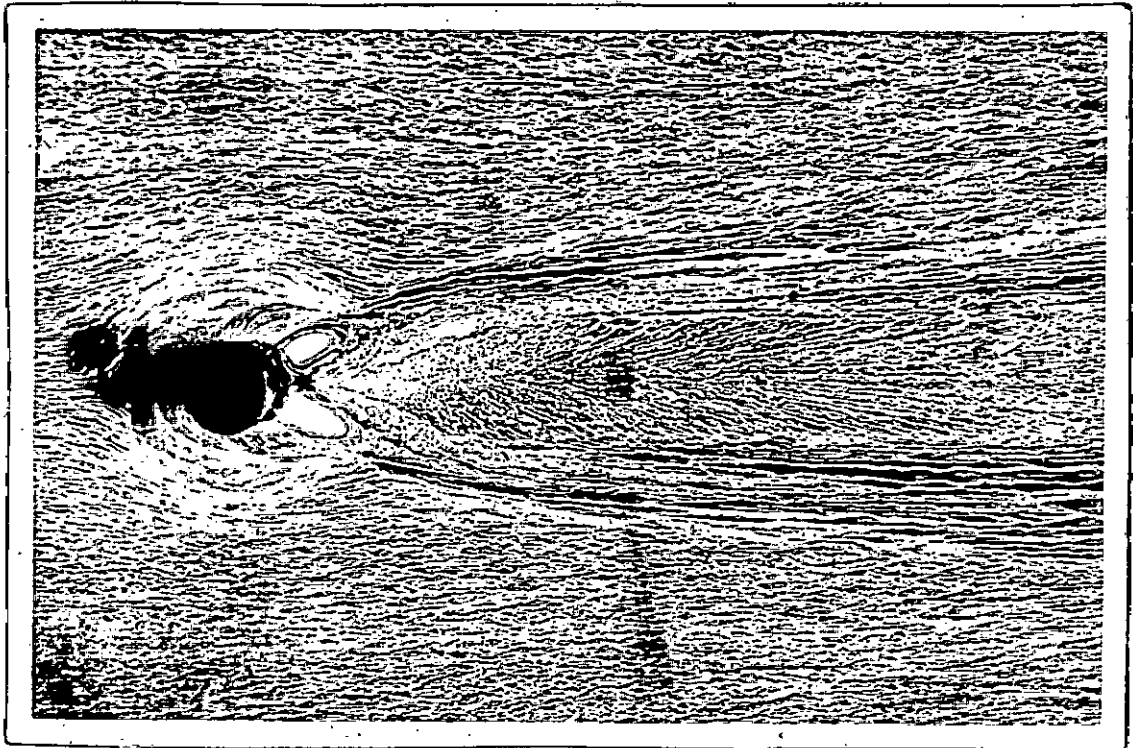
FLOW VISUALISATION



DIRECTION OF FLOW →

Re. No.  $9.8 \times 10^4$

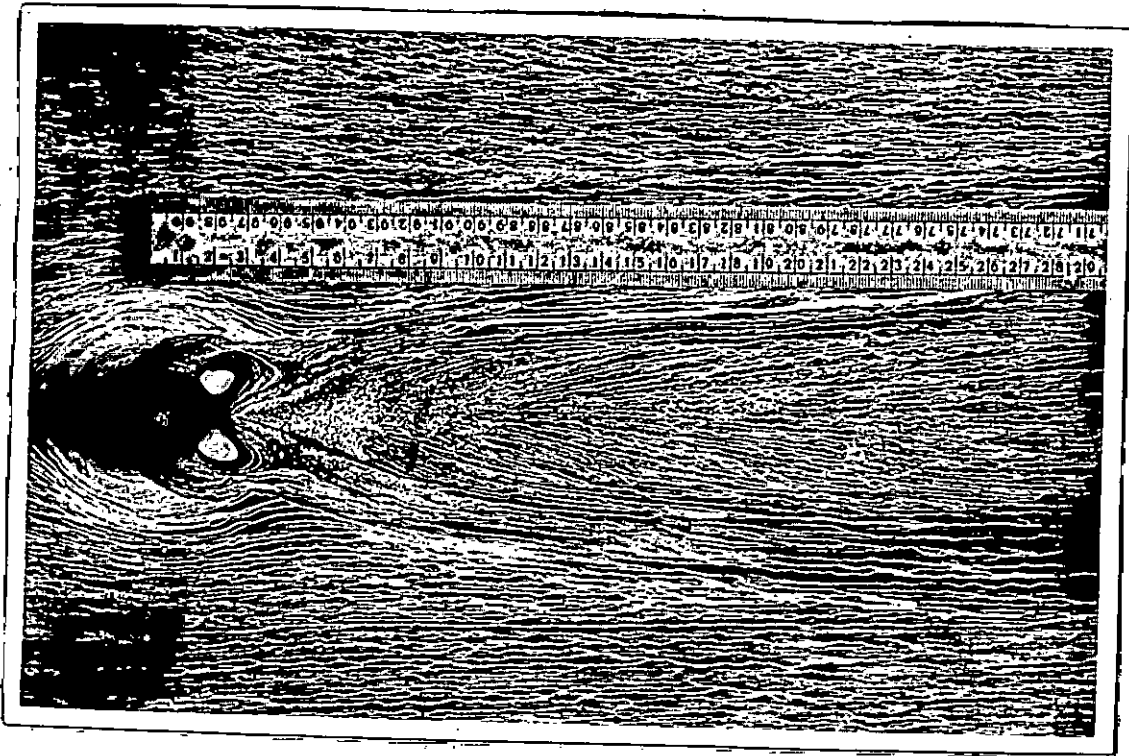
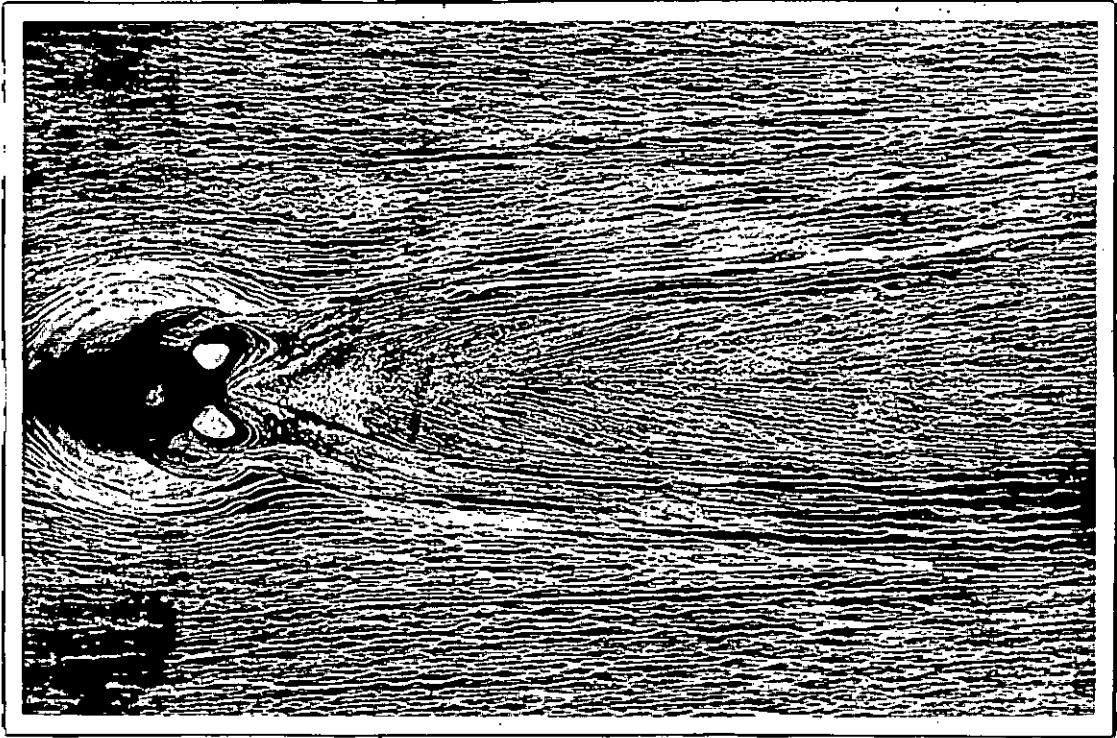
Fig. 6.24 Flow Pattern of Undisturbed Flow.



DIRECTION OF FLOW →

Re. No. =  $9.8 \times 10^4$

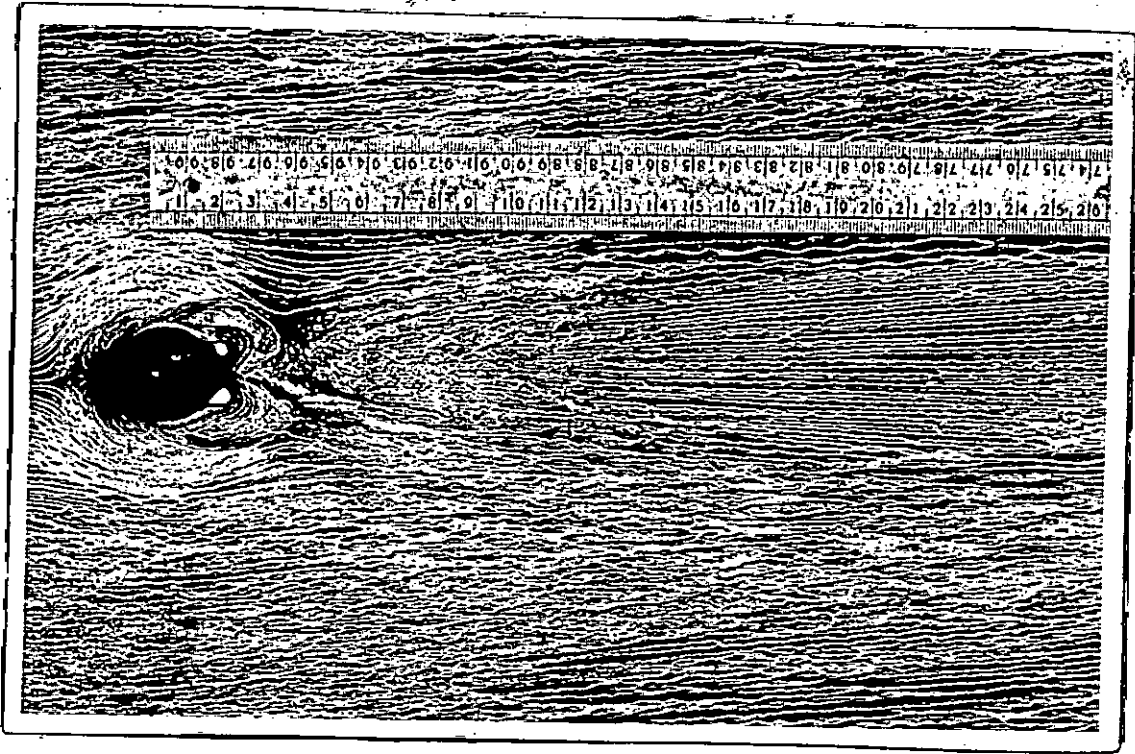
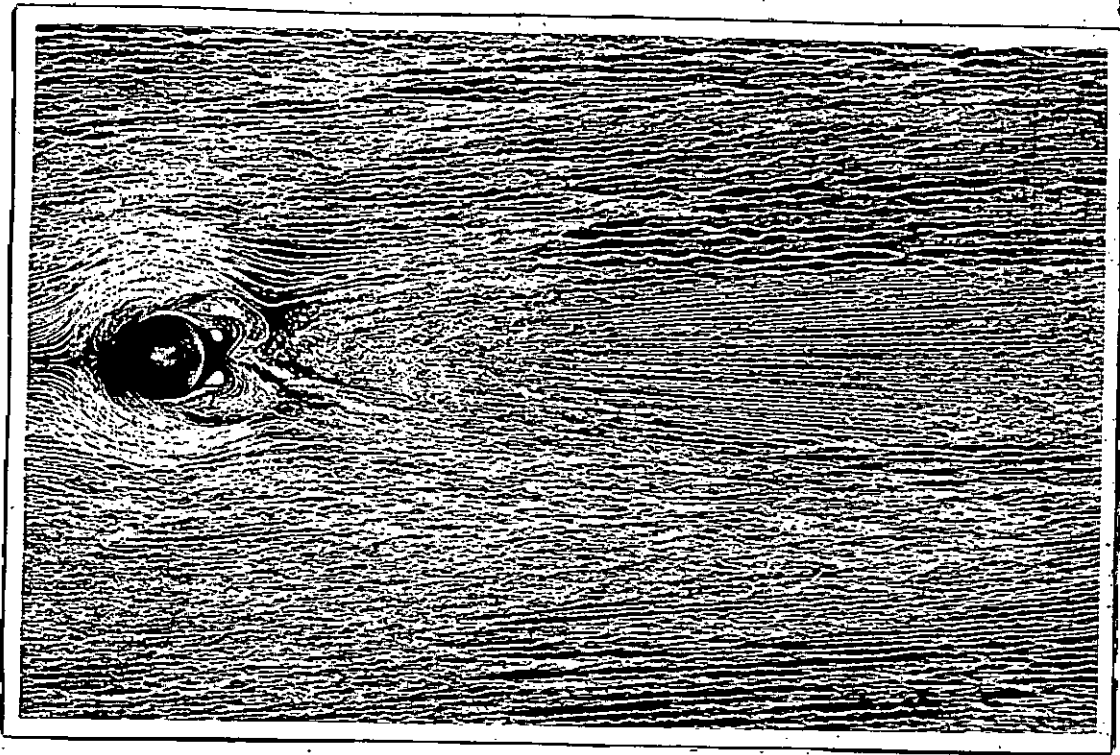
Fig. 6.25 Flow Pattern for the Right Circular Cylinder.



DIRECTION OF FLOW →

Re.No. =  $9.8 \times 10^4$

Fig. 6.26 Flow Pattern for the Rounded Head Cylinder.



DIRECTION OF FLOW →  
Re.No. =  $9.8 \times 10^4$

Fig. 6.27 Flow Pattern for the Cone.

PLOTS OF  $Y/\delta$  VS. FLOW ANGLE

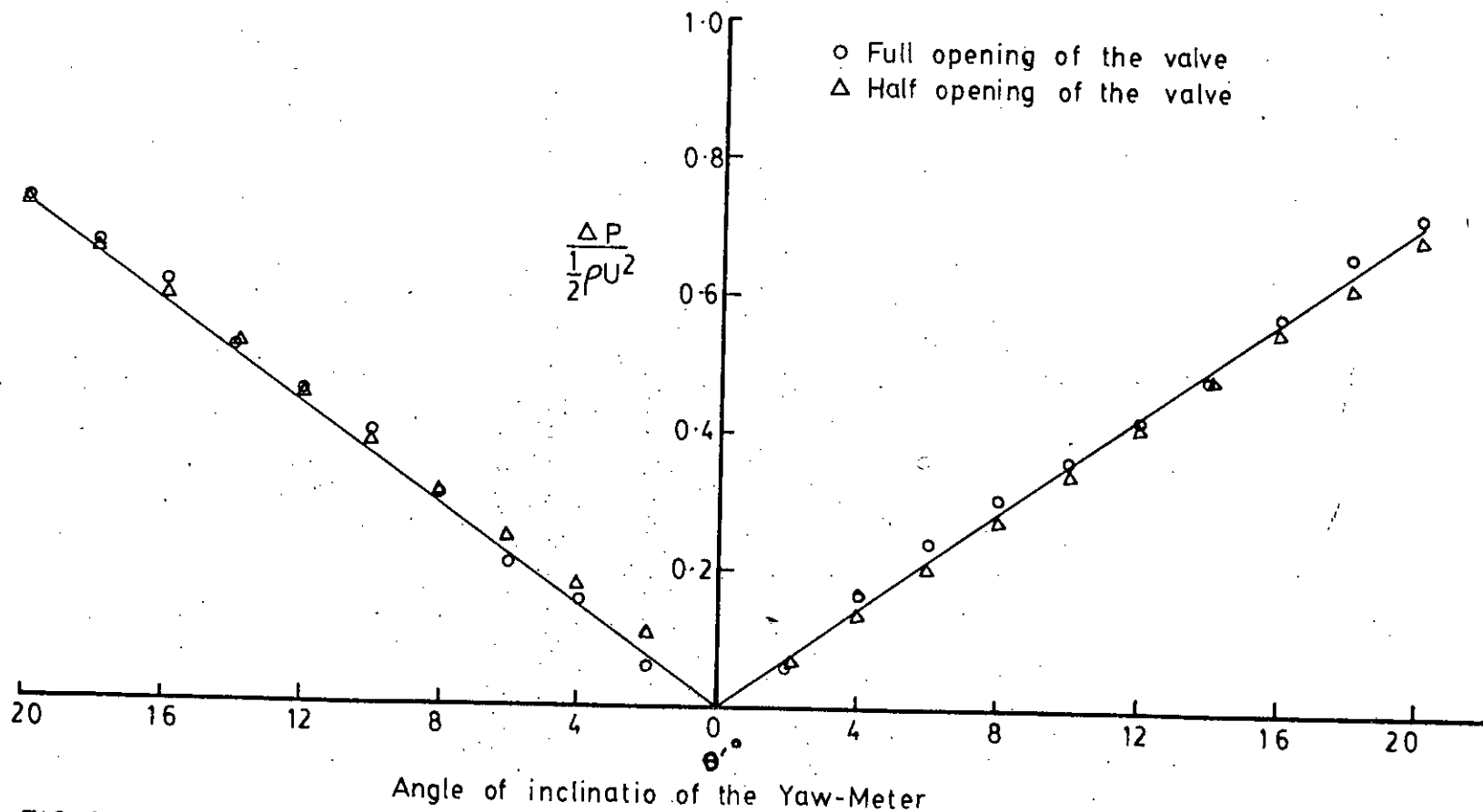


FIG. 6.28 CALIBRATION OF THE YAW-METER



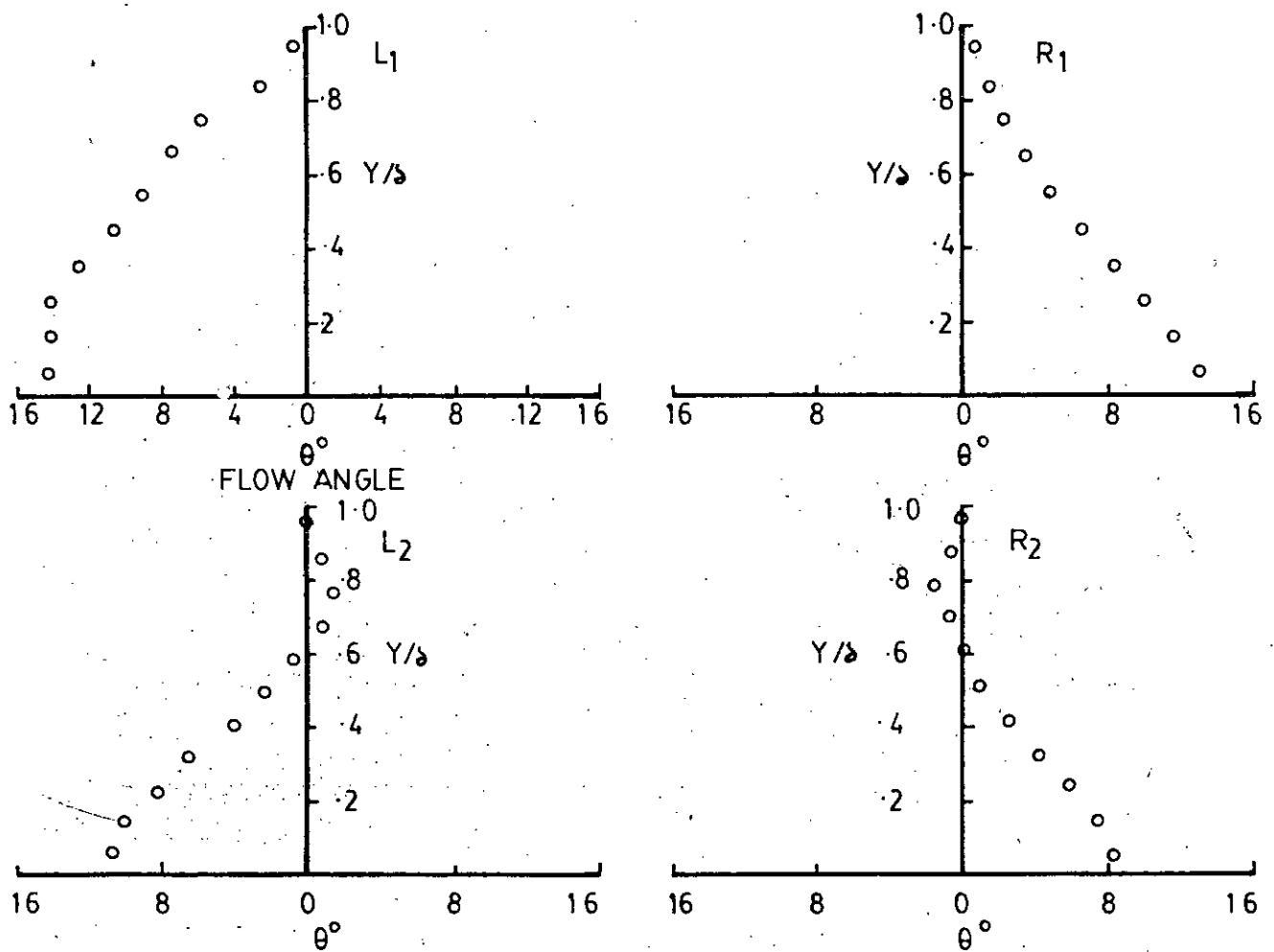


FIG. 6-29  $Y/\delta$  VERSUS FLOW ANGLE FOR THE RIGHT CIRCULAR CYLINDER

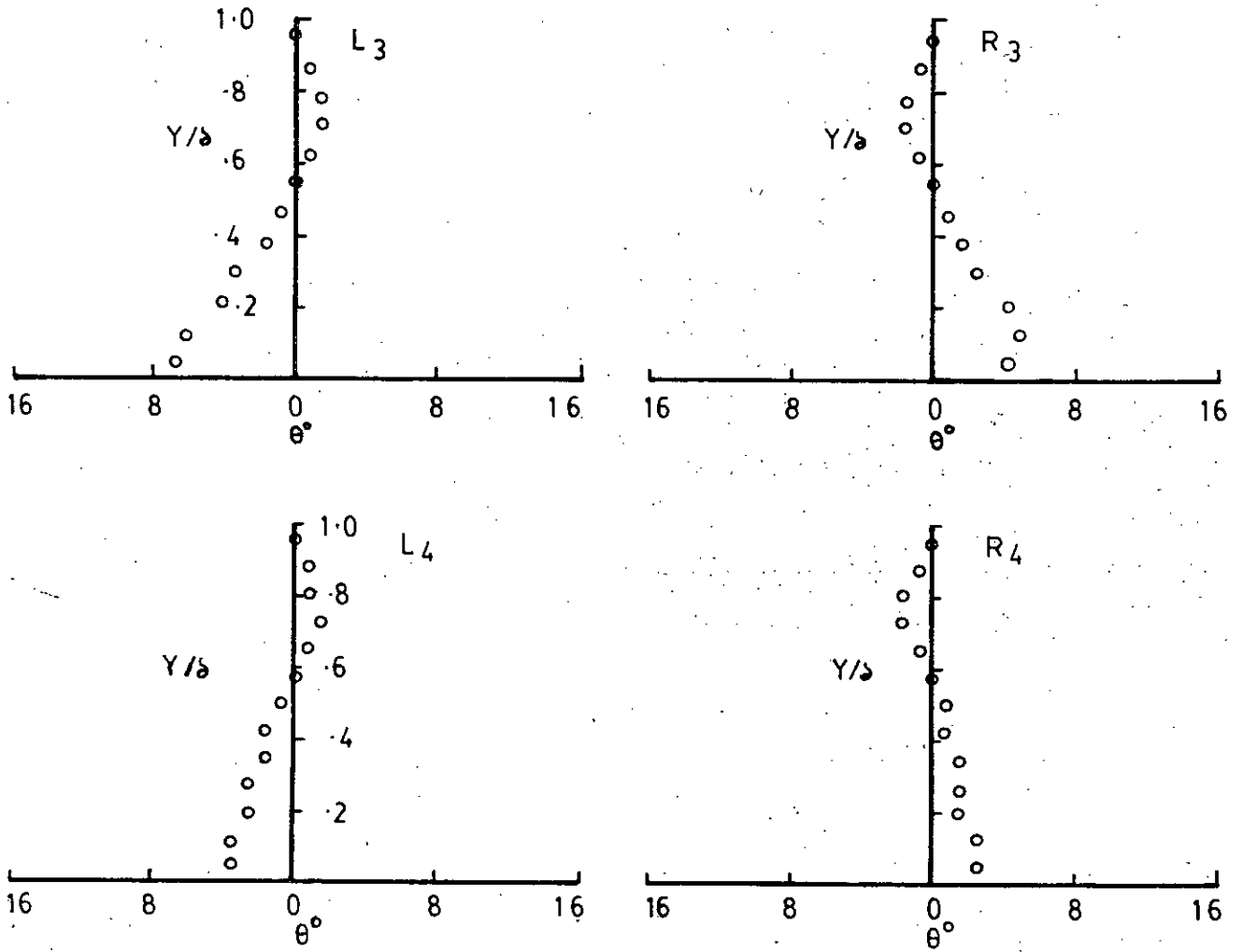


FIG. 6-30.  $Y/\delta$  VERSUS FLOW ANGLE FOR THE RIGHT CIRCULAR CYLINDER

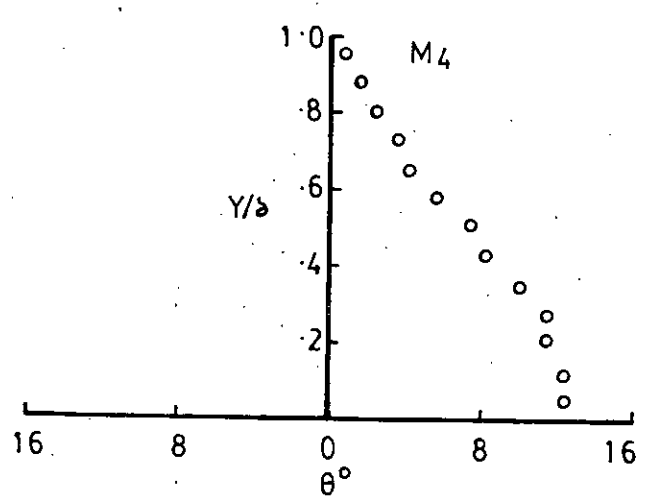
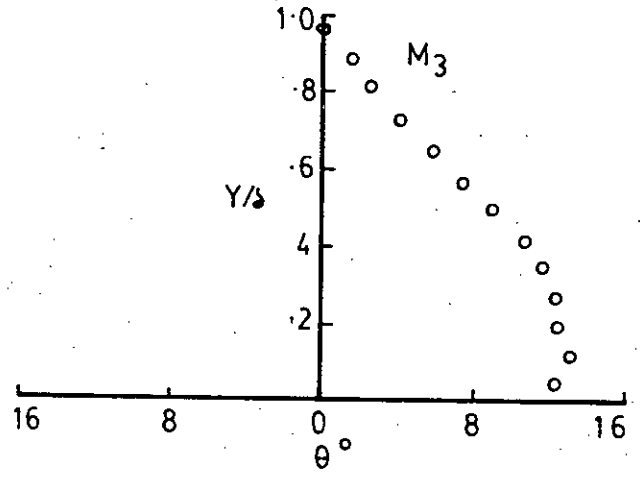
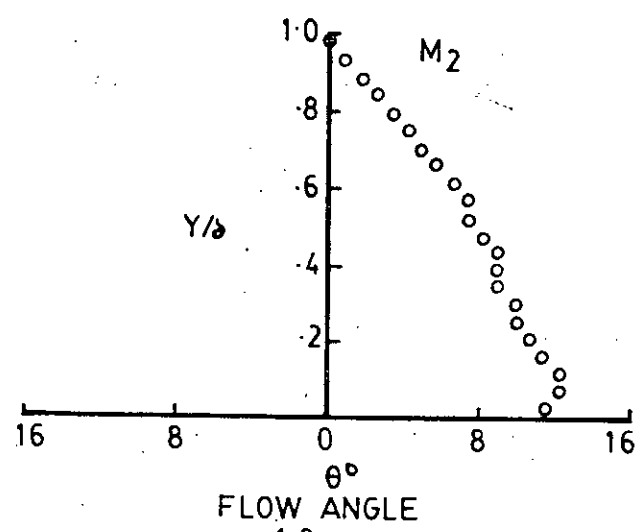
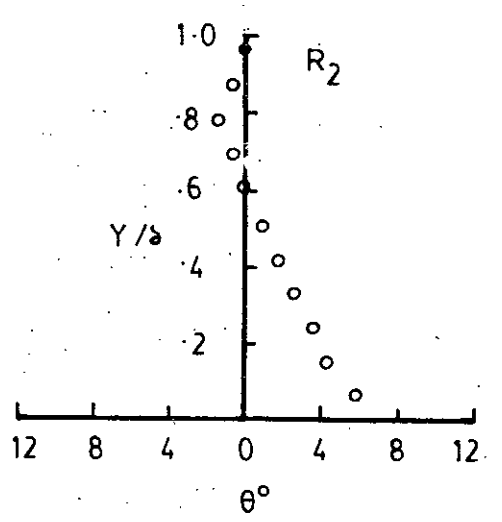
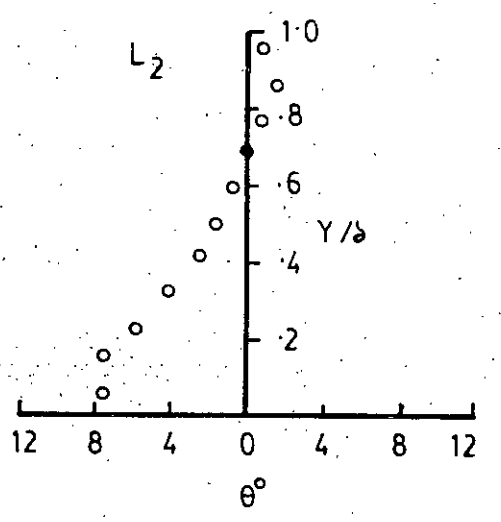
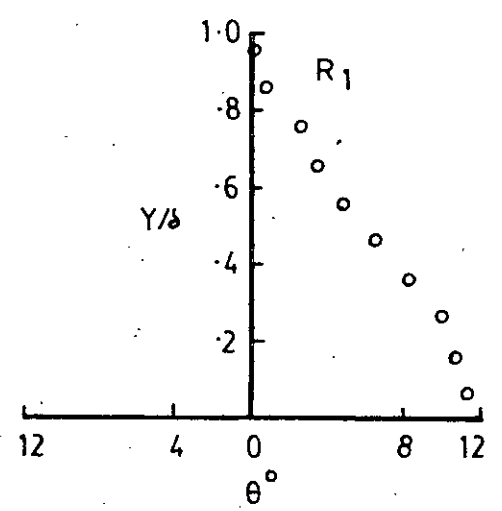
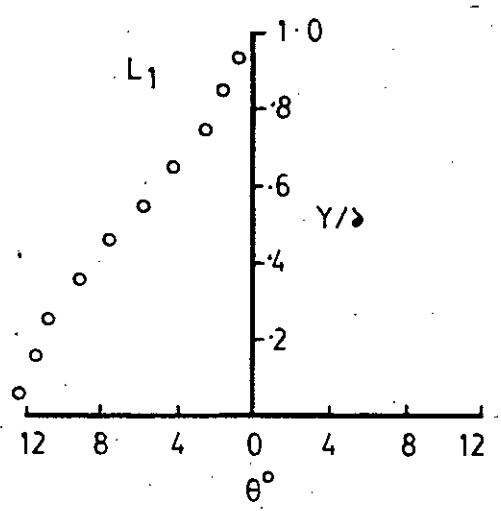
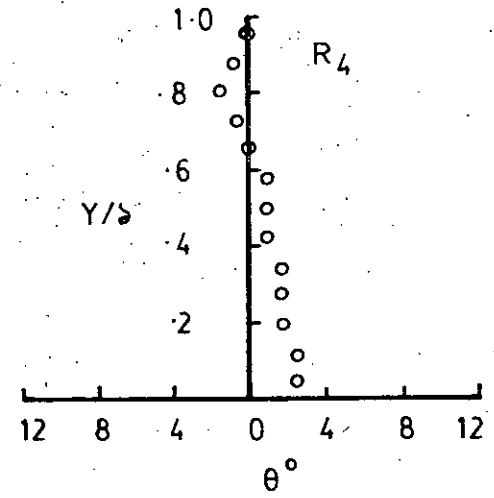
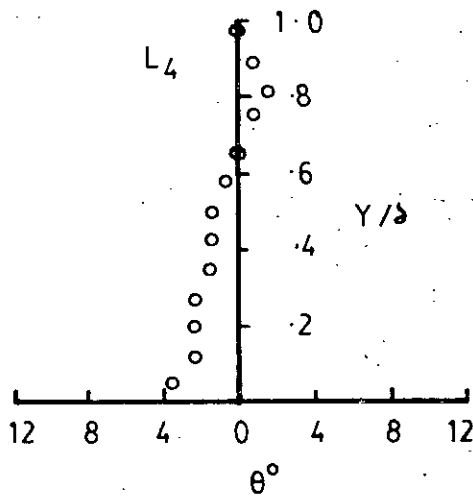
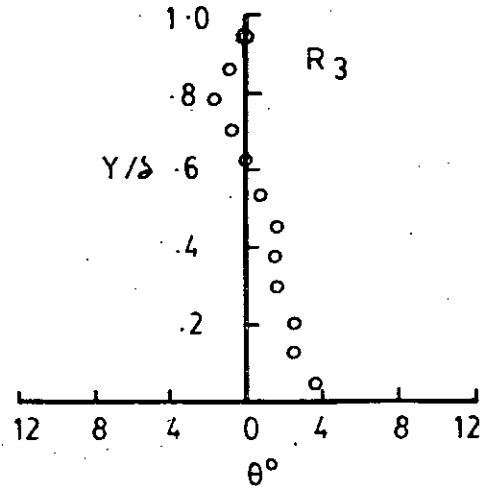
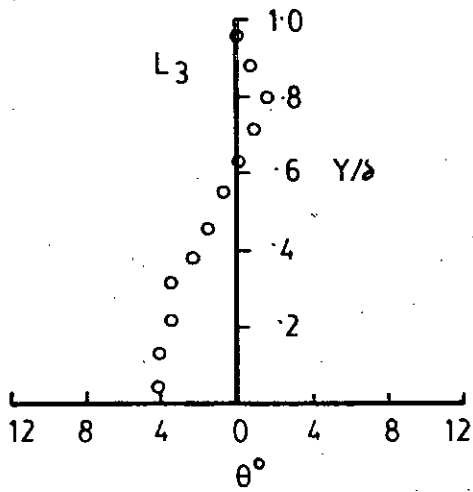


FIG. 6-31  $Y/\delta$  VERSUS FLOW ANGLE FOR THE RIGHT CIRCULAR CYLINDER



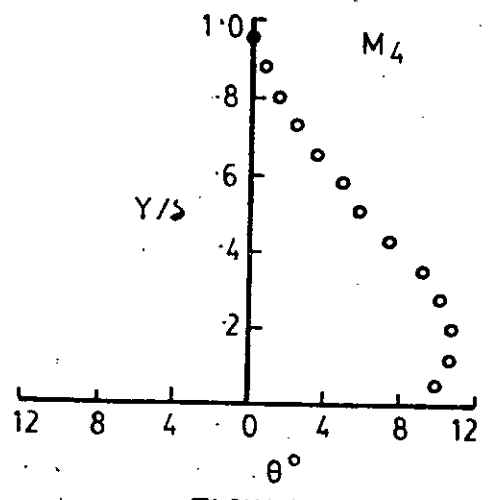
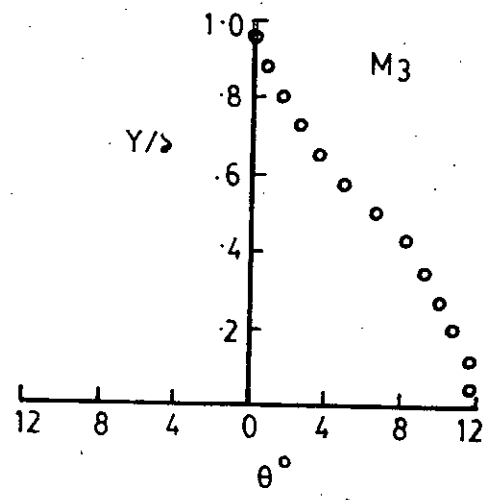
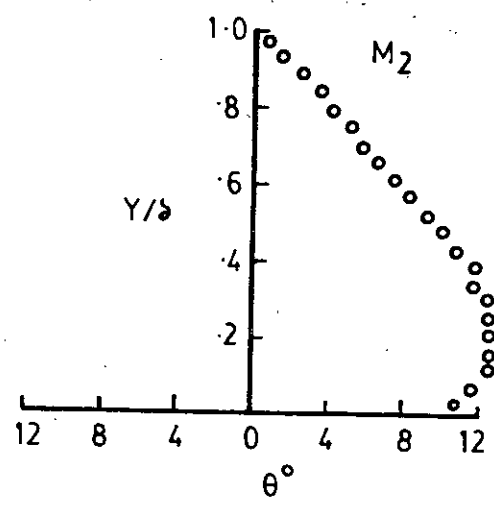
FLOW ANGLE

FIG-6-32 PLOTS OF  $Y/d$  VERSUS FLOW ANGLE FOR THE ROUNDED HEAD CYLINDER



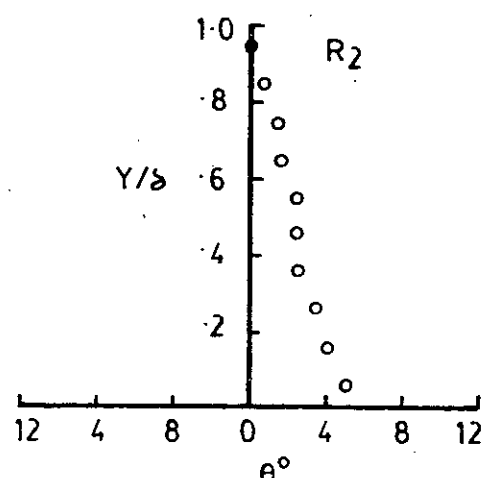
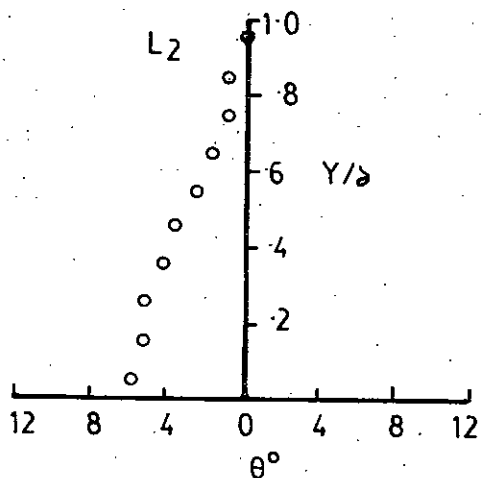
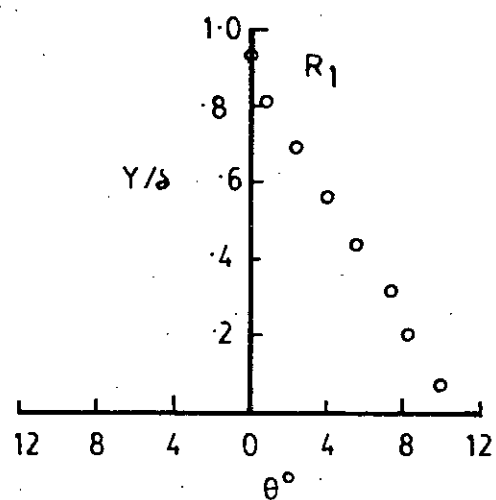
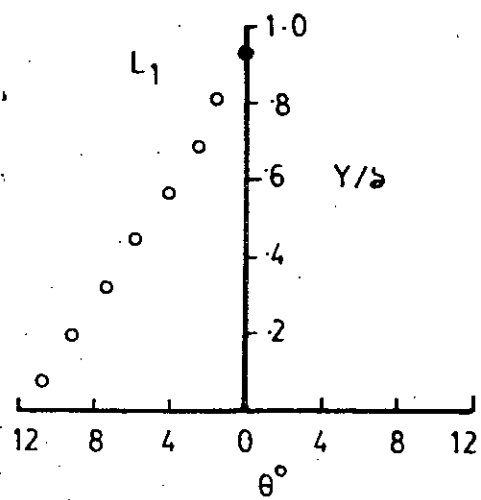
FLOW ANGLE

FIG. 6-33 PLOTS OF  $Y/\delta$  VERSUS FLOW ANGLE FOR THE ROUNDED HEAD CYLINDER



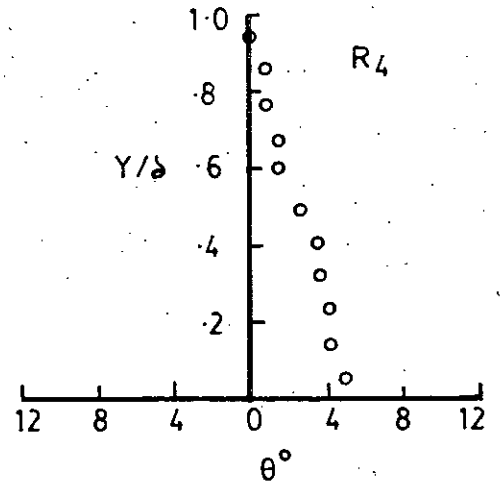
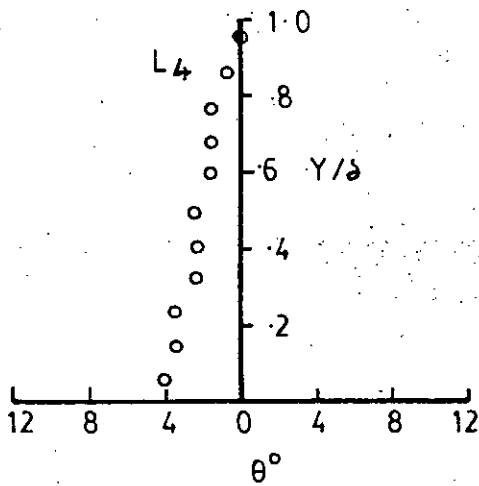
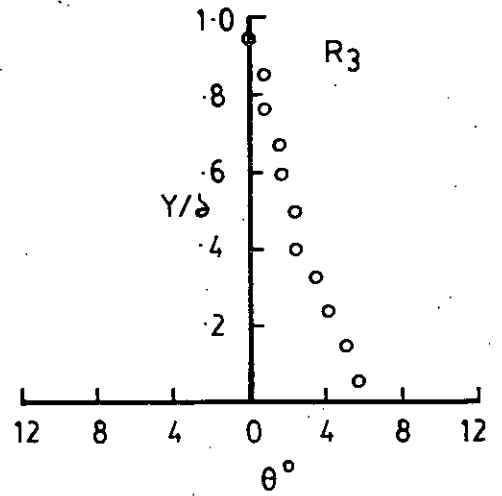
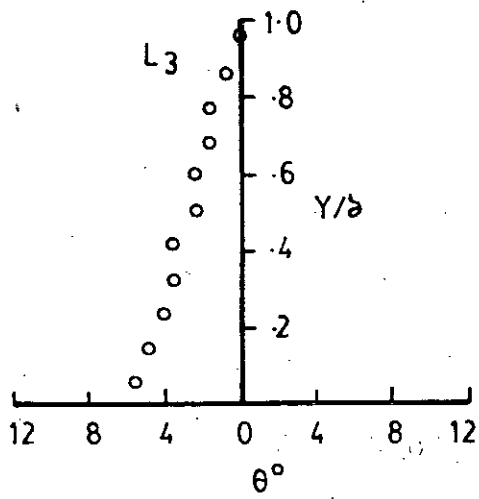
FLOW ANGLE

FIG.6-34  $Y/\delta$  VERSUS FLOW ANGLE FOR THE ROUNDED HEAD CYLINDER



FLOW ANGLE

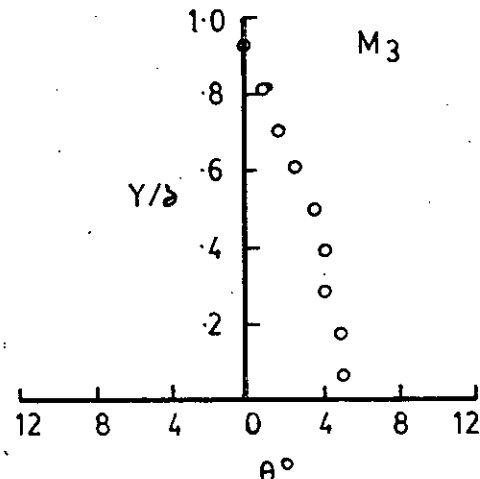
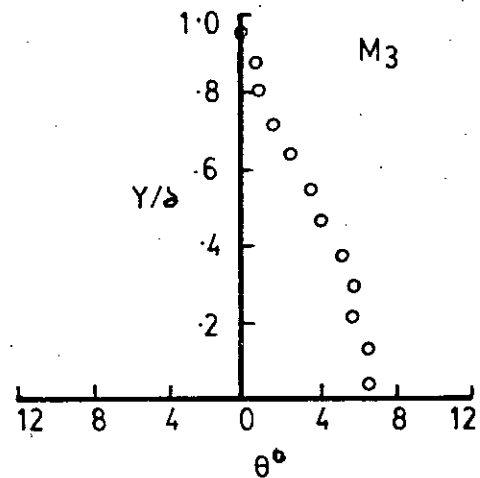
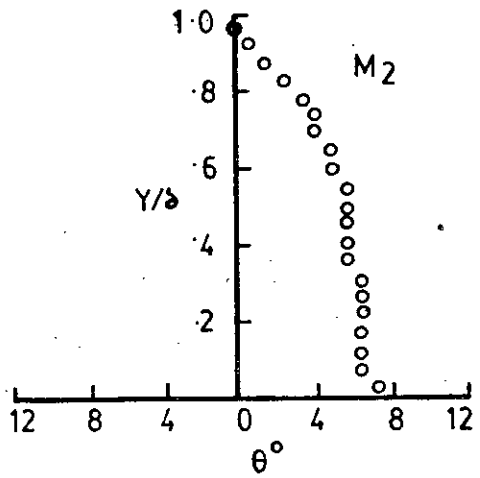
FIG. 6.35 PLOTS OF  $Y/\delta$  VERSUS FLOW ANGLE FOR THE CONE



FLOW ANGLE

FIG. 6-36 PLOT OF Y/d VERSUS FLOW ANGLE FOR THE CONE





FLOW ANGLE

FIG. 6.37 PLOTS OF  $Y/\delta$  VERSUS FLOW ANGLE FOR THE CONE

HODOGRAPH

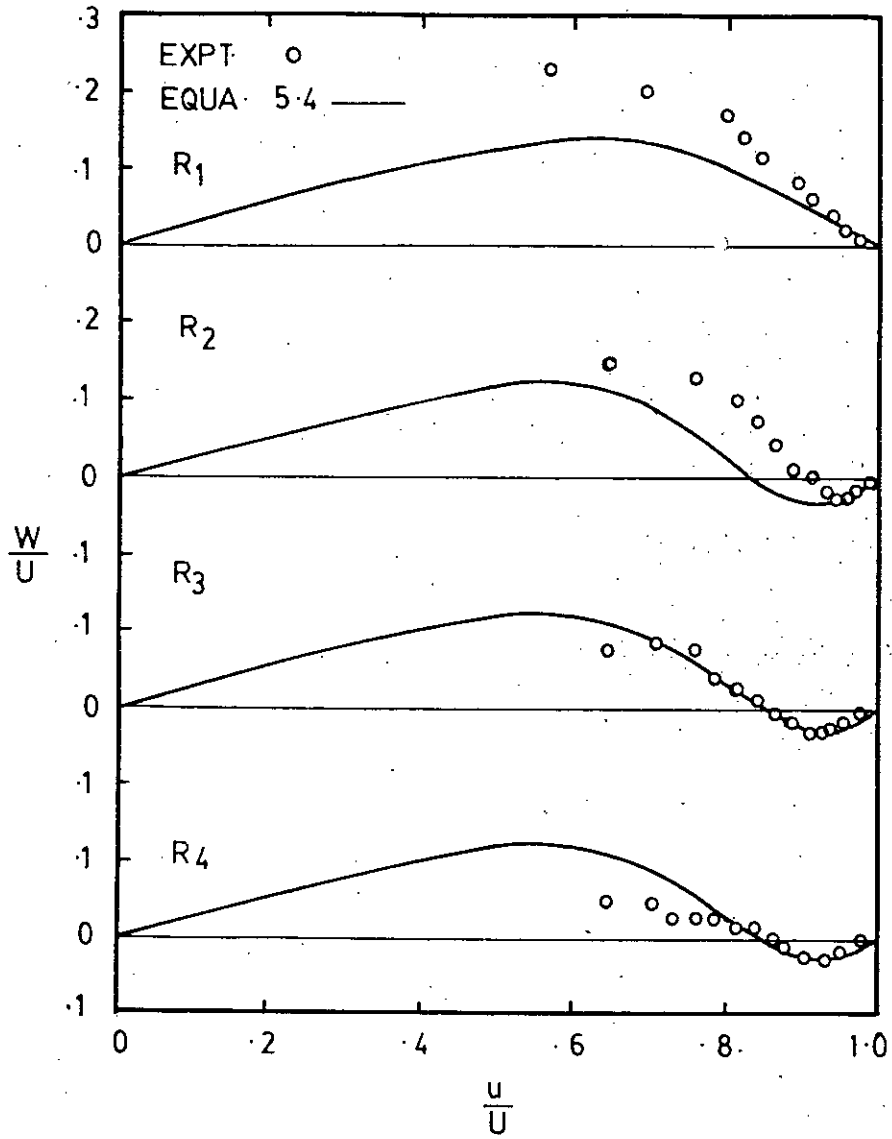


FIG. 6-38 HODOGRAPH FOR THE RIGHT CIRCULAR CYLINDER

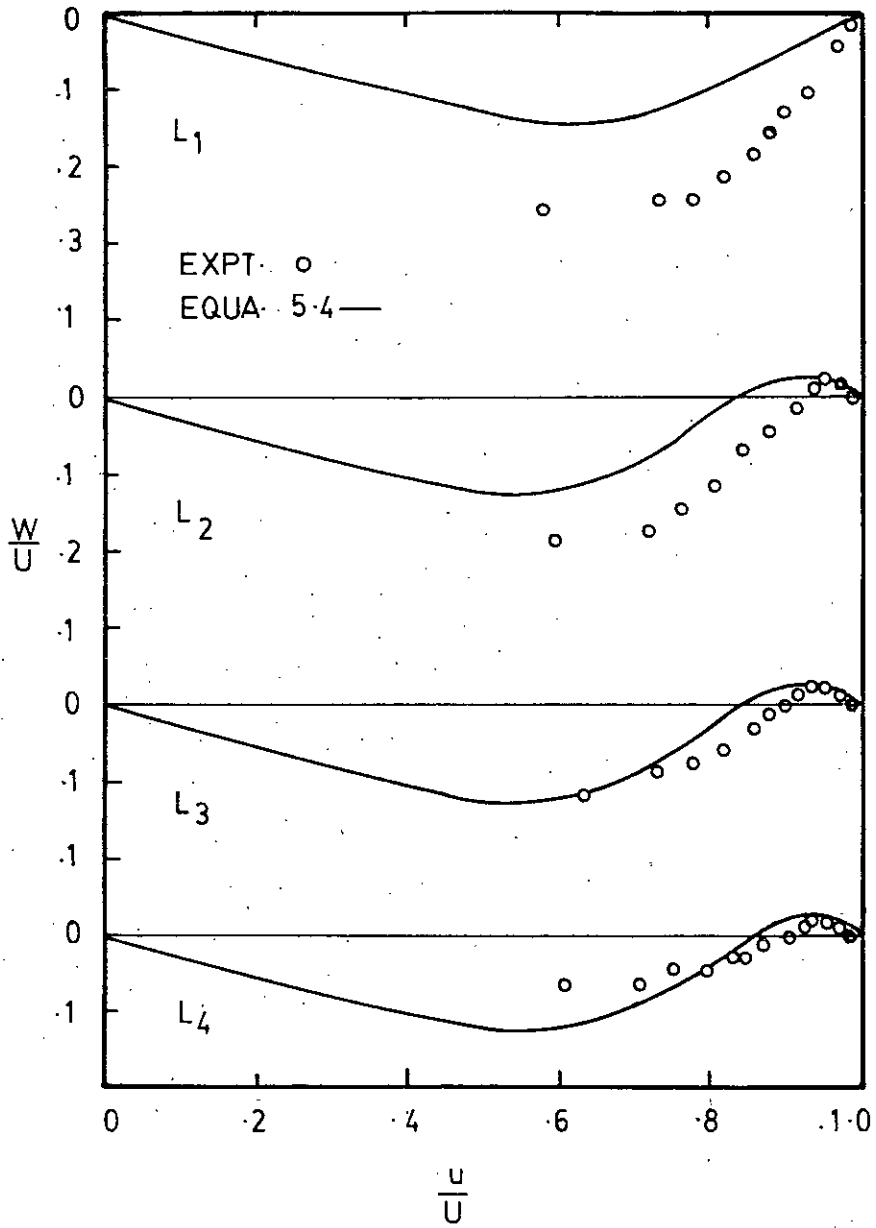


FIG. 6.39 HODOGRAPH FOR THE RIGHT CIRCULAR CYLINDER

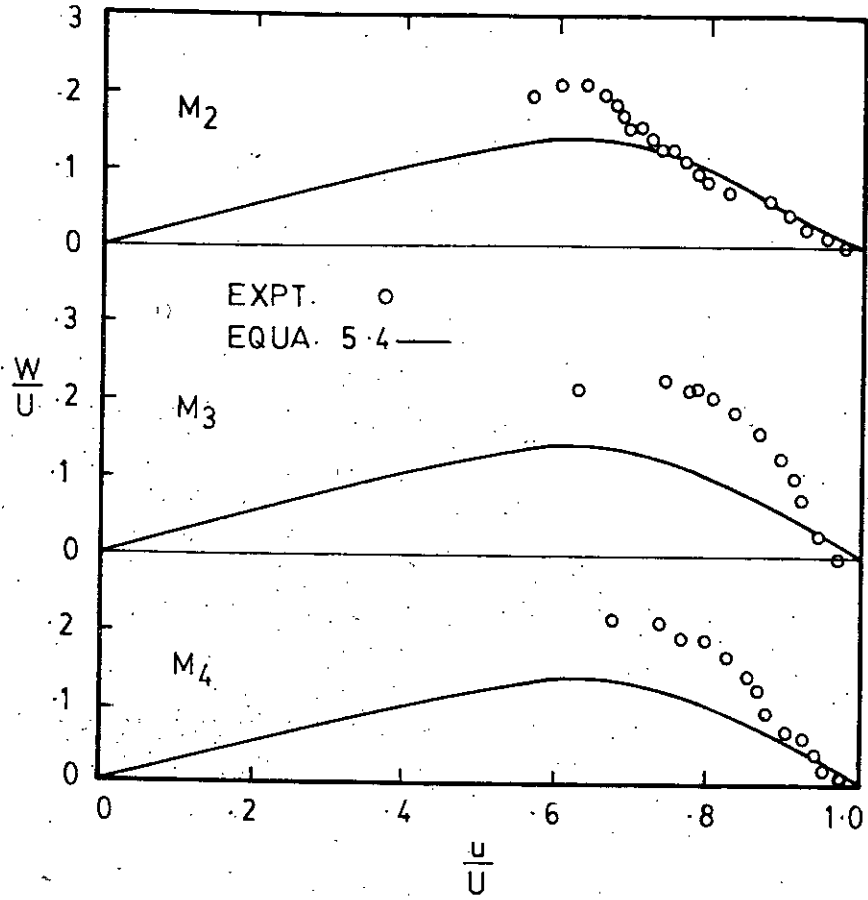


FIG. 6.40 HODOGRAPH FOR THE RIGHT CIRCULAR CYLINDER

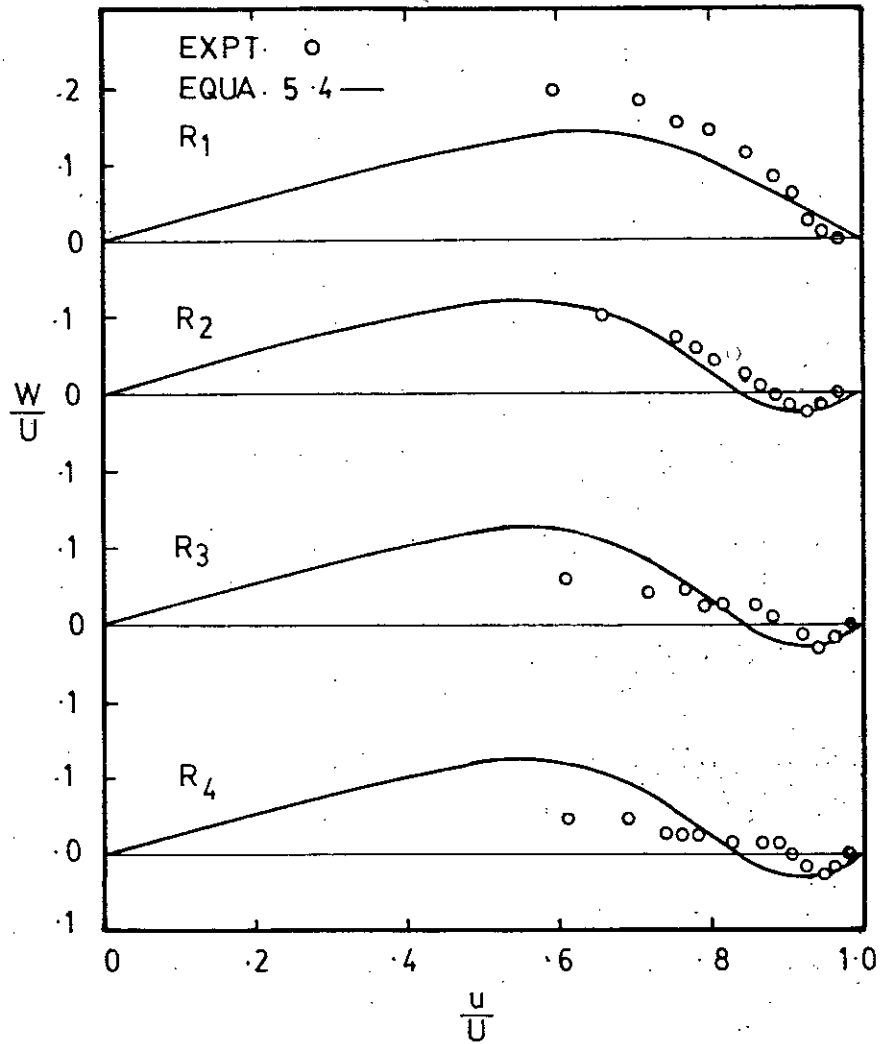


FIG. 6.41 HODOGRAPH FOR THE ROUNDED HEAD CYLINDER

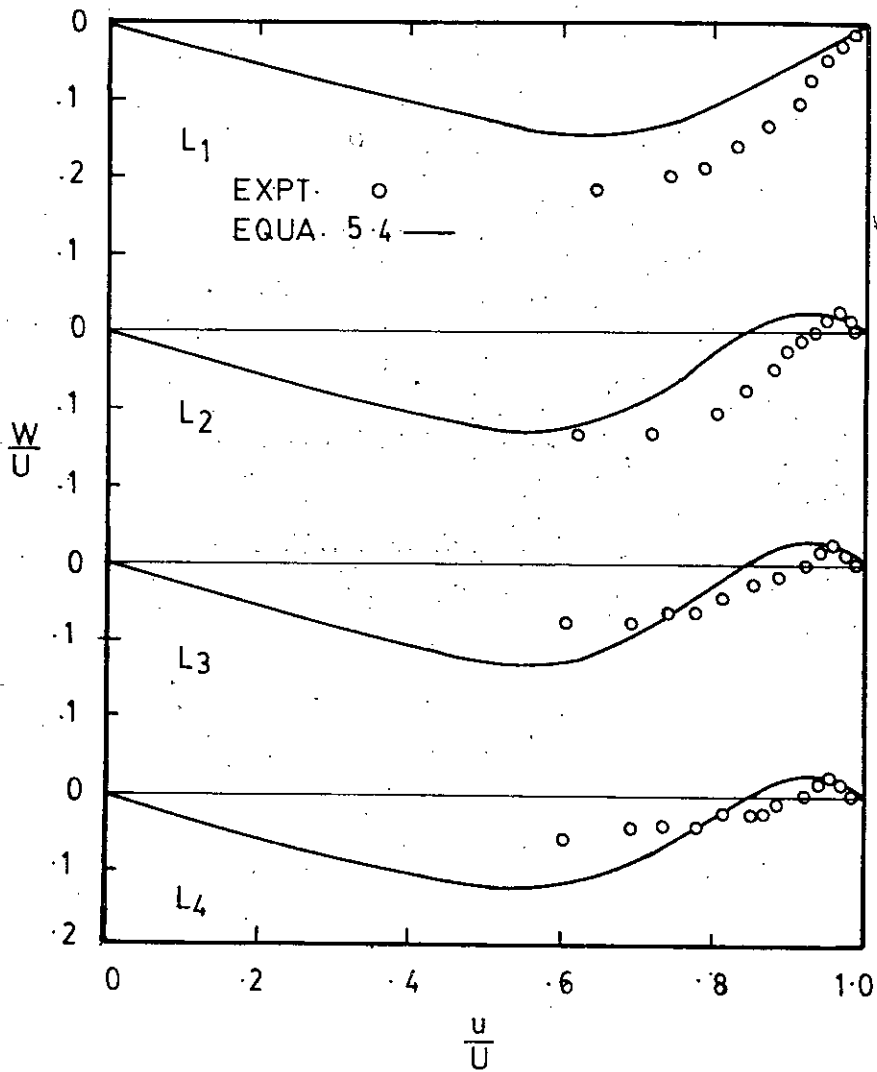


FIG. 6-42 HODOGRAPH FOR THE ROUNDED HEAD CYLINDER

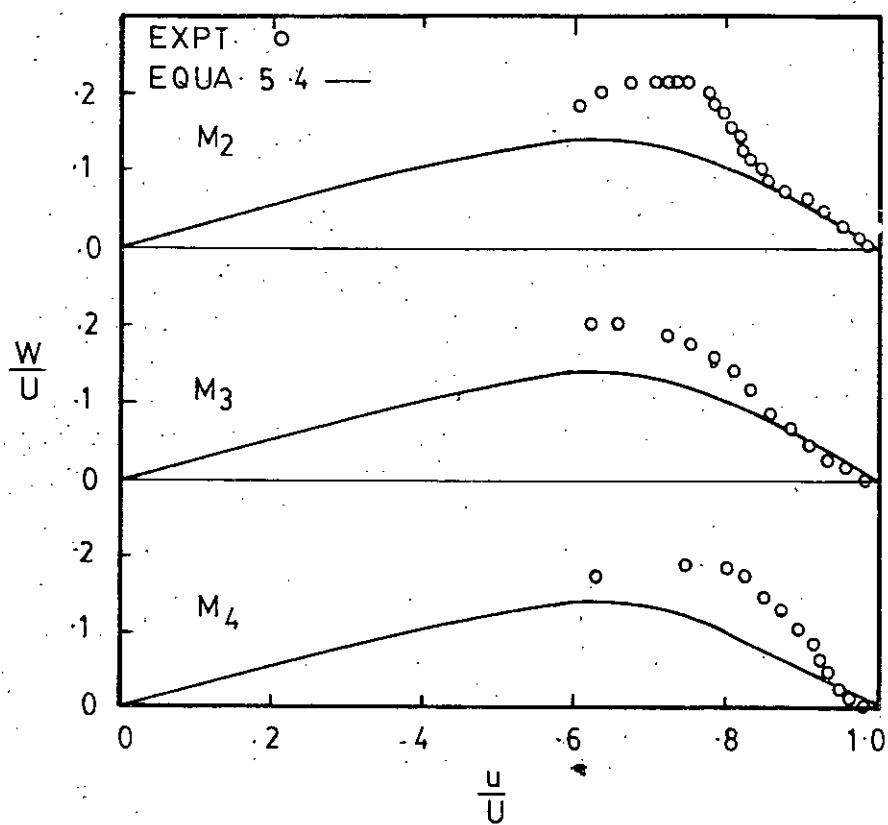


FIG. 6-43 HODOGRAPH FOR THE ROUNDED HEAD CYLINDER



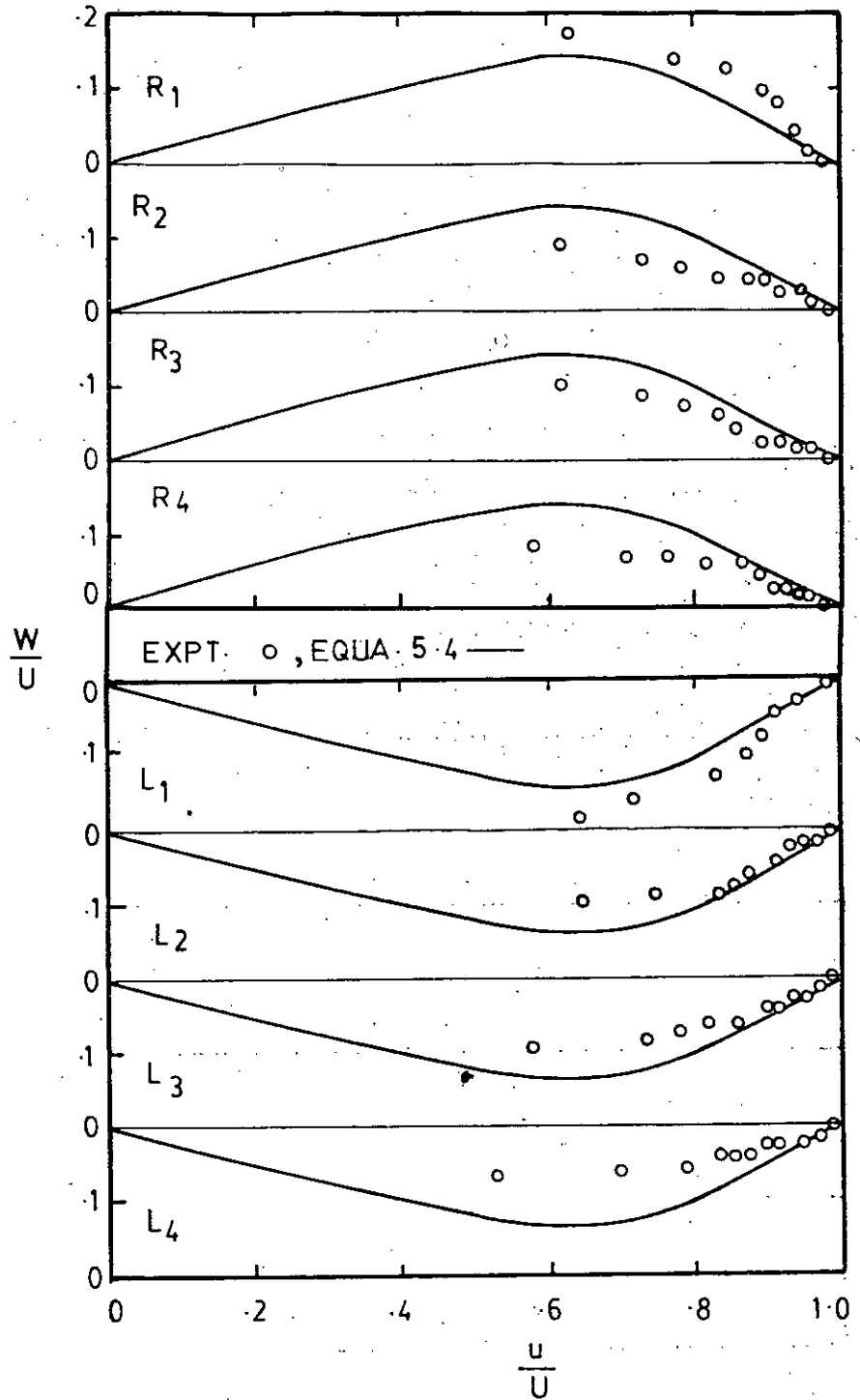


FIG. 6.44 HODOGRAPH FOR THE CONE

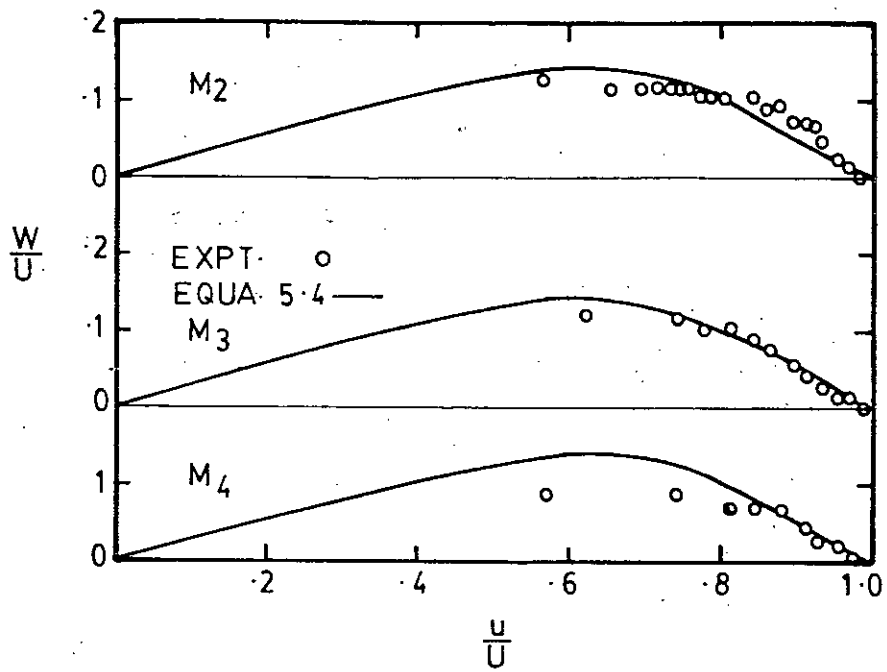


FIG. 6.45 HODGRAPH FOR THE CONE

## APPENDIX

### Two-tube Yawmeter

There are two common ways by which flow direction can be measured with pressure probes. In the first method a symmetrical arrangement of sensing holes is used and known as 'null-reading' or equibalanced method. In this method the probe is oriented at a position by which same pressure is recorded at each hole and the flow direction is then related to the geometry of the probe. In the second method the probe remains stationary and the steady flow comes at different angle of attack. The observed pressure differences between the camphered tubes are measured and a non-dimensional pressure difference,  $\Delta p / \frac{1}{2} \rho U^2$  versus angle of flow is plotted for calibration of the yawmeter. The pressure differences in the camphered tubes increase with increase angle of flow direction. In the 'null-reading' method of measurement error due to the sensing probe i.e. yaw meter is added with the error of the angle measurements, in addition, during measurements rotation of the probe is sometimes become difficult. On the other hand use of simple yawmeter does not need arrangement of rotation and it gives reliable values of the flow angles. For these reasons multi-tube yawmeters are generally used in three-dimensional flows. There are many types of yawmeters, e.g. claw, diverging 2-tube, 2-tube, conrad, chiesel, pyramid, conical, etc.

For simplicity of the construction a simple two-tube yawmeter (1958) was used for the present investigation and a calibration of the yawmeter was presented in Fig. 28.

According to Bryer and Pankhurst (1971), the sensitivity of yawmeter can be expressed as  $\Delta p / \frac{1}{2} \rho U^2$ , where  $\Delta p$  is the pressure difference between the two sensing-holes and  $\psi$  is the yaw angle. The smallest change of flow angle  $\Delta \psi$  which can be measured by a given system can be expressed by the equation,  $\Delta \psi = \Delta p_{\min} / (C_p)_{\psi} \frac{1}{2} \rho U^2$ , where  $\Delta p_{\min}$  is the minimum pressure difference that can be read on the manometer and  $(C_p)_{\psi}$  is the yawmeter sensitivity. For the present experiment the yaw meter sensitivity is .160 and the flow angle is detectable to better than  $.11^\circ$  at a free stream velocity of 25 fps and with a minimum reading of .025 cm of water head in the inclined manometer.

